2015

Thiol-ene Scaffolds as Synthetic Augments and Silicate Ceramics as Osteogenic Components for Bone Tissue Engineering Applications

Cong Chen
Louisiana State University and Agricultural and Mechanical College

THIOL-ENE SCAFFOLDS AS SYNTHETIC AUGMENTS AND SILICATE CERAMICS AS OSTEOGENIC COMPONENTS FOR BONE TISSUE ENGINEERING APPLICATIONS

A Dissertation

Submitted to the Graduate Faculty of the
Louisiana State University and
Agricultural and Mechanical College
in partial fulfillment of the
requirements for the degree of
Doctor of Philosophy

in

The Donald W.Clayton Graduate Program
in Engineering Science

by
Cong Chen
B.Tech., Jiangnan University, 2009
M.S., Louisana State Univeristy, 2011
August, 2015

♥

To my beloved parents without whom

I would not have come so far...

ACKNOWLEDGMENTS

I would like to thank God for his blessings towards achieving this goal in my life and my family for their encouragement and unconditional support. Mom and Dad, I owe all my success to you. I would like to express my gratitude towards my parents for their parental love and for making me the person that I am today.

Most of all, I would like to thank Dr. Hayes for accepting me as his research assistant and for their guidance and advice. He has been my mentor and has offered me his support at all times. I am very thankful to him for having given me the opportunity to work on interesting projects and for his constant encouragement and faith in me. His constant enthusiasm and zeal during my research have made my research work really interesting. I would also like to thank Dr. Monroe, Dr. Aita and Dr. Nguyen for serving on my committee. Their timely and valuable inputs to my project are highly appreciated.

I would also like to thank Dr. Pojman and Dr. Boldor for all their help and valuable advice when I needed it. I am also grateful to Dr. Lopez for letting me work in her laboratory and for encouraging me to give my best at all times. I would like to thank all my colleagues and fellow graduate students at Biological & Agricultural Engineering Department. Special thanks go to Leah Garber, Dr. Ammar Qureshi, Dr. Akanksha Kanitkar, Dr. Del Piero, Dr. Dongmei Cao, Mollie Smoak, Katie Hogan, Elizabeth Jee, Ms. Ying Xiao, Forum Shah, Carmel Fargason, Dr. Thomas Scherr, Dr. Andre Zanetti and Dr. Michelle Walker for their help and assistance with my research. I would also like to extend my gratitude to Ms. Angie and Ms. Donna for their valuable support while working in BAE department. They have been great friends from whom I have gotten to learn a lot.

TABLE OF CONTENTS

ABSTRACT

Bone tissue engineering approaches using polymer/ceramic composites show promise as effective biocompatible, absorbable, and osteoinductive materials. A novel class of *in situ* polymerizing thiol-acrylate based copolymers synthesized via an amine-catalyzed Michael addition was studied for its potential to be used in bone defect repair. Both pentaerythritol triacrylate-co-trimethylolpropane tris(3-mercaptopropionate) (PETA-co-TMPTMP) and PETA-co-TMPTMP with hydroxyapatite composites were fabricated in solid cast and foamed forms. These materials were characterized chemically and mechanically followed by an *in vitro* evaluation of the biocompatibility and chemical stability in conjunction with human adipose-derived mesenchymal pluripotent stem cells (hASC). The solid PETA-co-TMPTMP with and without hydroxyapatite (HA) exhibited compressive strength in the range of 7-20 MPa, while the cytotoxicity and biocompatibility results demonstrate higher metabolic activity of hASC on PETA-co-TMPTMP than on a polycaprolactone control. SEM imaging of hASC show expected spindle shaped morphology when adhered to copolymer. Micro-CT analysis indicates open cell interconnected pores. Foamed PETA-co-TMPTMP HA composite shows promise as an alternative to FDA-approved biopolymers for bone tissue engineering applications.

The results of the six week *in vivo* biocompatibility study using a posterior lumbar spinal fusion model demonstrate that PETA:HA can be foamed *in vivo* without serious adverse effects at the surgical site. Additionally, it was demonstrated that cells migrate into the interconnected pore volume are found within centers of ossification.

Because the natural mechanical strength of materials is highly dependent on the crystal structure, four different silicate-derived ceramics—diopside, akermanite, monticellite, and merwinite have been synthesized and evaluated for their potential as bone augments and grafts. This sparks our interest in the fabrication of polycaprolactone (PCL)/ceramic composites for potential use as scaffolds. Akermanite and monticellite exhibit better osteogenic properties than diopside and merwinite, suggesting that they might be the optimal material for fabricating bone scaffolds.

CHAPTER 1. INTRODUCTION

Biomaterial matrices are widely used to deliver genetic material and/or inductive biochemical signal, which allow developmental control over the delivered stem cells to some extent. Lots of studies using stem cell-scaffold constructs in regenerative medicine and showed promising results (Levi & Longaker, 2011b).

1.1 Current biomaterials used in hASC bone tissue engineering strategies

1.1.1 Biological materials

Biologic scaffolds composed of naturally occurring extracellular matrix (ECM) facilitate constructive remodeling of tissues when used with site specific cells. The use of endogenous stem cells, modulation of the host innate immune response, and influence of cell differentiation could cause the remodeling process (Crapo et al., 2013). ECM materials are typically prepared with decellularization of source tissues, such as adipose and nervous system tissue, and then made into sheets, powder, or hydrogels. The decellularization is performed during ECM isolation in order to prevent inflammatory response and/or tissue rejection due to xenogeneic and allogeneic cellular antigens (Zanetti et al., 2013b). However, ECM still retain the structure and function original tissue to a large extent (Song & Ott, 2011) and could trigger desirable immunemediated responses at injury sites in multiple tissue types (Ariganello et al., 2011). Biologic scaffolds composed of ECM have been used in many studies to facilitate constructive remodeling in several tissues, including dura mater, bone, cartilage (Yang et al., 2008), cardiac muscles (Robinson et al., 2005), and peripheral and central nervous system(Crapo et al., 2013; Martini, 1994).

In other studies, fibrin hydrogel were used as bone scaffolds. hASC were initially loaded on a fibrin hydrogel and then the hASC-fibrin hydrogel was wrapped around an orthopaedic construct

to treat bone or cartilage defect (Hankemeier et al., 2007; Wang et al., 2010b). Therefore, the understanding of the biomechanical properties of the ECM loaded with hASC will be critical to future clinical use.

1.1.2 Synthetic polymers

Biocompatible synthetic polymers can be produced reproducibly in bulk and in highly purified forms. Polyester polymers such asPCL, PGA, PLLA and their copolymer PLGA, which have been shown to support hASC proliferation and differentiation, are the most popular synthetic polymeric materials in bone tissue engineering.(Guven et al., 2011; Jeon et al., 2008; Lee et al., 2011; Levi et al., 2010; Wang et al., 2010a)

Polycaprolactone (PCL)

Polycaprolactone (PCL) is formed through ring-opening polymerization and has repeating units of one ester group and five methylene groups. The degradation of PCL is done in two steps, random hydrolysis of ester bonds and weight loss due to the diffusion of oligomeric sort from the volume(Sabir et al., 2009). PCL degrades slowly and it can last for up to 2 years *in vivo*(van Gaalen et al., 2008) . As a versatile polymeric material, PCL has been made into nanofibers by eletrospinning and after seeding the cells on PCL nanofibers, mineralization and type I collagen were observed on the scaffolds(Yoshimoto et al., 2003).

Poly lactic acid (PLLA)

PLLA is produced by the cyclic dimer of lactic acid that exists as two optical isomers. D &L- lactate is the isomer in natural form, as well as DL-lactide, which is the synthetic mixture of D-lactide and L-lactide (Sabir et al., 2009). Poly (lactic acid) also can be degraded by the homogenous hydrolysis erosion, releasing non-biocompatible products (acids) that can

dramatically change the scaffold microenvironment leading to cell death. The biocompatibility of PLLA scaffolds could be improved by combining in collagen or BMP-2, and used to treat segmental defect model in rat. Neo bone tissue was observed after 12 week after implantation of PLLA scaffolds (Liao et al., 2004).

Poly glycolic acid (PGA)

PGA is a rigid thermoplastic material, with high melting temperature and more hydrophilic than PLA. It is not soluble in most organic solvents due to the high crystallinity (Sabir et al., 2009). PGA can be fabricated in various ways such as extrusion, injection, and compression molding. The properties and the degradation can be affected by the type of processing technique. PGA, when fabricated with triple amount of β-TCP, exhibited a strong ability for osteogenesis, mineralization and biodegradation for bone replacement (Cao & Kuboyama, 2010). PGA was also made into an injectable copolymer with PLA and demonstrated to be a suitable osteoconductive material to treat critical size bone defects (Rimondini et al., 2005).

Poly (D,L-lactide-co-glycolide) PLGA

Copolymerization of PLLA and PGA produce PLGA, which is amorphous, and has a slower degradation rate and weaker mechanical strength compared to PLLA. Bone scaffolds are also made of PLGA and have been demonstrate to accelerate bone healing. Furthermore, PLGA scaffolds induce more rapid bone formation than untreated controls (Karp et al., 2003). Marra *et al.* mixed HAP granules into poly(caprolactone) and PLGA blends and observed the formation of collagen layer on the scaffold.(Marra et al., 1999)

In comparison to the above techniques the amine catalyzed thiol-acrylate reaction utilized in this study is unique as it proceeds though as anionic step growth mechanism. Normally anionic polymerization mechanisms proceed via a chain growth mechanism. This amine catalyzed thiol-acrylate mechanism proceeds via a chain "process" with sequential chain transfer steps with each addition causing the polymerization to follow the rules and attributes of a step growth mechanism in terms of molecular weight and physical properties. The general reaction scheme below is described in Bounds *et al.*(Bounds et al.)

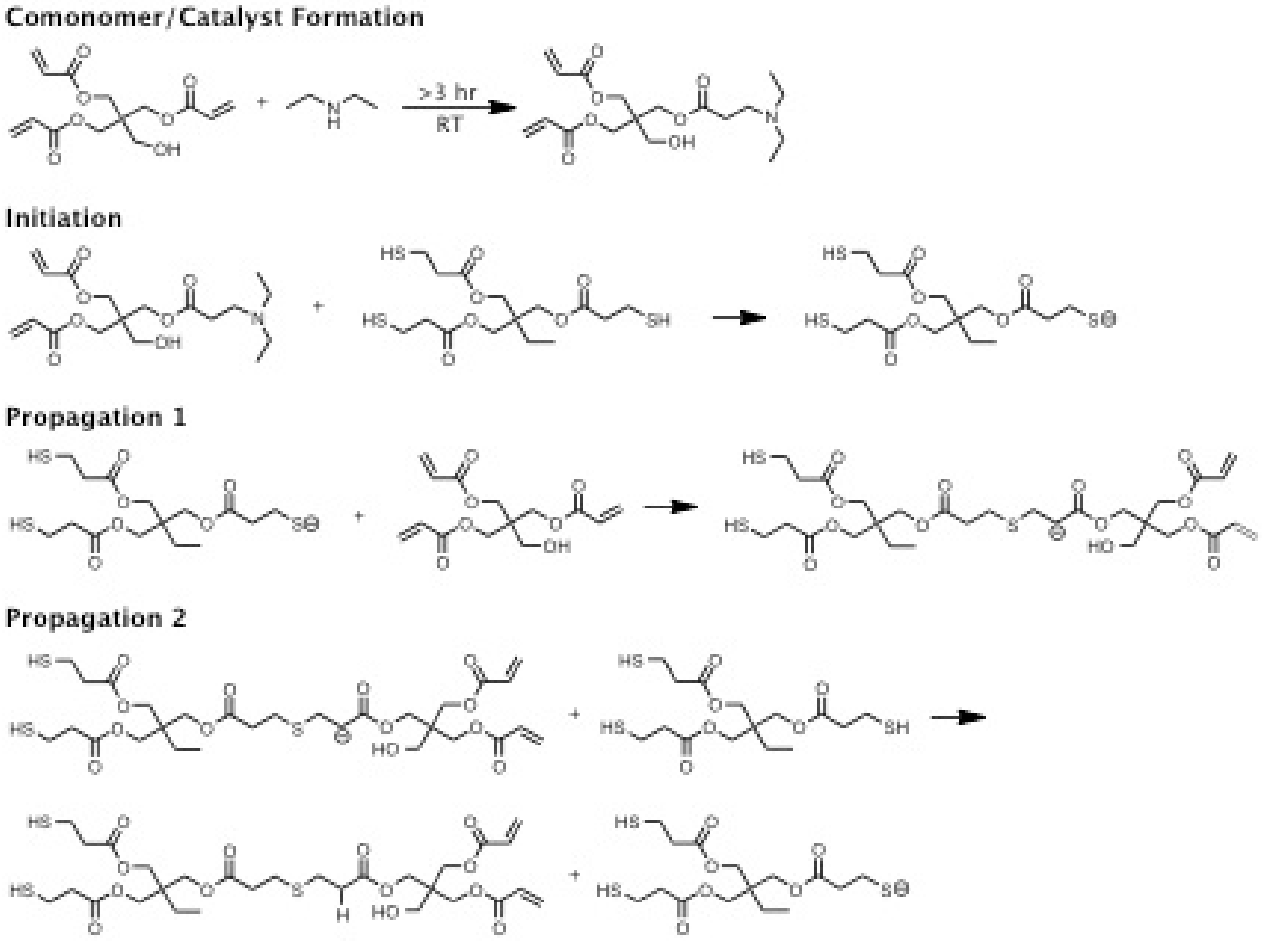

Figure 1.1 Scheme of Amine Catalyzed Thiol-Acrylate Reaction

1.1.3 Ceramics

Bone is composed of hydroxyapatite (HA) crystals distributed within an organic matrix with porosity and percent mineralization varying among bone types.(Pallua & Suscheck, 2010a) The use of calcium phosphate ceramics as bone substitutes dates back more than 30 years to the field of dental implantation(Ambard & Mueninghoff, 2006). However, one of the main disadvantage of calcium phosphates is their weak mechanical strength, especially they are brittle and have poor fatigue resistance (Vallet‐Regí & Ruiz‐Hernández, 2011). Highly porous bioceramics and scaffolds have even weaker mechanical strength. Consequently, for biomedical applications, calcium phosphates are primarily used as fillers and coatings. Kim et al observed higher alkaline phosphatase activity of the proliferated cells on porous ZrO2 bone scaffold coated with hydroxyapatite than pure ZrO_2 scaffolds(Kim et al., 2003a). It is generally agreed that ceramic biomaterials used in bone tissue engineering applications should mimic the natural bone structure to support cell attachment and migration within the porous materials (Zanetti et al., 2013b). β-tricalcium phosphate (β-TCP), is a synthetic apatite that shows great osteoconductive and osteoinductive properties compared to HA both *in vitro* and *in vivo* (Dong et al., 2002; Kwon et al., 2003; Yuan et al., 2001). Lately, Liu et al. evaluated the osteogenic potential of hASC loaded in β-TCP and akermanite scaffolds and demonstrated that Akermanite ($Ca_2MgSi_2O_7$) has a stable degradation rate and superior bone deposition compared to β-TCP constructs (Liu et al., 2008b). Furthermore, akermanite scaffolds are able to improve hASCs' osteogenic commitment since the cells have a strong affinity for Ca, Mg, and Si ions deposited on scaffold(Liu et al., 2008b). Diopside, another ceramic similar to akermanite, has been demonstrated to precipitate apatite mineral in simulated body fluid (SBF),(Iwata et al., 2004b)

support osteoblast culture(Wu & Chang, 2007a) and to form bone/ceramic interfaces in rabbit models of osteointegration.(Nonami & Tsutsumi, 1999) The bioactivity of diopside composites has also recently been explored in SBF. Sainz *et al*. evaluated the thermodynamic stability of a blend of wollatonite and diopside in finding that higher diopside content resulted in a more stable chemically stable substrate.(Sainz et al., 2010) Another recent study found that increased diopside content in Al_2O_3/diopside ceramic composites led to increased calcium deposition in SBF.(Zhang et al., 2010a) Zhang *et al*. found substantial mineral growth on the surface of HA/diopside composites immersed in SBF. Unfortunately, this study did not have adequate controls or analysis to determine the nature of the mineral formations.(Zhang et al., 2011) We are particularly interested this phase because of the dimensionality of the structure type. It is similar to akermanite and will expand our interest in understanding the role of structure and preparation in the strength and bioactivity of ceramics for bone scaffolding.

In addition to magnesium and silicon, strontium an alkaline earth element similar to calcium, has long been known as bioactive trace component of bone and has been explored as a treatment for osteoporosis.(Dahl et al., 2001; Shorr & Carter, 1952) Several recent studies have doped strontium into ceramics such calcium polyphosphate, hydroxyapatite, and hardystonite where in low percentages (wt/wt) strontium doped ceramics were found to up regulate osteogenic markers *in vitro* and increase bone volume *in vivo*. (Landi et al., 2007; Qiu et al., 2006; Tian et al., 2009; Zreiqat et al., 2010)

It is important to note that ceramic materials prepared in the techniques as published typically have impurities and are not crystalline. To correlate osteogenic properties with composition it is critical to study phase-pure materials and in the proposed project, we plan to prepare ceramics

with multiple heat treatments to reach sample equilibrium and carefully monitoring phase formation.

It is clear that scaffold technology plays a critical role in the success of the current stem cell based bone tissue engineering paradigms. While a variety of different materials, both ceramics and polymers, have been tested in combination with hASC, it has been noted by Lendeckel *et al*. and others that composite scaffolds may offer a better clinical outcome as a result of improved mechanical and biological properties.(Lendeckel et al., 2004) The study detailed in disseration will explore diopside, monticellite and merwinite, similar in composition to akermanite, as osteogenic components of PCL composites for potential use in bone defect repair.

1.2 Scaffolds fabrication method

Solvent casting

Solvent casting or particulate leaching is generally used to make scaffolds at room temperature. For this method, polymers like PLLA or PLGA dissolved in an organic solvent such as chloroform first and then into a mold containing solid crystals. These salt crystals are insoluble in the organic solvent, however, could be leached out by immersing the scaffold in water to form a pore structure within the scaffold (Liao et al., 2002; Mozafari et al., 2010).

Using different size and morphology of the salt crystals could change the pore size and porosity of scaffolds. The disadvantages of the this method include the extensive use of toxic organic solvents, long time required for solvent removal (days-to-weeks), residual particles in the scaffolds, as well as insufficient interconnectivity (Hutmacher, 2000).

Thermally induced phase separation.

High volume of inter-connected micropore structure of bone scaffolds could be created through thermal precipitation method (Hutmacher, 2000). Briefly, the polymer was dissolved in organic solvents (1,4-dioxane or dimethylcarbonate) to produce a homogeneous mixture then mixed with ceramics powder.

The solution was freeze under -70^{o}C for 24 hours and freeze-dry in a vacuum oven till reaching a constant weight (Maquet et al., 2004). Such method could be used to prepare PCL/Hydroxyapatite (Zargarian & Haddadi-Asl, 2010), PLLA/TCP composite scaffolds (Xiong et al., 2002).

Material Injections

Injectable pastes have been developed for use as a fixation material or to fabricate bone constructs for cell ingrowth or proceeding. Injectable materials have an advantage over pre-sculpted scaffolds since they can conform to any shape that they are pressed into. In this method, polymerization can be done *in situ* (Shin et al., 2003; Temenoff & Mikos, 2000). Injectable calcium phosphate cements (CPC) have been widely used for filling of bone defects near the joint since 1980s but they have a low flexural and tensile strength (Brown & Chow, 1983; Larsson, 2010; LeGeros et al., 1982).

Generally, properties of the injectable materials, such as viscosity, setting time, and initial mechanical strength, are important for their potential application as bone scaffolds. By using material injections, the material can fill the gaps in the defect regardless of defect shape and also it is easy to incorporate bioactive and therapeutic agents by mixing them together with the injectable materials(Di Martino et al., 2005).

Gas-Foaming Process

Gas foaming process can also be used to fabricate polymer foams with high porosity without using highly toxic organic solvents (Cooper, 2000; Harris et al., 1998; Mooney et al., 1996).

Carbon dioxide (CO_2) is usually used as gas porogen for foaming the polymer. Solid polymers are saturated with CO_2 when exposed to high pressure of CO_2 gas. By using this approach, the porosity of polymer foam can reach up to 93% with pore size around 100 μm. However, gas-foaming results in a closed pore surface and with only 10–30% of interconnected pores.

Combing particulate leaching method with gas foaming could significantly improve the pores interconnectivity of scaffolds (Liu & Ma, 2004). However, completely eliminating closed pores is still a great challenge (Mooney et al., 1996).

3D Printing

Rapid prototyping, especially 3D printing, is becoming more and more popular to create custom implants based on individual need (Leukers et al., 2005). 3D Printing uses ink-jet printing technology to precisely place a ‘‘binder’’ solution on a bed of powder. It glues the powder together in a cross-sectional layer; any powdered material, including polymers, metals, or ceramics can be fused using an ink-jet head in theory (Stevens et al., 2008).

A starch-based polymer powders (corn starch, dextran and gelatin) was made via 3D printing process (Lam et al., 2002). Furthermore, hydroxyapatite scaffolds has been successfully fabricated by 3D printing technology and cells proliferated deep into the structure forming close contact to Hydroxyapatite granules (Leukers et al., 2005).

Other applied scaffold fabrication technologies

Other techniques for scaffold fabrication also include membrane lamination, fabrication of non-woven, emulsion freeze drying, supercritical-fluid technology and fused deposition modeling. Table 1.1summarizes the key characteristics and parameters of the techniques currently used.

Table 1.1 Key characteristics and parameters of the techniques currently used

Fabrication technology	Processing	Material properties required for processing	Porosity in %	Architecture
Membrane lamination	Solvent bonding	Soluble	<85	Irregular pore structure
Fabrication of non-woven	Carding, Needling, Plate pressing	Fibers	*<95*	Insufficient mechanical properties
Emulsion freeze drying	Casting	Soluble	*<97*	High volume of inter-connected micropore structure
Supercritical-fluid technology	Casting	Amorphous	*10-30*	High volume of non-interconnected micropore structure
Fused deposition modelling	Solid free form fabrication	Thermoplastic	*<90*	100% interconnected macropore structure (triangles, pentagons, honey comb, etc.),design and fabrication layer by layer

1.3 Animal models used in bone tissue engineering

Rat is one of the most commonly used animals in medical research. However, there are significant dissimilarities between rat and human bone. In addition, rats are improper for emulating multiple implants simultaneously due the limitations of (Mooney & Siegel, 2005). Other animal models have been established to study parameters that affect bone healing.

These animal models include dog (mongrel, beagle, foxhound, terrier, and bulldog), rabbit, guinea pig, and sheep. Growth factors, bone graft scaffolds, and macroscopic/microscopic

changes after different treatment were studies by using these models(Grynpas et al., 2002; Reichert et al., 2013; Viateau et al., 2007; Wang et al., 2010b).

Rodents

The most commonly used lab animal model is the rat. Rats are inexpensive, easy to raise and they do not carry the societal concerns compared with other larger animal models (Liebschner, 2004). Multiple bone implants surgery models, such as spinal fusion, cranial defect and long bone defect have been used on rats and demonstrated great success (Burdick et al., 2003; Cook et al., 1994; Lopez et al., 2009). Bone turnover and the effect of diet on this process since all types of rodents have been studied so extensively in research.

There are, however, disadvantages in the use of rats and mice: they have a limited naturally occurrence of basic multicellular unit based remodeling; another limitation is the absence of impaired osteoblast function during the late stages of estrogen deficiency (Liebschner, 2004). It is also impossible to collect large blood samples or obtain several biopsies in such a small animal for long term studies(Mooney & Siegel, 2005) .

Canine

The dog model is the most commonly used animal model for studying the spinal fusion process. A lot of literatures compare canine and human bone with regard to the usefulness of the dog as a model for human orthopaedic conditions. A major disadvantage of these dog models is that solid fusion always occurs, which is different from clinical situations in humans(Liebschner, 2004).

Trabecular bone from the distal femur of human's and dog's is similar in terms of mechanical and mass properties, but differs in ultimate strain resistance, indicating that canine

trabecular bone is able to withstand higher compressive strains before failure than human bone (Choi & Goldstein, 1992). Callewart et al. evaluated the dog spinal fusion method to determine the rate of fusion after decortication with autogenous bone grafting versus dicortication alone and found out 100% of the decorticated facets with iliac graft and 75% of the facet sites with decortication alone were determined to be fused after 6 months by manual testing (Schimandle & Boden, 1994) .

Sheep and Goats

The number of using sheep is increasing over the last decade and sheep were widely used in orthopedic research involving fractures, osteoporosis, bone-lengthening and osteoarthritis. Adult sheep weigh more similar human's body and have long bones of dimensions suitable for the implantation of human implants (Newman et al., 1995).

The bone structure of the sheep is quite different from human being histologically although sheep bones are relatively close to human bones.

In sheep, bone contains principally of primary bone (de Kleer, 2006) in contrast to the largely secondary, haversian bone composition in humans(Eitel et al., 1981). Kon et al. (Kon et al., 2000) have evaluated the potential of BMSCs (bone marrow derived stem cells) to repair bone defects in vivo in a sheep model.

They created a critical size defect in the sheep tibia and implanted an appropriately designed porous scaffold made of pure HA into the missing segment. Ceramics scaffolds were either seeded with BMSCs or left empty.

Even though bone formation was histologically observed in both cell-seeded and not seeded implants, in the former bone formation was found to occur both within the internal

macropore space and around the HAC cylinder while in the latter bone formation was limited mostly to the outer surface and was not observed in most of the inner pores. Furthermore in an indentation assay, the stiffness of the complex HA-bone material was found to be higher in cell-seeded implants than in constructs alone.

Table 1.2 Summary of four key attributes in terms of similarity between animal and human bone (Pearce et al., 2007)

	Canine	Sheep/Goat	Rodents
Macrostructure	++	+++	+
Microstructure	++	+	+
Bone Composition	+++	+++	+
Bone Remodelling	++	+++	++

1.4 Reference

Ambard, A.J., Mueninghoff, L. 2006. Calcium Phosphate Cement: Review of Mechanical and Biological Properties. *Journal of Prosthodontics*, **15**(5), 321-328.

Ariganello, M.B., Simionescu, D.T., Labow, R.S., Michael Lee, J. 2011. Macrophage differentiation and polarization on a decellularized pericardial biomaterial. *Biomaterials*, **32**(2), 439-449.

Bounds, C.O., Goetter, R., Pojman, J.A., Vandersall, M. Preparation and application of microparticles prepared via the primary amine-catalyzed michael addition of a trithiol to a triacrylate. *Journal of Polymer Science Part A: Polymer Chemistry*, **50**(3), 409-422.

Brown, W., Chow, L. 1983. A new calcium-phosphate setting cement. *Journal of Dental Research*. AMER ASSOC DENTAL RESEARCH 1619 DUKE ST, ALEXANDRIA, VA 22314. pp. 672-672.

Burdick, J.A., Frankel, D., Dernell, W.S., Anseth, K.S. 2003. An initial investigation of photocurable three-dimensional lactic acid based scaffolds in a critical-sized cranial defect. *Biomaterials*, **24**(9), 1613-1620.

Cao, H., Kuboyama, N. 2010. A biodegradable porous composite scaffold of PGA/β-TCP for bone tissue engineering. *Bone*, **46**(2), 386-395.

Choi, K., Goldstein, S.A. 1992. A comparison of the fatigue behavior of human trabecular and cortical bone tissue. *Journal of biomechanics*, **25**(12), 1371-1381.

Cook, S.D., Baffes, G.C., Wolfe, M.W., SAMPATH, T.K., Rueger, D.C. 1994. Recombinant human bone morphogenetic protein-7 induces healing in a canine long-bone segmental defect model. *Clinical orthopaedics and related research*, **301**, 302-312.

Cooper, A.I. 2000. Polymer synthesis and processing using supercritical carbon dioxide. *Journal of Materials Chemistry*, **10**(2), 207-234.

Crapo, P.M., Tottey, S., Slivka, P.F., Badylak, S.F. 2013. Effects of Biologic Scaffolds on Human Stem Cells and Implications for CNS Tissue Engineering. *Tissue Engineering Part A*, **20**(1-2), 313-323.

Dahl, S., Allain, P., Marie, P., Mauras, Y., Boivin, G., Ammann, P., Tsouderos, Y., Delmas, P., Christiansen, C. 2001. Incorporation and distribution of strontium in bone. *Bone*, **28**(4), 446-453.

de Kleer, V. 2006. Development of bone. *Bone in Clinical Orthopedics. G. Sumner-Smith. Philadelphia, WB Saunders Co*, 1-80.

Di Martino, A., Sittinger, M., Risbud, M.V. 2005. Chitosan: a versatile biopolymer for orthopaedic tissue-engineering. *Biomaterials*, **26**(30), 5983-5990.

Dong, J., Uemura, T., Shirasaki, Y., Tateishi, T. 2002. Promotion of bone formation using highly pure porous< i> β</i>-TCP combined with bone marrow-derived osteoprogenitor cells. *Biomaterials*, **23**(23), 4493-4502.

Eitel, F., Klapp, F., Jacobson, W., Schweiberer, L. 1981. Bone regeneration in animals and in man. *Archives of orthopaedic and traumatic surgery*, **99**(1), 59-64.

Grynpas, M., Pilliar, R., Kandel, R., Renlund, R., Filiaggi, M., Dumitriu, M. 2002. Porous calcium polyphosphate scaffolds for bone substitute applications in vivo studies. *Biomaterials*, **23**(9), 2063-2070.

Guven, S., Mehrkens, A., Saxer, F., Schaefer, D.J., Martinetti, R., Martin, I., Scherberich, A. 2011. Engineering of large osteogenic grafts with rapid engraftment capacity using mesenchymal and endothelial progenitors from human adipose tissue. *Biomaterials*, **32**(25), 5801-9.

Hankemeier, S., van Griensven, M., Ezechieli, M., Barkhausen, T., Austin, M., Jagodzinski, M., Meller, R., Bosch, U., Krettek, C., Zeichen, J. 2007. Tissue engineering of tendons and ligaments by human bone marrow stromal cells in a liquid fibrin matrix in immunodeficient rats: results of a histologic study. *Archives of orthopaedic and trauma surgery*, **127**(9), 815-821.

Harris, L.D., Kim, B.-S., Mooney, D.J. 1998. Open pore biodegradable matrices formed with gas foaming.

Hutmacher, D.W. 2000. Scaffolds in tissue engineering bone and cartilage. *Biomaterials*, **21**(24), 2529-2543.

Iwata, N.Y., Lee, G.-H., Tokuoka, Y., Kawashima, N. 2004. Sintering behavior and apatite formation of diopside prepared by coprecipitation process. *Colloids and Surfaces B: Biointerfaces*, **34**(4), 239-245.

Jeon, O., Rhie, J.W., Kwon, I.K., Kim, J.H., Kim, B.S., Lee, S.H. 2008. In vivo bone formation following transplantation of human adipose-derived stromal cells that are not differentiated osteogenically. *Tissue engineering. Part A*, **14**(8), 1285-94.

Karp, J.M., Shoichet, M.S., Davies, J.E. 2003. Bone formation on two‐dimensional poly (DL‐lactide‐co‐glycolide)(PLGA) films and three‐dimensional PLGA tissue engineering scaffolds in vitro. *Journal of Biomedical Materials Research Part A*, **64**(2), 388-396.

Kim, H.-W., Lee, S.-Y., Bae, C.-J., Noh, Y.-J., Kim, H.-E., Kim, H.-M., Ko, J.S. 2003. Porous ZrO2 bone scaffold coated with hydroxyapatite with fluorapatite intermediate layer. *Biomaterials*, **24**(19), 3277-3284.

Kon, E., Muraglia, A., Corsi, A., Bianco, P., Marcacci, M., Martin, I., Boyde, A., Ruspantini, I., Chistolini, P., Rocca, M. 2000. Autologous bone marrow stromal cells loaded onto porous hydroxyapatite ceramic accelerate bone repair in critical - size defects of sheep long bones. *Journal of biomedical materials research*, **49**(3), 328-337.

Kwon, S.-H., Jun, Y.-K., Hong, S.-H., Kim, H.-E. 2003. Synthesis and dissolution behavior of β-TCP and HA/β-TCP composite powders. *Journal of the European Ceramic Society*, **23**(7), 1039-1045.

Lam, C.X.F., Mo, X., Teoh, S.-H., Hutmacher, D. 2002. Scaffold development using 3D printing with a starch-based polymer. *Materials Science and Engineering: C*, **20**(1), 49-56.

Landi, E., Tampieri, A., Celotti, G., Sprio, S., Sandri, M., Logroscino, G. 2007. Sr-substituted hydroxyapatites for osteoporotic bone replacement. *Acta Biomaterialia*, **3**(6), 961-969.

Larsson, S. 2010. Calcium phosphates: what is the evidence? *Journal of orthopaedic trauma*, **24**, S41-S45.

Lee, J.S., Lee, J.M., Im, G.I. 2011. Electroporation-mediated transfer of Runx2 and Osterix genes to enhance osteogenesis of adipose stem cells. *Biomaterials*, **32**(3), 760-8.

LeGeros, R., Chohayeb, A., Shulman, A. 1982. Apatitic calcium phosphates: possible dental restorative materials. *J Dent Res*, **61**, 343.

Lendeckel, S., Jodicke, A., Christophis, P., Heidinger, K., Wolff, J., Fraser, J.K., Hedrick, M.H., Berthold, L., Howaldt, H.-P. 2004. Autologous stem cells (adipose) and fibrin glue used to treat widespread traumatic calvarial defects: case report. *Journal of Cranio-Maxillofacial Surgery*, **32**(6), 370-373.

Leukers, B., Gülkan, H., Irsen, S.H., Milz, S., Tille, C., Schieker, M., Seitz, H. 2005. Hydroxyapatite scaffolds for bone tissue engineering made by 3D printing. *Journal of Materials Science: Materials in Medicine*, **16**(12), 1121-1124.

Levi, B., James, A.W., Nelson, E.R., Vistnes, D., Wu, B., Lee, M., Gupta, A., Longaker, M.T. 2010. Human adipose derived stromal cells heal critical size mouse calvarial defects. *PloS one*, **5**(6), e11177.

Levi, B., Longaker, M.T. 2011. Concise Review: Adipose‐Derived Stromal Cells for Skeletal Regenerative Medicine. *Stem Cells*, **29**(4), 576-582.

Liao, C.J., Chen, C.F., Chen, J.H., Chiang, S.F., Lin, Y.J., Chang, K.Y. 2002. Fabrication of porous biodegradable polymer scaffolds using a solvent merging/particulate leaching method. *Journal of biomedical materials research*, **59**(4), 676-681.

Liao, S.S., Cui, F.Z., Zhang, W., Feng, Q.L. 2004. Hierarchically biomimetic bone scaffold materials: Nano-HA/collagen/PLA composite. *Journal of Biomedical Materials Research Part B: Applied Biomaterials*, **69B**(2), 158-165.

Liebschner, M.A. 2004. Biomechanical considerations of animal models used in tissue engineering of bone. *Biomaterials*, **25**(9), 1697-1714.

Liu, Q., Cen, L., Yin, S., Chen, L., Liu, G., Chang, J., Cui, L. 2008. A comparative study of proliferation and osteogenic differentiation of adipose-derived stem cells on akermanite and β-TCP ceramics. *Biomaterials*, **29**(36), 4792-4799.

Liu, X., Ma, P.X. 2004. Polymeric scaffolds for bone tissue engineering. *Annals of biomedical engineering*, **32**(3), 477-486.

Lopez, M.J., McIntosh, K.R., Spencer, N.D., Borneman, J.N., Horswell, R., Anderson, P., Yu, G., Gaschen, L., Gimble, J.M. 2009. Acceleration of spinal fusion using syngeneic and allogeneic adult adipose derived stem cells in a rat model. *Journal of Orthopaedic Research*, **27**(3), 366-373.

Maquet, V., Boccaccini, A.R., Pravata, L., Notingher, I., Jérôme, R. 2004. Porous poly (< i> α</i>-hydroxyacid)/Bioglass< sup>®</sup> composite scaffolds for bone tissue engineering. I: preparation and in vitro characterisation. *Biomaterials*, **25**(18), 4185-4194.

Marra, K.G., Szem, J.W., Kumta, P.N., DiMilla, P.A., Weiss, L.E. 1999. In vitro analysis of biodegradable polymer blend/hydroxyapatite composites for bone tissue engineering. *Journal of Biomedical Materials Research*, **47**(3), 324-335.

Martini, R. 1994. Expression and functional roles of neural cell surface molecules and extracellular matrix components during development and regeneration of peripheral nerves. *Journal of neurocytology*, **23**(1), 1-28.

Mooney, D.J., Baldwin, D.F., Suh, N.P., Vacanti, J.P., Langer, R. 1996. Novel approach to fabricate porous sponges of poly (D, L-lactic-co-glycolic acid) without the use of organic solvents. *Biomaterials*, **17**(14), 1417-1422.

Mooney, M.P., Siegel, M.I. 2005. Animal models for bone tissue engineering. *Encyclopedia of Biomaterials and Biomedical Engineering. New York: Marcel Dekker*, 1-19.

Mozafari, M., Moztarzadeh, F., Rabiee, M., Azami, M., Maleknia, S., Tahriri, M., Moztarzadeh, Z., Nezafati, N. 2010. Development of macroporous nanocomposite scaffolds of gelatin/bioactive glass prepared through layer solvent casting combined with lamination technique for bone tissue engineering. *Ceramics International*, **36**(8), 2431-2439.

Newman, E., Turner, A., Wark, J. 1995. The potential of sheep for the study of osteopenia: current status and comparison with other animal models. *Bone*, **16**(4), S277-S284.

Nonami, T., Tsutsumi, S. 1999. Study of diopside ceramics for biomaterials. *Journal of Materials Science: Materials in Medicine*, **10**(8), 475-479.

Pallua, N., Suscheck, C.V. 2010. *Tissue engineering: from lab to clinic*. Springer Verlag.

Pearce, A., Richards, R., Milz, S., Schneider, E., Pearce, S. 2007. Animal models for implant biomaterial research in bone: a review. *Eur Cell Mater*, **13**(1), 1-10.

Qiu, K., Zhao, X.J., Wan, C.X., Zhao, C.S., Chen, Y.W. 2006. Effect of strontium ions on the growth of ROS17/2.8 cells on porous calcium polyphosphate scaffolds. *Biomaterials*, **27**(8), 1277-1286.

Reichert, J.C., Berner, A., Siamak Saifzadeh, D., Hutmacher, D.W. 2013. Preclinical Animal Models for Segmental Bone Defect Research and Tissue Engineering. in: *Regenerative Medicine*, Springer, pp. 1023-1064.

Rimondini, L., Nicoli-Aldini, N., Fini, M., Guzzardella, G., Tschon, M., Giardino, R. 2005. In vivo experimental study on bone regeneration in critical bone defects using an injectable

biodegradable PLA/PGA copolymer. *Oral Surgery, Oral Medicine, Oral Pathology, Oral Radiology, and Endodontology*, **99**(2), 148-154.

Robinson, K.A., Li, J., Mathison, M., Redkar, A., Cui, J., Chronos, N.A., Matheny, R.G., Badylak, S.F. 2005. Extracellular matrix scaffold for cardiac repair. *Circulation*, **112**(9 suppl), I-135-I-143.

Sabir, M.I., Xu, X., Li, L. 2009. A review on biodegradable polymeric materials for bone tissue engineering applications. *Journal of Materials Science*, **44**(21), 5713-5724.

Sainz, M.A., Pena, P., Serena, S., Caballero, A. 2010. Influence of design on bioactivity of novel CaSiO3-CaMg(SiO3)2 bioceramics: in vitro simulated body fluid test and thermodynamic simulation. *Acta Biomater*, **6**(7), 2797-807.

Schimandle, J.H., Boden, S.D. 1994. Spine update the use of animal models to study spinal fusion. *Spine*, **19**(17), 1998-2006.

Shin, H., Quinten Ruhe, P., Mikos, A.G., Jansen, J.A. 2003. In vivo bone and soft tissue response to injectable, biodegradable oligo (poly (ethylene glycol) fumarate) hydrogels. *Biomaterials*, **24**(19), 3201-3211.

Shorr, E., Carter, A. 1952. The usefulness of strontium as an adjuvant to calcium in the remineralization of the skeleton in man. *Bulletin of the Hospital for Joint Diseases*, **13**(1), 59.

Song, J.J., Ott, H.C. 2011. Organ engineering based on decellularized matrix scaffolds. *Trends in Molecular Medicine*, **17**(8), 424-432.

Stevens, B., Yang, Y., Mohandas, A., Stucker, B., Nguyen, K.T. 2008. A review of materials, fabrication methods, and strategies used to enhance bone regeneration in engineered bone tissues. *Journal of Biomedical Materials Research Part B: Applied Biomaterials*, **85B**(2), 573-582.

Temenoff, J.S., Mikos, A.G. 2000. Injectable biodegradable materials for orthopedic tissue engineering. *Biomaterials*, **21**(23), 2405-2412.

Tian, M., Chen, F., Song, W., Song, Y., Chen, Y., Wan, C., Yu, X., Zhang, X. 2009. In vivo study of porous strontium-doped calcium polyphosphate scaffolds for bone substitute applications. *Journal of Materials Science: Materials in Medicine*, **20**(7), 1505-1512.

Vallet‐Regí, M., Ruiz‐Hernández, E. 2011. Bioceramics: from bone regeneration to cancer nanomedicine. *Advanced Materials*, **23**(44), 5177-5218.

van Gaalen, S., Kruyt, M., Meijer, G., Mistry, A., Mikos, A., van den Beucken, J., Jansen, J., de Groot, K., Cancedda, R., Olivo, C., Yaszemski, M., Dhert, W. 2008. Chapter 19 - Tissue engineering of none. in: *Tissue Engineering*, (Eds.) C. van Blitterswijk, P. Thomsen, A. Lindahl, J. Hubbell, D.F. Williams, R. Cancedda, J.D. de Bruijn, J. Sohier, Academic Press. Burlington, pp. 559-610.

Viateau, V., Guillemin, G., Bousson, V., Oudina, K., Hannouche, D., Sedel, L., Logeart‐Avramoglou, D., Petite, H. 2007. Long‐bone critical‐size defects treated with tissue‐engineered grafts: A study on sheep. *Journal of orthopaedic research*, **25**(6), 741-749.

Wang, C.Z., Chen, S.M., Chen, C.H., Wang, C.K., Wang, G.J., Chang, J.K., Ho, M.L. 2010a. The effect of the local delivery of alendronate on human adipose-derived stem cell-based bone regeneration. *Biomaterials*, **31**(33), 8674-83.

Wang, W., Li, B., Li, Y., Jiang, Y., Ouyang, H., Gao, C. 2010b. In vivo restoration of full-thickness cartilage defects by poly (lactide-co-glycolide) sponges filled with fibrin gel, bone marrow mesenchymal stem cells and DNA complexes. *Biomaterials*, **31**(23), 5953-5965.

Wu, C., Chang, J. 2007. Degradation, bioactivity, and cytocompatibility of diopside, akermanite, and bredigite ceramics. *Journal of Biomedical Materials Research Part B: Applied Biomaterials*, **83B**(1), 153-160.

Xiong, Z., Yan, Y., Wang, S., Zhang, R., Zhang, C. 2002. Fabrication of porous scaffolds for bone tissue engineering via low-temperature deposition. *Scripta Materialia*, **46**(11), 771-776.

Yang, Q., Peng, J., Guo, Q., Huang, J., Zhang, L., Yao, J., Yang, F., Wang, S., Xu, W., Wang, A., Lu, S. 2008. A cartilage ECM-derived 3-D porous acellular matrix scaffold for in vivo cartilage tissue engineering with PKH26-labeled chondrogenic bone marrow-derived mesenchymal stem cells. *Biomaterials*, **29**(15), 2378-2387.

Yoshimoto, H., Shin, Y.M., Terai, H., Vacanti, J.P. 2003. A biodegradable nanofiber scaffold by electrospinning and its potential for bone tissue engineering. *Biomaterials*, **24**(12), 2077-2082.

Yuan, H., De Bruijn, J., Li, Y., Feng, J., Yang, Z., De Groot, K., Zhang, X. 2001. Bone formation induced by calcium phosphate ceramics in soft tissue of dogs: a comparative study between porous α-TCP and β-TCP. *Journal of materials science: materials in medicine*, **12**(1), 7-13.

Zanetti, A.S., Sabliov, C., Gimble, J.M., Hayes, D.J. 2013. Human adipose‐derived stem cells and three‐dimensional scaffold constructs: A review of the biomaterials and models currently used for bone regeneration. *Journal of Biomedical Materials Research Part B: Applied Biomaterials*, **101**(1), 187-199.

Zargarian, S.S., Haddadi-Asl, V. 2010. A nanofibrous composite scaffold of PCL/hydroxyapatite-chitosan/PVA prepared by electrospinning. *Iran Polym J*, **19**, 457-468.

Zhang, M., Liu, C., Sun, J., Zhang, X. 2011. Hydroxyapatite/diopside ceramic composites and their behaviour in simulated body fluid. *Ceramics International*, **37**(6), 2025-2029.

Zhang, M., Liu, C., Zhang, X., Pan, S., Xu, Y. 2010. Al2O3/diopside ceramic composites and their behaviour in simulated body fluid. *Ceramics International*, **36**(8), 2505-2509.

Zreiqat, H., Ramaswamy, Y., Wu, C., Paschalidis, A., Lu, Z.F., James, B., Birke, O., McDonald, M., Little, D., Dunstan, C.R. 2010. The incorporation of strontium and zinc into a calcium-silicon ceramic for bone tissue engineering. *Biomaterials*, **31**(12), 3175-3184.

CHAPTER 2 THIOL-ACRYLATE NANOCOMPOSITE FOAMS FOR CRITICAL SIZE BONE DEFECT REPAIR: A NOVEL BIOMATERIAL[1]

2.1 Introduction

Bone tissue engineering shows promise as an alternative strategy to current surgical techniques to replace or restore the function of traumatized, damaged, or lost bone.(Gaalen et al., 2008; Pallua & Suscheck, 2010a) Over the past several decades, bone grafts have advanced as standard treatment to augment or accelerate bone regeneration.(Pallua & Suscheck, 2010a) Autogenous cancellous bone grafts have long been used to facilitate bone regrowth, although quantity is limited and surgical procedures for graft harvest are required. Allogeneic bone grafts are costly, require time-consuming bone banking procedures, and have high potential for disease transmission. Neither technique provides a clinically convenient method for conformal filling of a critical sized bone defect compared to a proposed injectable biomaterial providing mechanical support and biological cues to support bone regrowth.

To date, a clear trend towards the use of composite scaffolds as an alternative to allogenic or autogenic bone can be observed in many of the current models.(Hwang & Todo, 2012; Liu et al., 2012; Ravichandran et al., 2012; Wu et al., 2012) Native bone is composed of naturally occurring hydroxyapatite (HA) crystals distributed within an organic matrix, with porosity and percent mineralization varying among bone types.(Pallua & Suscheck, 2010b) Synthetic HA has been widely used in bone scaffold fabrication because it possesses osteogenic properties.(Jeon et al., 2012; Ohba et al., 2012) While several of these studies involved the use of extracellular matrix or other natural occurring compounds such as collagen, decellularized bone or chitosan, synthetic polymers can be highly pure, readily reproducible and have adaptable mechanical,

[1]Reprinted with the permission of Journal of Biomedical Materials Research Part A (Appendix A)

chemical, and biological properties to suit specific clinical applications. Much of the research utilizing synthetic polymers in hASC-combined tissue engineering has been focused on hybrid cell/scaffold constructs using degradable polyester polymers such as poly(lactide-co-glycolide) (PLGA), poly(L-lactide) (PLLA), and poly-ε-caprolactone (PCL).

Thiol-ene chemistry possesses many advantageous properties for tissue engineering applications.[2-5] Specifically thiol-acrylate chemistry has already been used in biomedical applications, but has only been explored in photolytically polymerized systems.(Rydholm et al., 2005; Rydholm et al., 2008; Rydholm et al., 2006) Thiol-acrylate polymers synthesized via an amine-catalyzed Michael addition reaction have not been explored for biomedical applications. Scheme 1 displays how the general reaction proceeds by the formation of a catalyst/comonomer molecule through the Michael addition of the secondary diethylamine across the double bond found in acrylate monomers. These activated acrylates were then individually mixed with a thiol comonomer (TMPTMP). This *in situ* tertiary amine catalyzed Michael addition proceeds via a chain "process" due to the sequential chain transfer step after each addition. The Michael addition reaction causes the polymerization to follow the rules and attributes of a step-growth mechanism in terms of molecular weight and physical properties.

In this study, the synthesis and characterization of a novel class of thiol-acrylate copolymers(Bounds et al.) has been reported. The tunable gel times and mechanical properties were determined. A series of biocompatibility tests indicate this new synthetic polymer is capable of supporting human adipose derived stromal cell culture. Furthermore, SEM and micro-CT studies illustrate the morphology of solid and foamed PETA-co-TMPTMP HA composites.

These materials are a potentially transformative class of novel biomaterials with the application for *in situ* conformal polymerization at the site of trauma.

2.2 Materials and Methods

2.2.1 Preparation of thiol-acrylate materials

All chemicals were used as received. Trimethylolpropane triacrylate (TMPTA), poly(ethylene glycol) diacrylate(PEGDA) (MW 700), poly(ethylene glycol) diacrylate (PEGDA) (575), poly-caprolactone(PCL), trimethylolpropane ethoxylate triacrylate (TMPeTA) (MW 912), trimethylolpropane ethoxylate triacrylate (TMPeTA)(MW 692), trimethylolpropane tris(3-mercaptopropianate) (TMPTMP) were obtained from Aldrich. Diethylamine (DEA) was obtained with 99% purity from AGROS organics, and pentaerythritol triacrylate (PETA) was obtained from Alfa Aesar.

Several compositions consisting of TMPTMP with di- or tri-functional acrylates listed above were prepared in a 1:1 functionality ratio. These solutions were subjected to hASC cytotoxicity and mass loss tests that are further explained below. PETA-co-TMPTMP was selected for further experimentation. Twenty stock solutions containing PETA with DEA content ranging from 2.8-35.1% were prepared and subjected to mechanical testing. The 16.1% DEA concentration was chosen not only for its maximum mechanical strength, but also its gel time allowed for an appropriate time range needed for mixing and application of the material.

The preparation of the foamed composite material was prepared by adding 16.1% PETA/DEA stock solution to TMPTMP in a 1:1 molar functionality ratio followed by 3 hours of mixing. HA (20% wt/wt) was added to the PETA-co-TMPTMP solution and cast into cylindrical

molds (10x10mm). The foamed composite copolymer was prepared by pouring the PETA-co-TMPTMP with HA into a 250 mL pressurized spray canister using 7g-compressed nitrous oxide as a gaseous porogen. The foamed composite copolymer was expelled from the canister into the same cylindrical molds used for solid casting. The same foamed procedure was used for the solid copolymer without HA. Another 20% HA foamed sample was prepared *in vitro* by foaming directly into a beaker containing stromal cell medium instead of cylindrical molds to test the impact of physiological solution on polymerization and foam structure.

2.2.2 Mechanical testing

Compression testing was performed on four specimens of each scaffold type with cylindrical geometry of 10 mm × 10 mm at room temperature using a hydraulic universal testing machine (Instron Model 5696, Canton, MA, USA) at an extension rate of 0.5 mm/min to a maximum compression strain of 90%. These scaffold types included foamed PETA-co-TMPTMP with HA(20%), *in vitro* foamed PETA-TMPTMP with HA(20%), foamed PETA-co-TMPTMP without HA, and solid PETA-co-TMPTMP.

2.2.3 hASC isolation and culture

Liposuction aspirates from subcutaneous adipose tissue were obtained from three donors. All tissues were obtained with informed consent under a clinical protocol reviewed and approved by the Institutional Review Board at the Pennington Biomedical Research Center. Isolation of hASC was performed as described elsewhere.(Gimble et al., 2010) The initial passage of the primary cell culture was referred to as “Passage 0” (p0). The cells were passaged after trypsinization and plated at a density of 5,000 cells/cm^2 (‘‘Passage 1’’) for expansion on T125

flasks in order to attain 80%. Passage 2 of each individual was used for cell viability test after acute exposure to the scaffold medium extractives and on scaffolds after loading using a spinner flask.

2.2.4 Mass loss test

Composite copolymer-HA (foam and solid) mass loss as a function of composition was analyzed with PCL foam prepared through thermally induced phase separation(Zanetti et al., Accepted October 4, 2012) serving as a positive control and solid cast PETA composite providing an internal comparison for previous experiments. All samples were normalized to the initial mass before media exposure.

The samples were incubated on an orbital shaker with 5mL stromal media at 37^{o}C and 200rpm/min for 7 days.

2.2.5 Extract cytotoxicity

The extracts from the mass loss test were filtered (0.22 μm pore size) and pipetted (100 μL/well) into a 96-well plate previously sub-cultured with hASC (2,500 cells/well) and incubated in a CO_2 incubator at 37^{o}C containing 5% CO_2 for 24 hours. The cellular viability on scaffold cultures was determined using the Alamar blue assay by adding 10 μL Alamar blue reagent to each well and re-incubated at 37^{o}C in 5% CO_2 for 2 h. The fluorescence was measured at an excitation wavelength of 530 nm and an emission wavelength of 595 nm using a fluorescence plate reader. The tissue culture treated plastic 96-well plate served as a control substrate.

2.2.6 hASC loading on scaffolds and culture

5 μL (1.0×104 cells/μL) of Passage 2 of each donor (n = 3) were pooled and directly loaded on the top of each sample. After 30 min of incubation at 37 ^{o}C and 5% CO_2, the opposite

side of each sample was loaded with the same number of cells by the same approach. Experimental groups included: PETA-co-TMPTMP solid, PETA-co-TMPTMP foam, PETA-co-TMPTMP+HA solid, PETA-co-TMPTMP+HA foam, PCL solid and PCL foam. Scaffolds loaded with hASC were immediately transferred to new 48-well plates and cultured in stromal media (DMEM, 10% FBS, and 1% triple antibiotic solution) for 7 days followed by sample collection to assess cell viability with Alamar blue stain.

2.2.7 In vitro hASC viability on scaffolds with alamar blue stain

The viability of cells within the scaffolds in stromal media was determined after 7 days using an Alamar Blue™ metabolic activity assay. The scaffolds were removed from culture, washed three times in PBS, and incubated with 10% Alamar Blue™ in Hank's balanced salt solution (HBSS) without phenol red (pH 7) for 90 min. Aliquots (100 μL) of Alamar Blue™/HBSS were placed in a 96-well plate in triplicate, and the fluorescence was measured at an excitation wavelength of 530 nm and an emission wavelength of 595 nm using a fluorescence plate reader.

2.2.8 In vitro hASC viability on scaffolds with picogreen

Scaffolds were sectioned using forceps and then incubated with 0.5 mL proteinase K (0.5 mg/mL) at 56ºC overnight. The mixture was centrifuged for 5 minutes at 108g, and 50 μl aliquots of the mixture were mixed with 50 μl Picogreen dye solution (0.1 g/mL, Invitrogen) in 96-well plates. Samples were excited at 480 nm and total DNA concentration was compared to the live control. Scaffold without cells were used to subtract the background fluorescence emission from all readings.

2.2.9 SEM analysis

The solid precast PETA-co-TMPTMP polymer was placed in a 12-well plate to form a thin layer (1mm thickness). The polymers seeded with stem cells were fixed first for 30mins by 2% glutaraldhyde (GA) (made with 2parts Cocadylate, 1part 8% GA and 1 part distilled H_2O). The samples were subjected to a dehydration procedure by using 30-100% ethanol solution increasing by 10% increment every 30 minutes. 100% HDMS (Hexamethyldisilazane) was added to the samples to replace the dried air and ethanol overnight. A conductive platinum coating was applied using EMS550X sputter coater for 2 minutes followed by standard SEM analysis. *In situ* and *in vitro* foamed samples were also subjected to standard SEM analysis.

2.2.10 Micro-CT analysis

Three PETA-co-TMPTMP foams were fabricated with pressurized extrusion foaming as described with the first two foams having 0 and 20%HA content. The third sample also had a 20%HA content, but was foamed into stromal media (*in vitro*). Samples were sliced into 1-2 mm approximate cuboids of 10-15 mm height. Samples were imaged with 11 keV monochromatic x-rays with 2.5 μm/px resolution at the tomography beamline at the Center for Advanced Microstructures and Devices (Louisiana State University, Baton Rouge, LA). Projections numbered 720 corresponding to $\Delta\theta=0.25$; projection exposure time varied between 2 and 4 seconds, but reconstruction algorithms ensure normalized data. The two different datasets are directly comparable, both as an aggregate dataset and as slices. Reconstruction data are 16-bit signed integer with mean air intensity scaled to zero. Pore size was measured using ImageJ 64.

Volume renderings were generated from the three foamed samples 3D data using Avizo 7.0.1 (Visualization Services Group). Two overlapping sub-volumes are rendered

simultaneously, one with a red-orange-white colormap corresponding to trithiol-triacrylate foam, and the other with a blue-green colormap corresponding to hydroxyapatite inclusions. Orthogonal slices were created using ImageJ and have equivalent scale, brightness, contrast, and grey map settings.

2.2.11 Statistical analysis

All results were expressed as mean ± SEM. Normality of the data was confirmed using the Shapiro-Wilk test ($P < 0.001$). Data were analyzed with one or two-way analysis of variance (ANOVA), followed by Tukey's minimum significant difference (MSD) post hoc test for pairwise comparisons of main effects. For all comparisons, a P-value < 0.05 was considered significant.

2.3 Results and Discussion

Thiol-acrylate chemistry incorporates nearly all of the materials used in the synthesis process into one complete network greatly reducing the risks of leaching toxic monomers and short chain oligomers as is observed with other techniques.(Burdick & Anseth, 2002; Nuttelman et al., 2006) Additionally, bioactive compounds such as peptides can be copolymerized as has been demonstrated with photoinitiated thiol-acrylate chemistries.(Salinas & Anseth, 2008) Third, and perhaps most importantly, these materials can rapidly polymerize *in situ* and in an *in vitro* environment through an attached tertiary amine, self-catalyzed "chain" process.

These materials have broadly tunable mechanical and chemical properties in that many compositions of polymer chain repeating units with thiol and acrylate moieties can be created using the same approach and biocompatible reaction scheme. By varying the number of

functional moieties, straight chain, branched and cross-linked compositions can be synthesized. However, for *in situ* polymerization to be practical, gel times must be tunable across a range from minutes to hours, which is easily achievable using this thiol-acrylate system. The strength of these materials can also be manipulated by varying the initial DEA concentration, as the functionality and cross-link density are both a function of the DEA concentration. This is caused by the first Michael addition with the secondary amine, which results in the loss of an acrylate functionality to the trifunctional acrylate. The 16.1% DEA concentration was chosen for further analysis as a potential bone repair composite because it possessed the highest Young's Modulus and could be optimized to have a 15-20 minute gel time while forming a material with suitable flexural strength. PETA was the most attractive acrylate in terms of biocompatibility and mass loss data.

In Figure 2.1, the conversion of Alamar blue by PETA and PETA+HA polymers is statistically the same as the tissue culture treated plastic and PCL control samples and similar to other materials tested. The mass loss over a week of exposure to physiological solution is represented in Figure 2.2.

Both PETA and PETA+HA demonstrated greater stability than other experimental materials tested with similar losses to PCL. Greater physiological stability is considered an asset in the proposed application as bone regeneration time is often on the order of weeks to months.(van Gaalen et al., 2008) PETA containing polymers and composites degraded much more rapidly than PETA, and the stability correlates with the molecular weight of the oligomer.

While not explored in this study these polymers may have utility in other applications, such as wound care, where rapid degradation may be seen as a positive attribute.

Biomimicry of the complex mechanical properties of native tissues proves elusive; native tissue presents unique mechanical properties of nonlinear viscoelasticity and strain-dependent moduli.(Freed et al., 2009)

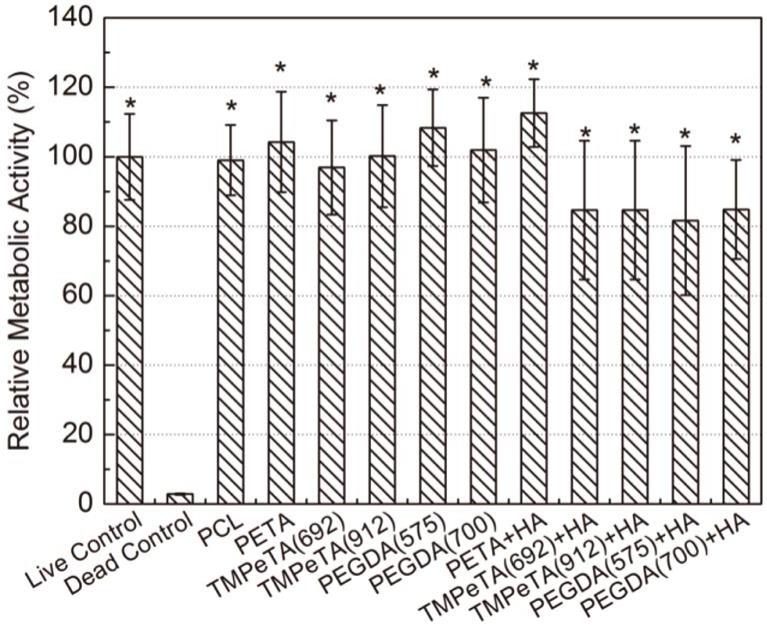

Figure 2.1 Relative metabolic activity of hASC in thiol-acrylate extractives as measured by Alamarblue fluorescent conversion. Relative fluorescent units have been normalized to live control. Asterisk indicates the sample is significantly different from dead control

The compressive strength of human cortical and cancellous bone are 130-180 MPa and 4-12 MPa, respectively.(Rezwan et al., 2006) The mechanical testing of solid/foam PETA-co-TMPTMP materials is shown in Figure 2.3.

Additionally, it was found that the maximal compressive strength of this PETA-co-TMPTMP+HA polymer at 90% strain is 19.23 ± 1.39 MPa while the pure PETA-co-TMPTMP

polymer is 7.71 ± 0.09 MPa. This result indicated that the introduction of ceramics improves the mechanical strength of the PETA copolymer similar to previously published results.(Hong et al., 2008; Reynaud et al., 2001) The compressive strength of PETA-co-TMPTMP+HA foam is 0.72 ± 0.07MPa while the pure PETA-co-TMPTMP foam is 0.14 ± 0.02MPa.

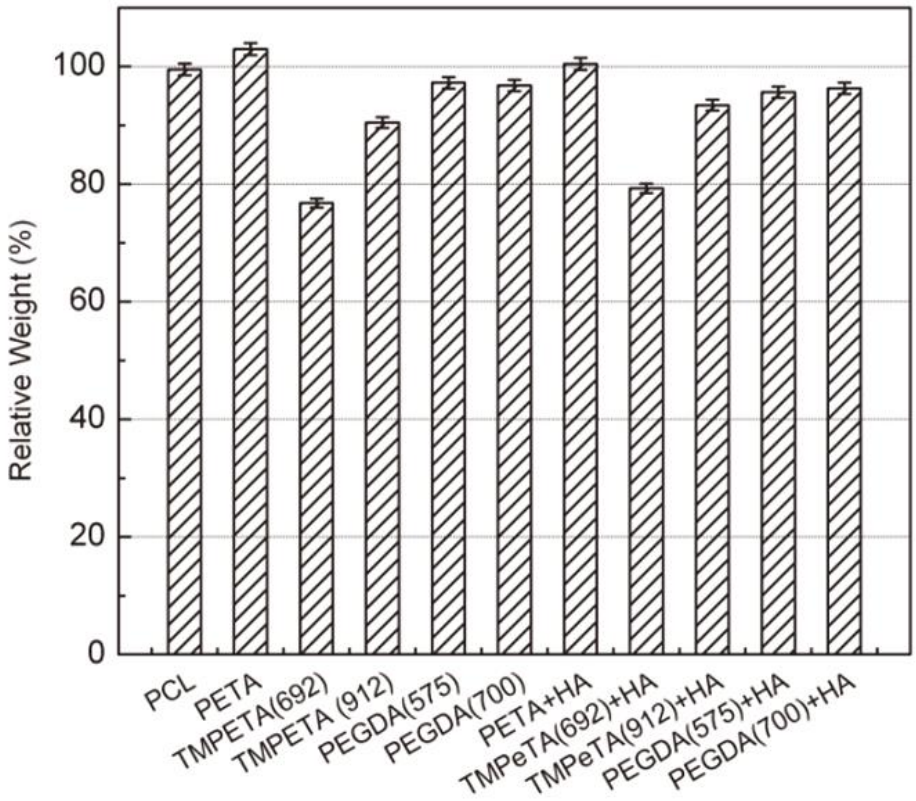

Figure 2.2 Mass loss after 7 days of incubation in stromal media. Samples are normalized to the starting mass for each sample

The foamed polymer has decreased mechanical strength compared to the solid polymer due to the large porosity. The mechanical properties of the copolymer polymerized *in vitro*, 0.84 ± 0.05 MPa, and *in situ*, 0.85 ± 0.06 MPa, in physiological media were very similar, indicating the presence of aqueous physiological media during the polymerization and foam structure formation has little impact on morphology and mechanical properties.

2.3.1 Mass balance

The polymer samples were extracted for 7 days in the stromal medium in order to determine the extent of mass loss.

These extracts were later used in cytotoxicity testing. The copolymer-HA composite foam and solid cast copolymer were found to have significantly greater mass loss than the PCL control foam.

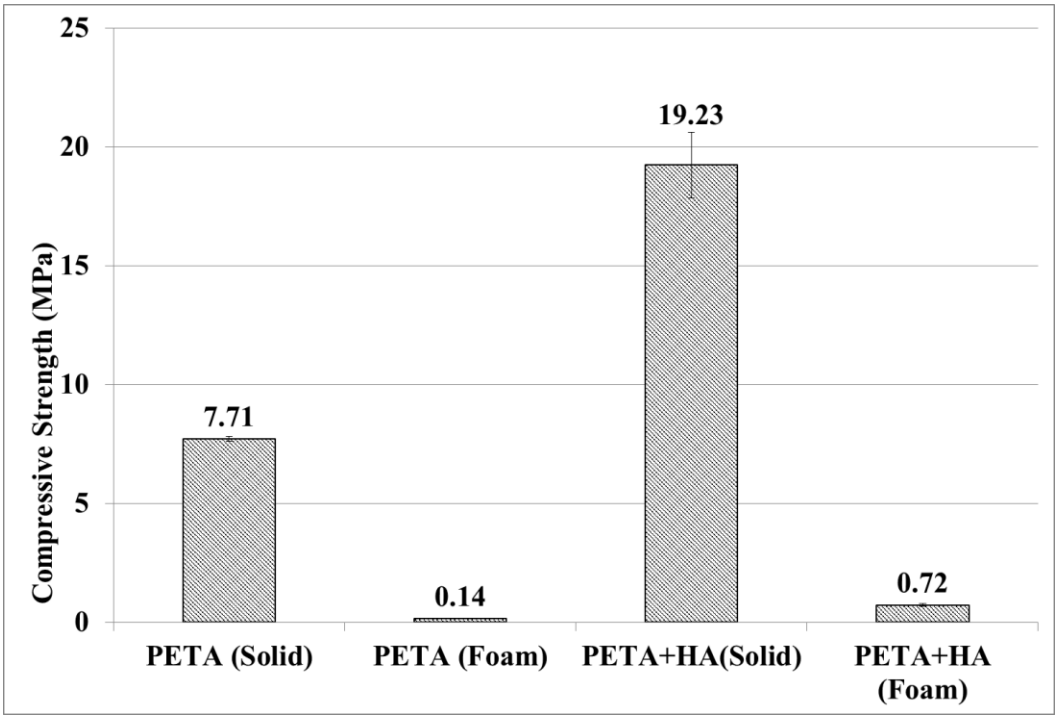

Figure 2.3 Compressive strength tested using hydraulic universal testing machine at an extension rate of 0.5mm/min to a maximum compression strain of 90%.

The mass loss is believed to occur as a result of hydrolytic chain scission in a manner similar to the degradation of PCL in physiological solutions.(Pitt et al., 1981) The PCL sample increased in mass likely as a result of mineralization or non-specific protein deposition (Figure 2.4). Similarly to PLLA and PGA, the degradation of PCL occurs by bulk or surface hydrolysis of

ester linkages resulting in a byproduct of caproic acid.(Ahn et al., 2009) At high concentrations of these degradation products, local tissue acidity may increase, resulting in adverse responses such as inflammation or fibrous encapsulation.(van Gaalen et al., 2008)

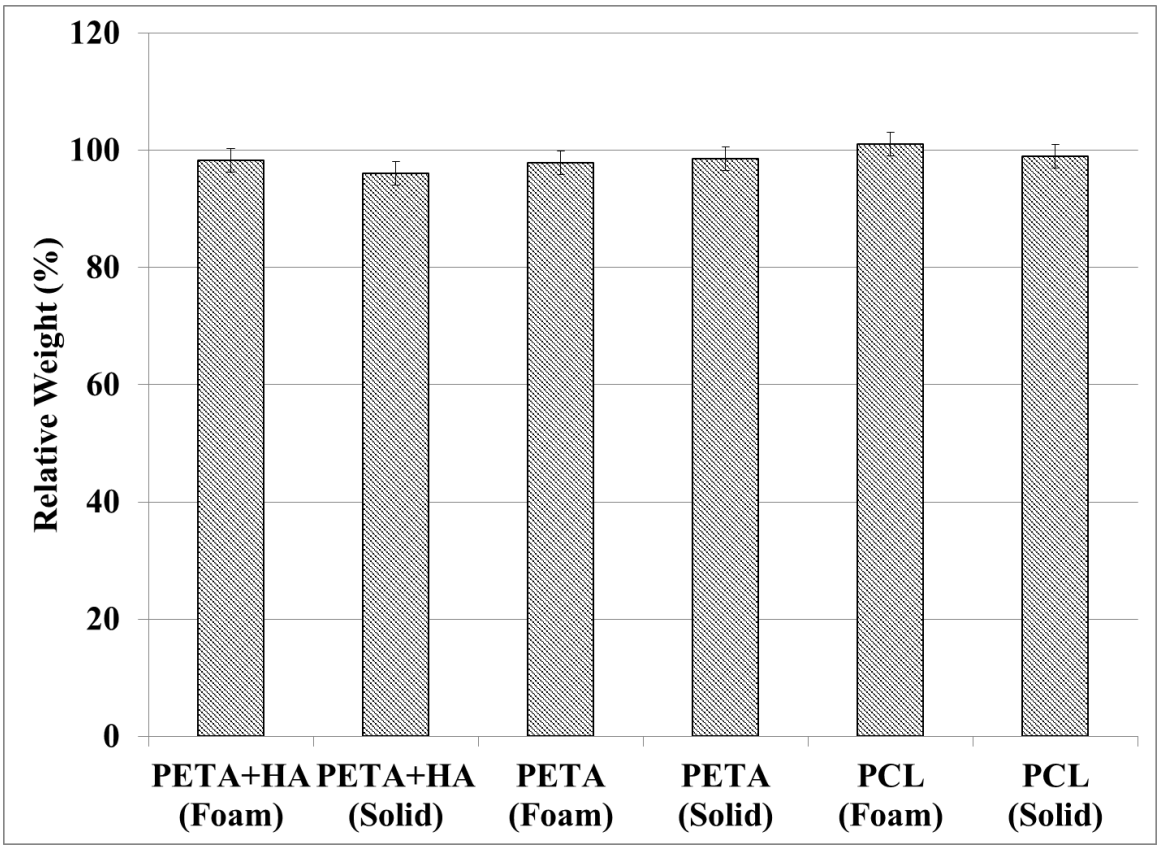

Figure 2.4 Mass loss of foamed samples after 7 days of incubation in stromal media. Samples are normalized to the staring mass of each sample.

2.3.2 Cytotoxicity test

PCL foam was fabricated by thermally induced phase separation from 1,4-dioxane followed by lyophilization.(Zanetti et al., Accepted October 4, 2012) Tissue culture treated polystyrene served as a positive control, while ethanol treated hASC served as a negative control. Cells

exposed to both the copolymer and copolymer+HA composite (solid and foam) extracts had significantly higher metabolic activity than the dead control or cells exposed to the PCL extract (Figure 2.5A). The reduction of hASC metabolic activity cultured on PCL does not correlate with a significant mass loss (Figure 2.4), indicating that this reduction in activity is likely not related to the generation of acidic PCL degradation products.

2.2.3 Biocompatibility test of hASC cells on the polymer

The ability of the PETA-co-TMPTMP polymer to support hASC cell adhesion and short-term culture was evaluated using Alamar blue metabolic activity assays and SEM to examine cell morphology. Cells were cultured on solid cast PETA and PETA-HA (20% wt/wt) composite samples for 4 days in stromal media and assayed for fluorescent Alamar blue conversion; styrene treated tissue culture plates served as a positive control. Compared to the positive control, hASC cultured on both the copolymer and the copolymer-HA composite had significantly lower metabolic activity (Figure 2.5B). Additionally, it appears that cells cultured on the copolymer-HA composite have significantly lower metabolic activity than cells on the non-composite. This may be a result of reduced metabolic activity associated with the differentiation of stem cells exposed to HA, a known osteogenic compound, and may not be indicative of reduced biocompatibility.(Rydholm et al., 2005) Based on Figure 2.5C, PETA foam demonstrates a relatively higher metabolic activity than solid PETA-HA composite and PCL foam, but significantly lower metabolic activity than cells on tissue cultured treated styrene. Although the foam PETA copolymer has a much larger surface area than solid PETA copolymer, the results

indicated that both forms of PETA copolymer supports hASC growth around the same level compared to the positive control.

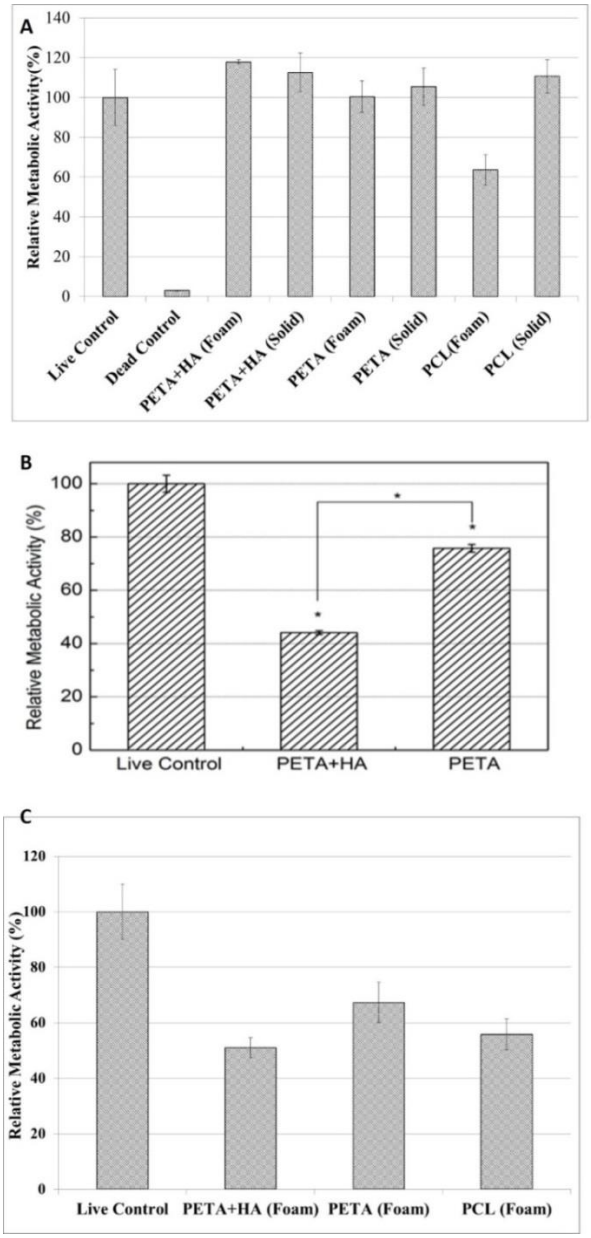

Figure 2.5 Relative metabolic activity of hASC as determined by Alamarblue conversion. Asterisks indicate the sample is significantly different from live control. The results are normalized to the live control. A: Exposure to 7 day stromal media extracts from PETA, PETA-HA, and PCL foams and solids. B: Cultured on solid cast PETA and PETAHA composites. C: hASC cultured on foamed PETA and PETA-HA composites.

2.2.4 DNA quantification on scaffolds (Picogreen assay)

DNA content of hASC cultured on all pure PETA, PETA composite, and PCL scaffolds was compared as a relative measure of cell viability and proliferation. After 4 days, the highest DNA content was observed in the PETA (20% HA) scaffold, 66.7% of the TCP control. The relative DNA content of the pure PETA and PCL scaffolds are approximately 56% and 65% of the live control respectively (Figure 2.6). The DNA content from cells cultured on all experimental samples are similar indicating that the total number of cells does not vary significantly with composition. This result is in contrast to the metabolic activity results (Figure 2.5a), which indicate a significantly reduced metabolic activity for cells grown on composite PETA/HA samples. This further supports the hypothesis that these cells on PETA/HA are likely in a reduced metabolic state as a result of early stage osteogenic differentiation.(Liu et al., 2008b)

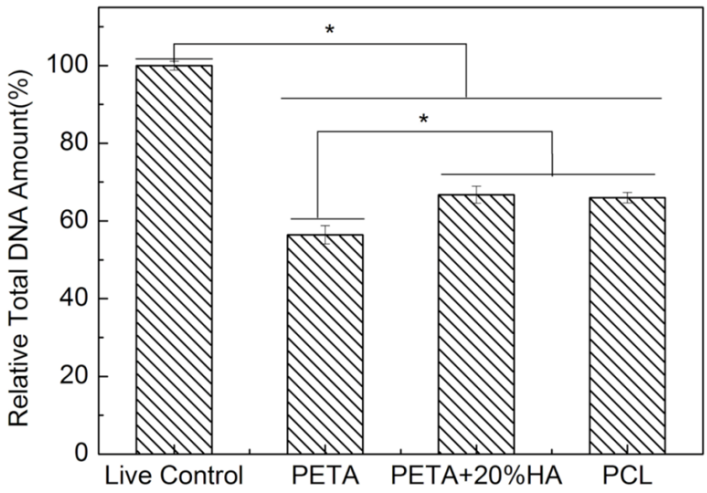

Figure 2.6 Relative total DNA amount as determined by picogreen assay for hASC cultured on foamed PETA and PETA-HA composites. The results are normalized to the live control. Asterisks indicate significant difference among the samples

2.2.5 SEM analysis.

The PETA-co-TMPTMP foam materials were found to have a largely closed celled structure with a pore size ranging from ~200-300 μm (Figure 2.7 right).

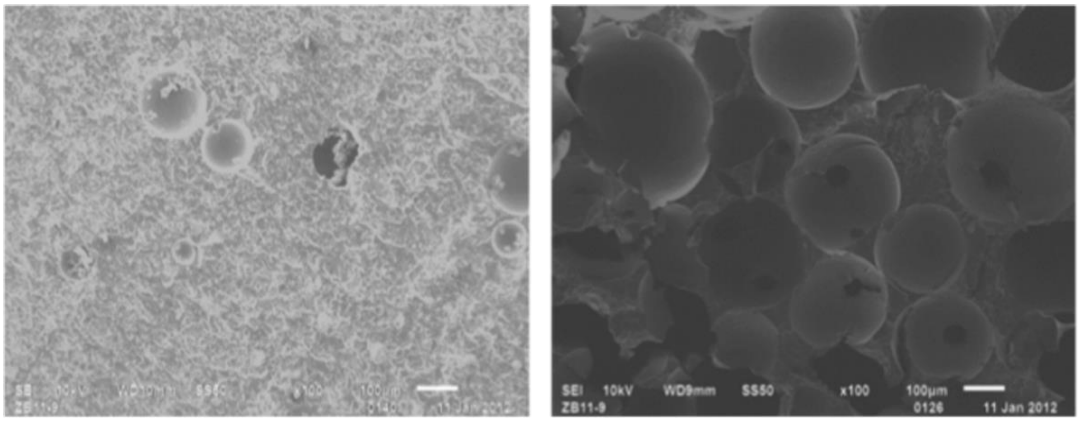

Figure 2.7 SEM image of PETA polymers in solid (left) and foamed (right) forms. Magnification is ×100 with scale bars of 100μm

A comparative image of the cast solid copolymer of the same composition can be seen in the left panel of Figure 2.7. The bubbles in the solid sample (Figure 2.7 left) are likely a result of air introduced during the mixing procedure.

The size of the pores found in the foamed sample fall within the range of pores found in native cancellous bone.(Hulbert et al., 1970) hASC morphology analysis was performed after culturing the human ASC cultured for 7 days on the solid cast PETA films.

The cells were fixed and imaged by SEM in an effort to evaluate the morphology of hASC on the thiol-acrylate copolymer.

From these images, it appears that hASC adhere well and take on the expected spindle shaped morphology during culture on the thiol-acrylate copolymer films (Figure 2.8).

It is likely the thiol groups impart a negative charge to the PETA co-polymer, potentially increasing the adhesion, spreading, and proliferation of hASC cells on these surfaces compared to neutral surfaces.(Kumar et al., 2010; Schneider et al., 2004)

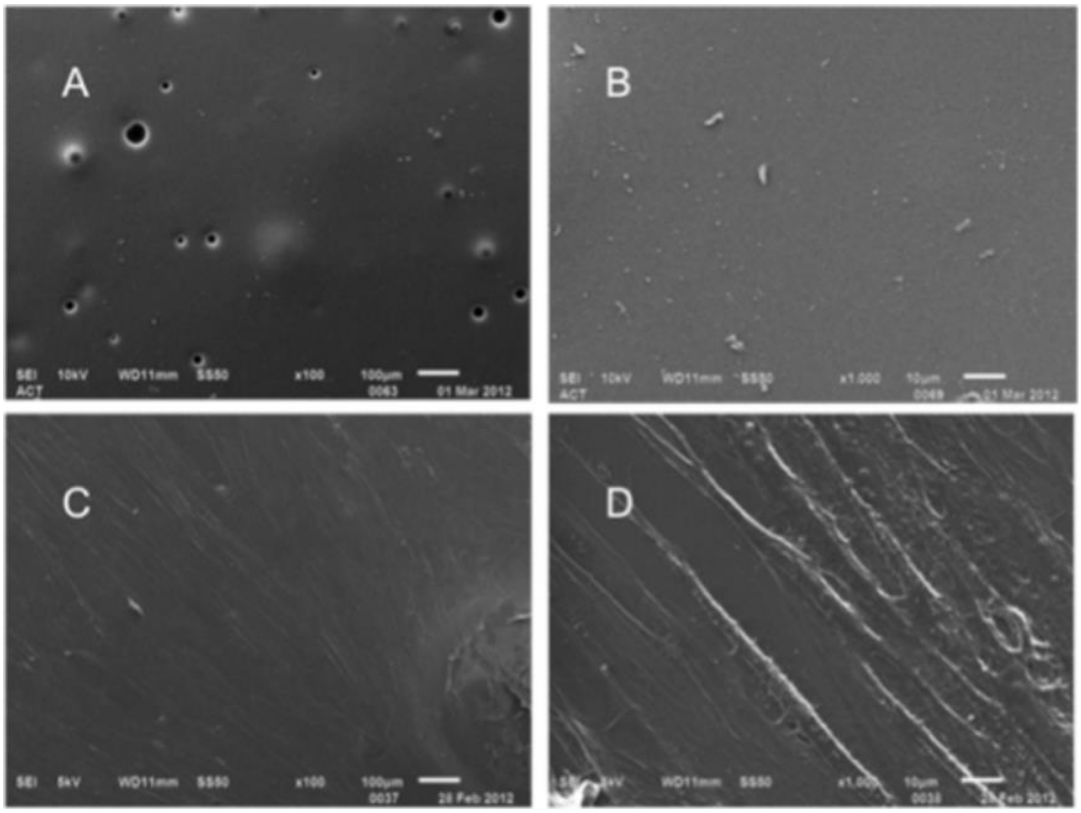

Figure 2.8 SEM images of PETA solid cast polymer films (A&B) and hASC after culture for 7 days on PETA films. Magnification is ×100 (A&C) and×1000 (B&D), scale bars are 100 and 10µm, respectively.

At lower magnification (100×) (Figure 2.8C) a confluent cell population is seen spreading more or less uniformly across the surface, while at higher magnification (1000×) the aligned spindle shaped morphology of individual cells can be clearly seen (Figure 2.8D). Cell free controls (Figure 2.8A&B) are included in this image for comparison. SEM analysis indicates that there is no substantial difference between the *in vitro* and *in situ* (20%HA) foamed samples in terms of porosity and morphology **(**Figure 2.9A-D**)**.

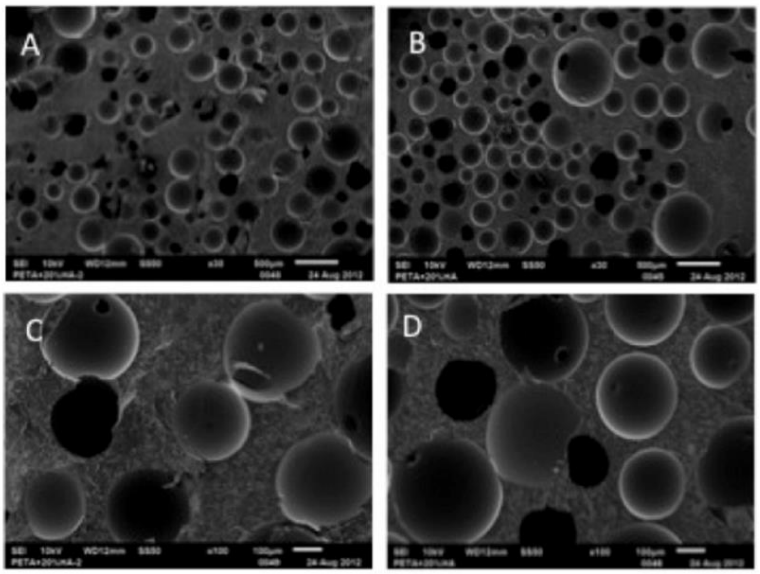

Figure 2.9 SEM images of in vitro PETA-co-TMPMP þ HA foam (A&C) and in situ PETA-co-TMPTMP+ HA foam (B&D). Magnification is ×100 (A&B) and×1000 (C&D), scale bars are 100 and 10 µm, respectively.

2.2.6 Micro-CT analysis

Micro-CT image data (Figure 2.10A-C) show good contrast between HA and polymer, confirming suitability of micro-CT as an appropriate study the HA distribution and pore morphology.

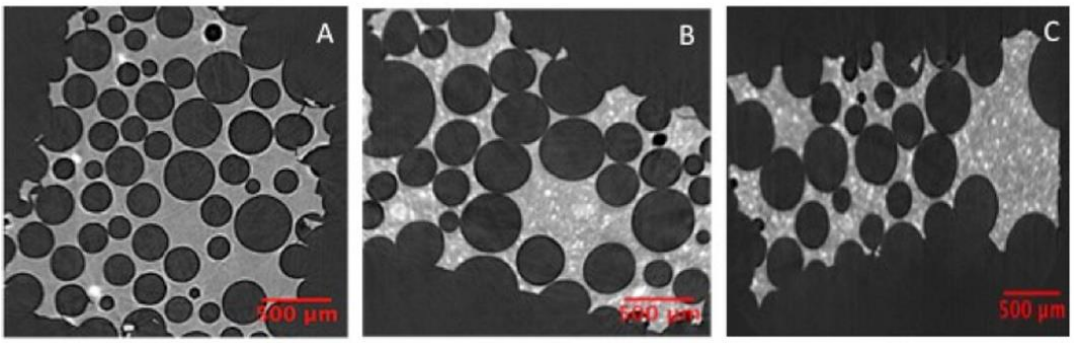

Figure 2.10 Micro Ct obtained orthogonal slices analyzed using Image J. Foamed PETA-co-TMPMP with 0% HA (A), and in situ PETA-co-TMPTMP foam (B), in vitro PETA-co-TMPMP foam (C) are all shown to have pore sizes ranging from 100 to 800 µm. The scale bar is 500 µm.

Volume renderings (Figure 2.11A) were generated from PETA-co-TMPTMP foam 3D data using Avizo 7.0.1 (Visualization Services Group).

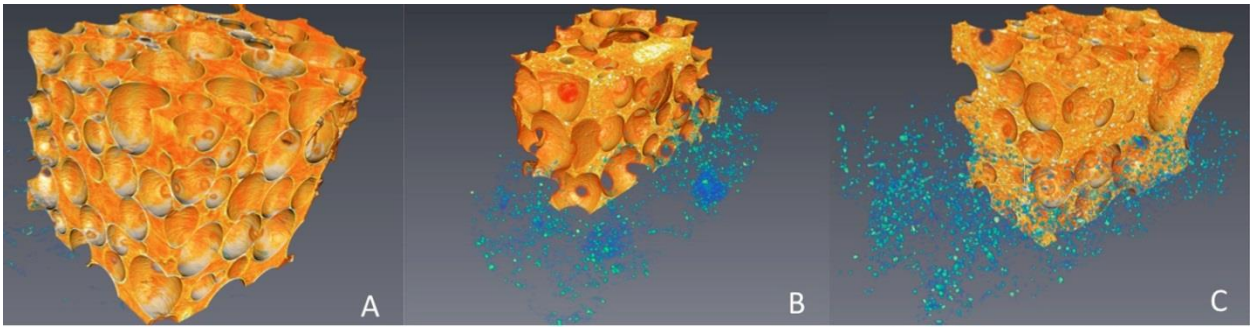

Figure 2.11 Micro Ct obtained 3D data with two overlapping subvolumes rendered simultaneously. Red–orange–white colormap corresponds to the PETA-co-TMPTMP foam, and the blue–green corresponds to HA inclusions. A: 0% HA foamed. B: In situ foamed 20% HA. C: In vitro foamed 20% HA.

Figures 2.11B (*in situ*) and Figure 2.11C (*in vitro*) were generated from PETA-co-TMPTMP with 20%HA foam 3D data. Two overlapping sub-volumes are rendered simultaneously, one with a red-orange-white colormap corresponding to thiol-acrylate foam, and the other with a blue-green colormap corresponding to hydroxyapatite inclusions.

Volume renderings indicate open-cell foam and interconnectivity. By providing an interconnected pore structure the support of cell migration, differentiation, nutrient support (Di Maggio et al., 2011; Lawrence & Madihally, 2008) and in some cases, the formation of blood vessels (Mehrkens et al., 2009; Papadimitropoulos et al., 2011; Scherberich et al., 2007) can be established. HA inclusions with the size of 10-50 microns were aggregated showing that a higher torque and speed of the stirrer are needed to achieve better homogeneity. Measurements using NIH ImageJ from these datasets indicate pores ranging from 100-500 microns for control (0% HA) and 20% HA having 125-800 microns.

2.3 Conclusion

The step growth nature of the amine catalyzed Michael addition reaction alleviated the concern of unreacted monomer or radicals leaching into the body as would typically occur using a chain-growth mechanism involving a free-radical process. *In situ* polymerization opens the opportunity for the development of absorbable foams for the conformal repair of critical sized tissue defects, which can be easily delivered in the clinical surgical setting. This represents a substantial improvement over PCL, which are foamed externally prior to surgical insertion, and methylmethacrylate bone cements, which are largely inert, non-porous, and permanent. The SEM analysis, mechanical testing, and micro CT data prove that there is no distinct difference between the PETA-co-TMPTMP foam made *in situ* and *in vitro*. While this material has many advantages, future work includes the development of a homogenous HA containing polymer network, osteogenic studies and improved mechanical strength of the foamed PETA-co-TMPTMP with varying HA amounts. It is clear that scaffold technology plays a critical role in the success of the current stem cell based bone tissue engineering paradigms. While a variety of different materials, both ceramics and polymers, have been tested in combination with hASC, Lendeckel et al. and others note that composite scaffolds may offer a better clinical outcome as a result of improved mechanical and biological properties.(Lendeckel et al., 2004) Calcium phosphate nanoscale ceramic particles of HA and β-TCP will be used as the inorganic osteogenic phase and thixotropic agent in future studies.

2.4 References

Ahn, H.H., Kim, K.S., Lee, J.H., Lee, J.Y., Kim, B.S., Lee, I.W., Chun, H.J., Kim, J.H., Lee, H.B., Kim, M.S. 2009. In vivo osteogenic differentiation of human adipose-derived stem

cells in an injectable in situ-forming gel scaffold. *Tissue engineering. Part A*, **15**(7), 1821-32.

Bounds, C.O., Goetter, R., Pojman, J.A., Vandersall, M. Preparation and application of microparticles prepared via the primary amine-catalyzed michael addition of a trithiol to a triacrylate. *Journal of Polymer Science Part A: Polymer Chemistry*, **50**(3), 409-422.

Burdick, J.A., Anseth, K.S. 2002. Photoencapsulation of osteoblasts in injectable RGD-modified PEG hydrogels for bone tissue engineering. *Biomaterials*, **23**(22), 4315-4323.

Di Maggio, N., Piccinini, E., Jaworski, M., Trumpp, A., Wendt, D.J., Martin, I. 2011. Toward modeling the bone marrow niche using scaffold-based 3D culture systems. *Biomaterials*, **32**(2), 321-9.

Freed, L.E., Engelmayr, G.C., Borenstein, J.T., Moutos, F.T., Guilak, F. 2009. Advanced Material Strategies for Tissue Engineering Scaffolds. *Advanced Materials*, **21**(32-33), 3410-3418.

Gaalen, S.v., Kruyt, M., Meijer, G., Mistry, A., Mikos, A., Beucken, J.v.d., Jansen, J., Groot, K.d., Cancedda, R., Olivo, C., Yaszemski, M., Dhert, W. 2008. Chapter 19 - Tissue engineering of bone. in: *Tissue Engineering*, (Eds.) B. Clemens van, T. Peter, L. Anders, H. Jeffrey, F.W. David, C. Ranieri, D.d.B. Joost, P.T.A.L.J.H.D.F.W.R.C.J.D.d.B. Jerome Sohier - Clemens van Blitterswijk, S. Jerome, Academic Press. Burlington, pp. 559-610.

Gimble, J.M., Guilak, F., Bunnell, B.A. 2010. Clinical and preclinical translation of cell-based therapies using adipose tissue-derived cells. *Stem Cell Research & Therapy*, **1**.

Hong, Z., Reis, R.L., Mano, J.o.F. 2008. Preparation and in vitro characterization of scaffolds of poly(l-lactic acid) containing bioactive glass ceramic nanoparticles. *Acta Biomaterialia*, **4**(5), 1297-1306.

Hulbert, S.F., Young, F.A., Mathews, R.S., Klawitter, J.J., Talbert, C.D., Stelling, F.H. 1970. Potential of ceramic materials as permanently implantable skeletal prostheses. *Journal of Biomedical Materials Research*, **4**(3), 433-456.

Hwang, S., Todo, M. 2012. Characterization of compressive deformation behavior of multi-layer porous composite materials for articular tissue engineering. *Journal of Mechanical Science and Technology*, **26**(7), 1999-2004.

Jeon, B.J., Jeong, S.Y., Koo, A.N., Kim, B.C., Hwang, Y.S., Lee, S.C. 2012. Fabrication of porous PLGA microspheres with BMP-2 releasing polyphosphate-functionalized nano-hydroxyapatite for enhanced bone regeneration. *Macromolecular Research*, **20**(7), 715-724.

Kumar, D., Gittings, J.P., Turner, I.G., Bowen, C.R., Bastida-Hidalgo, A., Cartmell, S.H. 2010. Polarization of hydroxyapatite: Influence on osteoblast cell proliferation. *Acta Biomaterialia*, **6**(4), 1549-1554.

Lawrence, B.J., Madihally, S.V. 2008. Cell colonization in degradable 3D porous matrices. *Cell Adhesion & Migration*, **2**(1), 9-16.

Lendeckel, S., Jodicke, A., Christophis, P., Heidinger, K., Wolff, J., Fraser, J.K., Hedrick, M.H., Berthold, L., Howaldt, H.-P. 2004. Autologous stem cells (adipose) and fibrin glue used to treat widespread traumatic calvarial defects: case report. *Journal of Cranio-Maxillofacial Surgery*, **32**(6), 370-373.

Liu, L., Wang, Y.Y., Guo, S.R., Wang, Z.Y., Wang, W. 2012. Porous polycaprolactone/nanohydroxyapatite tissue engineering scaffolds fabricated by combining NaCl and PEG as co-porogens: Structure, property, and chondrocyte-scaffold interaction in vitro. *Journal of Biomedical Materials Research Part B-Applied Biomaterials*, **100B**(4), 956-966.

Liu, Q., Cen, L., Yin, S., Chen, L., Liu, G., Chang, J., Cui, L. 2008. A comparative study of proliferation and osteogenic differentiation of adipose-derived stem cells on akermanite and β-TCP ceramics. *Biomaterials*, **29**(36), 4792-4799.

Mehrkens, A., Muller, A.M., Schafer, D., Jakob, M., Martin, I., Scherberich, A. 2009. Towards an intraoperative engineering of osteogenic grafts from the stromal vascular fraction of human adipose tissue. *Swiss Medical Weekly*, **139**(23-24), 23S-23S.

Nuttelman, C.R., Benoit, D.S.W., Tripodi, M.C., Anseth, K.S. 2006. The effect of ethylene glycol methacrylate phosphate in PEG hydrogels on mineralization and viability of encapsulated hMSCs. *Biomaterials*, **27**(8), 1377-1386.

Ohba, S., Wang, W., Itoh, S., Takagi, Y., Nagai, A., Yamashita, K. 2012. Acceleration of new bone formation by an electrically polarized hydroxyapatite microgranule/platelet-rich plasma composite. *Acta Biomaterialia*, **8**(7), 2778-2787.

Pallua, N., Suscheck, C.V. 2010a. *Tissue engineering: from lab to clinic*. Springer Verlag.

Pallua, N., Suscheck, C.V. 2010b. *Tissue Enginnering: from lab to clinic*. Springer Verlag.

Papadimitropoulos, A., Scherberich, A., Guven, S., Theilgaard, N., Crooijmans, H.J., Santini, F., Scheffler, K., Zallone, A., Martin, I. 2011. A 3D in vitro bone organ model using human progenitor cells. *Eur Cell Mater*, **21**, 445-58.

Pitt, C.G., Gratzl, M.M., Kimmel, G.L., Surles, J., Schindler, A. 1981. Aliphatic polyesters II. The degradation of poly (DL-lactide), poly (epsilon-caprolactone), and their copolymers in vivo. *Biomaterials*, **2**(4), 215-20.

Ravichandran, R., Venugopal, J.R., Sundarrajan, S., Mukherjee, S., Sridhar, R., Ramakrishna, S. 2012. Composite poly-L-lactic acid/poly-(alpha,beta)-DL-aspartic acid/collagen nanofibrous scaffolds for dermal tissue regeneration. *Materials Science & Engineering C-Materials for Biological Applications*, **32**(6), 1443-1451.

Reynaud, E., Jouen, T., Gauthier, C., Vigier, G., Varlet, J. 2001. Nanofillers in polymeric matrix: a study on silica reinforced PA6. *Polymer*, **42**(21), 8759-8768.

Rezwan, K., Chen, Q.Z., Blaker, J.J., Boccaccini, A.R. 2006. Biodegradable and bioactive porous polymer/inorganic composite scaffolds for bone tissue engineering. *Biomaterials*, **27**(18), 3413-3431.

Rydholm, A.E., Bowman, C.N., Anseth, K.S. 2005. Degradable thiol-acrylate photopolymers: polymerization and degradation behavior of an in situ forming biomaterial. *Biomaterials*, **26**(22), 4495-4506.

Rydholm, A.E., Held, N.L., Benoit, D.S.W., Bowman, C.N., Anseth, K.S. 2008. Modifying network chemistry in thiol-acrylate photopolymers through postpolymerization functionalization to control cell-material interactions. *Journal of Biomedical Materials Research Part A*, **86A**(1), 23-30.

Rydholm, A.E., Reddy, S.K., Anseth, K.S., Bowman, C.N. 2006. Controlling network structure in degradable thiol-acrylate biomaterials to tune mass loss behavior. *Biomacromolecules*, **7**(10), 2827-2836.

Salinas, C.N., Anseth, K.S. 2008. Mixed mode thiol-acrylate photopolymerizations for the synthesis of PEG-peptide hydrogels. *Macromolecules*, **41**(16), 6019-6026.

Scherberich, A., Galli, R., Jaquiery, C., Farhadi, J., Martin, I. 2007. Three-dimensional perfusion culture of human adipose tissue-derived endothelial and osteoblastic progenitors generates osteogenic constructs with intrinsic vascularization capacity. *Stem cells*, **25**(7), 1823-9.

Schneider, G.B., English, A., Abraham, M., Zaharias, R., Stanford, C., Keller, J. 2004. The effect of hydrogel charge density on cell attachment. *Biomaterials*, **25**(15), 3023-3028.

van Gaalen, S., Kruyt, M., Meijer, G., Mistry, A., Mikos, A., van den Beucken, J., Jansen, J., de Groot, K., Cancedda, R., Olivo, C., Yaszemski, M., Dhert, W. 2008. Chapter 19 - Tissue engineering of none. in: *Tissue Engineering*, (Eds.) C. van Blitterswijk, P. Thomsen, A. Lindahl, J. Hubbell, D.F. Williams, R. Cancedda, J.D. de Bruijn, J. Sohier, Academic Press. Burlington, pp. 559-610.

Wu, F., Wei, J., Liu, C.S., O'Neill, B., Ngothai, Y. 2012. Fabrication and properties of porous scaffold of zein/PCL biocomposite for bone tissue engineering. *Composites Part B-Engineering*, **43**(5), 2192-2197.

Zanetti, A.S., McCandless, G.T., Chan, J.Y., Gimble, J.M., Hayes, D.J. Accepted October 4, 2012. Characterization of novel akermanite:poly-ε-caprolactone scaffolds for human adipose-derived stem cells bone tissue engineering. *Journal of Tissue Engineering and Regenerative Medicine*.

CHAPTER 3 *IN VITRO* AND *IN VIVO* CHARACTERIZATION OF PENTAERYTHRITOL TRIACRYLATE-CO-TRIMETHYLOLPROPANE NANOCOMPOSITE SCAFFOLDS AS POTENTIAL BONE AUGMENTS AND GRAFTS[2]

3.1. Introduction

For the past several decades, the standard treatment to augment or accelerate bone regeneration has been the implantation of bone grafts. (Pallua & Suscheck, 2010a) Allogeneic bone grafts are costly, require time-consuming bone banking procedures, and have the potential for disease transmission. Autogenous bone grafts have long been used as bone replacements but require additional surgeries, which increase the risk of donor site morbidity and the burden on health care providers. (Ahlmann et al., 2002) Moreover, these techniques do not address the need for a clinically convenient and biodegradable method for conformally filling a critical sized bone defect while providing mechanical support and biological cues necessary to promote bone regrowth. Artificial composite scaffolds, whether bioderived, synthetic or hybrids, while studied extensively as alternatives for bone grafting and augmentation, have yet to see wide clinical adoption. (Zanetti et al., 2013b) Composite structures with calcium phosphates and magnesium silicates composing the bioactive ceramic portion, have been studied thoroughly to improve both the mechanical and osteogenic properties of scaffolds but an *in situ* polymerizing biodegradable bone augment or graft with biomimetic morphology and mechanical properties remains elusive. (Bohner, 2010; Hutmacher, 2000; Zanetti et al., 2013b) An initial study conducted by our group demonstrated the formation of a porous interconnected scaffold derived from the product of an amine-catalyzed Michael addition polymerization reaction.(Garber et al., 2013a) This thiol-acrylate reaction proceeds through a non-radical, step-growth process initiated

[2]Reprinted with the permission of Tissue Engineering Part A (Appendix B)

by an amine/acrylate co-monomer which is consumed in the reaction and incorporated into the growing polymer. Porous composite scaffolds made with this system were found to support human mesenchymal stromal/stem cell growth and to possess similar mechanical properties to cortical bone. (Sundelacruz & Kaplan, 2009)

The fabrication method of a scaffold can have a substantial impact on mechanical properties and bio-functionality by controlling porosity and interconnectivity. These factors influence cell attachment, proliferation, extracellular matrix production, and the transport of nutrients and wastes. (Degasne et al., 1999; Karageorgiou & Kaplan, 2005; Levine, 2008; Singh et al., 2009; Zanetti et al., 2012b) Solid freeform fabrication, thermal precipitation, gas foaming, and solvent casting followed by particulate leaching are the common approaches for making porous scaffolds for bone repair. (Karageorgiou & Kaplan, 2005; Levine, 2008) Except for gas foaming, these methods are not readily applicable to thermoset polymers due to their cross-linking densities and viscoelastic properties. Gas porogens and foaming apparatuses have the potential to be readily adapted to filling conformal defects in a clinical environment, similar to other surgical devices in use, such as fibrin sealant (Topart et al., 2005; Yeh & Tucker, 2005) and bone putty. (Gertzman & Sunwoo, 2000)

Herein we report on the *in vitro* characterization of the mechanical and osteoinductive properties of a gas foamed nanocomposite scaffold consisting of a thiol-acrylate copolymer with nanoscale hydroxyapatite (HA) inclusions. Scaffolds were prepared using a gas phase propellant and foaming agent to investigate the relationship of scaffold composition to morphology, mechanical properties, cytocompatibility, and osteogenic properties. The impact of varying HA

concentration in the PETA polymer on morphology is illustrated using SEM and micro-CT imaging. Mechanical testing was conducted to determine the compressive yield strength and modulus of the material. To evaluate cytocompatibility and osteogenic activity, human adipose derived mesenchymal stromal cells (hASC) were used as a model cell type. Metabolic activity, DNA content, calcium deposition, and the expression of the osteogenic markers alkaline phosphatase (*ALP*) and osteocalcin (*OCN*) were quantified with respect to scaffold composition. A six-week *in vivo* study was also conducted to assess the basic biocompatibility of the foamed composite and the feasibility of *in situ* foaming for a boney fusion model.

3.2 Materials and Methods

3.2.1 Preparation of thiol-acrylate materials

All chemicals were used as received: Trimethylolpropane tris(3-mercaptopropionate) (TMPTMP) was obtained from Aldrich, diethylamine (99% purity) (DEA) from AGROS organics, and pentaerythritol triacrylate from Alfa Aesar.

Scaffolds were prepared by formulating PETA with 16.1% DEA and adding TMPTMP in a 1:1 molar functionality ratio, followed by mixing with a stir rod for 3 hours as previously described.(Garber et al., 2013a) Several concentrations of copolymer PETA with HA were studied, the first number in the abbreviation connotes the polymer content while the second number provides the amount of HA found in the composite as a wt/wt percentage (100:0, 85:15, 80:20, 75:25). The mixtures were cast into cylindrical molds (5×10 mm) to form a solid scaffold. The foamed composite copolymer was prepared by pouring the PETA and HA (150 g in total)

into a 250 mL pressurized canister using 7 g-compressed nitrous oxide as a gas foaming agent. The foamed composite copolymer was expelled into the same cylindrical molds used for solid casting.

3.2.2 Mechanical testing

Solid and foamed scaffolds, molded to 6mm (diameter)×12mm(height) cylinder shape, were tested to determine maximal compressive strength and modulus. All scaffolds, solid, gas foamed or thermally precipitated, were subjected compression, and the ultimate compressive strength was reported at 30 percent strain. A universal testing machine (Instron Model 5696, Canton, MA, USA) was used at an extension rate of 0.5 mm/min.(Garber et al., 2013a)

3.2.3 Morphological analysis

All of the scaffolds were placed on the EMS550X sputter coater, which applied a conductive platinum coating for 4 minutes followed by standard SEM analysis. Human cadaver bone from knee area was obtained under LSU exempted IRB protocol HE 13-10 from the LSU Health Science Center.

3.2.4 Micro-CT analysis

Four PETA:HA (100: 0), (85:15), (80:20), (75:25) foams were fabricated by pressurized extrusion foaming and prepared as previously described.(Garber et al., 2013a) The imaging was conducted at the Center for Advanced Microstructures and Devices (Louisiana State University, Baton Rouge, LA) using a tomography beamline with 13 keV monochromatic x-rays with a 2.5 μm/px resolution. Projection exposure time varied from 2-4 seconds with $\Delta\theta$=0.25 corresponding

to the number of image slices (520). Reconstruction data were 16-bit signed integer with mean air intensity scaled to zero.

Avizo 7.0.1(Visualization Services Group) generated the volume renderings from the 3D data of the four foamed samples with two overlapping sub-volumes displayed simultaneously. The blue-green colormap represents the hydroxyapatite inclusions, and the red-orange colormap represents the copolymer foam. Image J generated 2-D orthogonal slices possessing grey colormap settings using the same data with a scale equivalent to the 3-D rendering. An approximate pore size was also measured using Image J. The orthogonal and micro-CT datasets were directly comparable, both as an aggregate dataset and as slices.

3.2.5 Porosity calculation based on micro-Ct

To analyze the three-dimensional data, two dimensional slices were read into a custom MATLAB code. For each slice the grayscale image was thresholded using Otsu's method (Otsu, 1975) and then converted into a binary image. Morphological operations were performed to remove small imaging artifacts, and isolate interior and exterior pores. After quantifying solid and void pixels, porosity was calculated as follows:

$$\varphi = \frac{V_{pores}}{V_{pores} + V_{solid}} \times 100\%$$

3.2.6 Adult stem cells isolation and culture

Liposuction aspirates from subcutaneous adipose tissue were obtained from three healthy adult subjects (male = 1 and females = 2) undergoing elective procedures. All tissues were

obtained with informed consent under a clinical protocol reviewed and approved by the Institutional Review Board at the LSU Pennington Biomedical Research Center and used under an exempted protocol at LSU A&M College. Isolation of hASC was performed as published.(Zanetti et al., 2012b) Passage 2 of each individual was used for *in vitro* hASC osteogenesis evaluation on tissue culture treated plastic or on scaffolds of different compositions. In both cases, hASC were cultured in either stromal (control - DMEM, 10% FBS, and 1% triple antibiotic solution) or osteogenic (DMEM, 10% FBS, 0.1 μM dexamethasone, 50 μM ascorbate-2-phosphate, 10 mM β-glycerophosphate, and 1% triple antibiotic solution) media for up to 21 days with media maintenance performed three times a week.

3.2.7 hASC loading on scaffolds and culture

All types of scaffolds were either molded or sculpted into 5 mm(diameter)×10mm(height) cylinder shape and gas sterilized afterwards. All the scaffolds were then submerged in stromal medium for 1hour before loading the hASCs. The same amount of second cell passages from all donors (n = 3) were pooled and directly loaded on a single face of each scaffold type at a concentration of 1.0×10^4 cells/μL for total volume of 5 μL. After 30 min of incubation in a saturated humidity atmosphere incubator at 37 °C and 5% CO_2, the same volume of hASCs containing solution were directly applied on the opposite side of each scaffold as previously described. (Zanetti et al., 2012b) Control groups included PCL:HA (100:0 and 80:20) scaffolds. Experimental groups included PETA:HA (100:0, 85:15, 80:20, 75:25) scaffolds. Scaffolds loaded with hASC were immediately transferred to 48-well plates and cultured in stromal or osteogenic media for 21 days. Cell medium were changed every 2-3 days. Triplicates were performed for each assay.

3.2.8 In vitro hASC metabolic activity on scaffolds

AlamarBlue™ (Life Technologies) is a useful measure of metabolic activity and is frequently used as an analog of cell viability and proliferation. All scaffold samples were seeded with hASC and cultured in stromal or osteogenic media for 21 days. The AlmarBlue™ conversion was measured at 7, 14, and 21 days The scaffolds were removed from culture, washed three times in Phosphate Buffered Saline (PBS), and incubated with 10% Alamar Blue™ in Hank's balanced salt solution (HBSS) without phenol red (pH 7) for 90 min. The fluorescence of three aliquots (100 μL) from each scaffold were measured at an excitation wavelength of 530 nm and an emission wavelength of 595 nm using a fluorescence plate reader (Wallac 1420 multilabel hts counter).

3.2.9 Alizarin red staining

hASC calcium deposition (triplicates of scaffolds alone and cell-scaffolds) was assessed after 7, 14, and 21 days of culture in control or osteogenic medium based on alizarin red staining. Wells were washed with 0.9% NaCl and fixed with 70% ethanol. Wells were stained with 2% alizarin red for 10 minutes and washed with DI water. Wells were destained with 10% cetylpyridinium chloride monohydrate for 4 hours at room temperature with constant agitation. Results were normalized to values from scaffolds cultured without cells for the same time periods.

3.2.10 In vitro quantification of DNA on scaffolds

Total DNA content was used to determine the number of cells on each scaffold as previously described.(Liu et al., 2008a) After triplicates of each scaffold were minced by a scalpel and the DNA was digested with 0.5 mL of 0.5mg/mL proteinase K (Sigma-Aldrich) at 56 ºC overnight,

aliquots (50 µL) were mixed with equal volumes of 0.1 g/mL Picogreen dye solution (Invitrogen) in 96-well plates. Samples were then excited at 480 nm with a plate reader (Wallac 1420 multilabel hts counter). Scaffolds without cells were used as negative controls.

3.2.11 Quantitative real-time polymerase chain reaction (QPCR)

Total RNA was extracted from triplicates of cell-scaffold constructs as previously described.(Zanetti et al., 2012b) Total RNA to cDNA EcoDry Premix (ClonTech) for cDNA synthesis. qRT-PCR was performed using 2× iTaq^{TM} SYBR$^{®}$ green supermix with ROX (Biorad) and primers for alkaline phosphatase (*ALP*) and osteoscalcin (*OCN*)(Zanetti et al., 2012b) to quantify osteogenic target gene expression of hASC loaded to scaffolds and cultured in either stromal or osteogenic media for 7, 14, and 21 days. Reactions were performed with a MJ Mini^{TM} Thermal Cycler (BioRad). The sequences of PCR primers (forward and backward, 50-30) were as follows: ALP, 5'-AATATGCCCTGGAGCTTCAGAA-3' and 5'-CCATCCCATCTCCCAGGAA-3';OCN, 5'-GCCCAGCGGTGCAGAGT-3' and 5'-TAGCGCCTGGGTCTCTTCAC-3'.Samples were normalized (ΔCt) against the house keeping gene 18S rRNA and the - ΔΔCt value of *ALP* and *OCN* in scaffolds cultured in osteogenic and control media was calculated using the ΔΔCt method.(Livak & Schmittgen, 2001b)

3.2.12 Statistical analysis

All results were expressed as mean ± SEM. Data was analyzed with one-way analysis of variance (ANOVA), followed by Tukey's minimum significant difference (MSD) post hoc test for pairwise comparisons of main effects. For all comparisons, a P-value < 0.05 was considered significant.

3.2.13 In vivo study

Scaffold Preparation and Surgical Implantation

Five male Fischer rats (Harlan Sprague-Dawley, Indianapolis, IN) were randomly assigned to three different treatments: (1) 1 rat was implanted with pre-sculpted PETA+20% HA, (2) 3 rats were implanted with PETA+20% foamed *in situ*, or (3) 1 rat was implanted with PETA+0% HA foamed *in situ* Stock/HA and TMPTMP/HA pre-polymer mixture were placed into a 250 mL pressurized spray canister with 7 g-compressed nitrous oxide as a gas foaming agent. The foamed composite copolymer was expelled from the canister onto a sterile surface. The solid composite was cut into a rectangle with dimensions (15 mm×10 mm×1 mm) for rat number 1. For rats 2, 3, and 4, the pre-polymer mixture was prepared as described above and foamed into a 5 mL syringe for surgical application. The process was the same for rat 5, but the formulation did not contain HA. The rat posterolateral lumbar spinal fusion surgery was performed as previously described (Aust et al., 2004). Prior to general anesthesia, rats received a subcutaneous injection of 0.5 mg/kg butorphanol (Torbugesic, Fort Dodge Animal Health) and 0.02 mg/kg glycopyrrolate (Robinul-V, Fort Dodge Animal Health, Fort Dodge, IA). Isoflurane was administered 20 minutes later in an induction chamber to induce anesthesia. The isoflurane was maintained at 1.5% via nose cone on a Bain circuit for the remainder of the procedure. The lumbar region was clipped and aseptically prepared with 70% isopropanol and betadine. A posterior midline skin incision was made over the lumbar spine. Two fascial incisions were made 3 mm lateral and parallel to the dorsal spinus processes. The L4 and L5 transverse processes were exposed with sharp and blunt dissection. A scalpel was used to decorticate each transverse process. Surgical sites were thoroughly lavaged with physiologic saline. In rat 1, solid scaffolds

were placed adjacent to both sides of the spine such that they spanned between the midpoint of each transverse process. For the remaining rats, 3 ml of each foamed scaffold was applied so that scaffold spanned between the center of each transverse process next to the spine. Fascial and subcutaneous incisions were closed separately with 3-0 polyglactin 910 (Vicryl, Ethicon) in a simple continuous pattern. Closure of the fascia around the implants effectively filled any potential space. A subcutaneous/subcuticular suture pattern was used to approximate skin edges, and tissue adhesive was used for skin closure (Vetbond, 3M). Scaffolds were harvested 3 (rat 3) or 6 (rats 1,2,4,5) weeks after implantation following euthanasia by CO_2 asphyxiation (Lopez et al., 2009). At 3 weeks, no significant results were shown in radiographs, micro-CT or histology analysis. Therefore, no results from Rat 3 were reported in the results and discussion sections.

Micro-CT Analysis

Immediately postmortem, two-dimensional (2-D) microcomputed tomography (μ-CT) imaging was performed (40 kV and 540 ms) to obtain 0.04 mm slices every 0.9°throughout a 360° rotation (SkyScan 1074, Skyscan n.v., Belgium). Three-dimensional (3-D) files were reconstructed from 2-D images. Measurements of 2-D and 3-D images were performed with AVIZO® Standard packages (FEITMVisualization Sciences Group). A density line was first drawn in void space with no tissue to measure the optical density (OD) of the image background. The line was then moved to L3 of the specimen's vertebral column to determine the OD of the tissue unaffected by the surgery. Lastly, the density line was moved between L4 and L5 of the specimen's vertebral column to calculate the OD of the area treated by the scaffolds. The density of the area treated by the implant was normalized by the densities of the void space and the

unaffected bone region in order to calculate the percentage of bone growth present in each specimen (Lopez et al., 2009).

$$OD = \log \frac{255}{Pixel\ value} \qquad \frac{OD_{Treated}}{OD_{Untreated}} \times 100 = \%\ new\ growth$$

Histology

Following imaging, spines were cut in half and fixed in neutral buffered formalin. One half of each spine was decalcified, paraffin embedded and longitudinal sections (5 um) were stained with hematoxylin and eosin. Microarchitecture was evaluated using Olympus BX46 microscope.

3.3. Results

3.3.1. SEM analysis

The foamed scaffold samples were analyzed using SEM to examine the trends in morphology. The morphology of the foam containing 0-20% HA was similar to cancellous human cadaver bone (Figure 3.1).

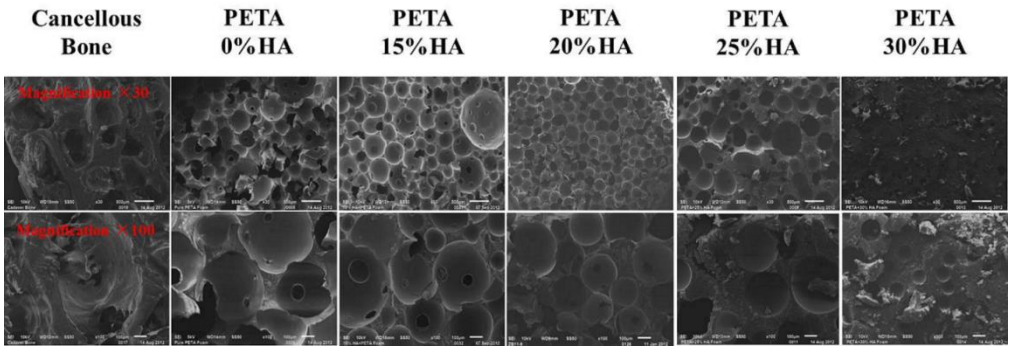

Figure 1 SEM analysis of PETA:HA (100:0), (85:15), (80:20), (75:25) scaffolds

The average pore diameters of PETA: HA 100:0 and 85:15 scaffolds were 250µm-300µm, with no significant difference between the two. PETA:HA 80:20 had a slightly smaller pore diameter of 150µm-200µm. The pore diameter of PETA:HA 75:25 was only 70µm-100µm. PETA:HA 70:30 had a pore diameter of less than 50µm. It is apparent from the results in Figure 3.1 that pore size is inversely related to HA content; pore diameter decreases as HA concentrations increase. Additionally, increasing HA content correlates with increased pore wall thickness and an apparent reduction in scaffold interconnectivity.

3.3.2. Micro-CT analysis and porosity calculation

There is a limitation associated with the amount of material that SEM can qualitatively analyze, reducing the generalizability of the data. To address this limitation, the interconnectivity, pore volume, and ceramic phase distribution of HA-PETA copolymer composites and PCL (control) were further analyzed by micro-CT. Micro-CT image analysis is a more senstivie method for estimating porosity of materials when compared to SEM, flow porosimetry, and gas adsorption. (Ho & Hutmacher, 2006) Volume renderings (Figure 3.2) were generated from PETA and PCL composite foam 3-D data using Avizo 7.0.1 (Visualization Services Group). Two overlapping sub-volumes were rendered simultaneously, one with a red-orange-white colormap corresponding to thiol-acrylate foam, and another with a blue-green colormap corresponding to hydroxyapatite additives. The porosity of PETA: HA (100:0, 85:15, and 80:20) are 66.9%, 72.0%, and 66.4% respectively (Figure 3.3A). It should be noted that an apparent transition in morphology occurred between 20% and 25% HA inclusions. As HA concentration increased from 20% to 25%, the porosity decreased significantly from 66.4% to 44.7%. When

HA concentration reaches 25%, the pore size is substantially reduced and the interconnected void volume appeared to decrease, resulting in a structure similar to a closed-cell foam (Figure 3.2K&L).

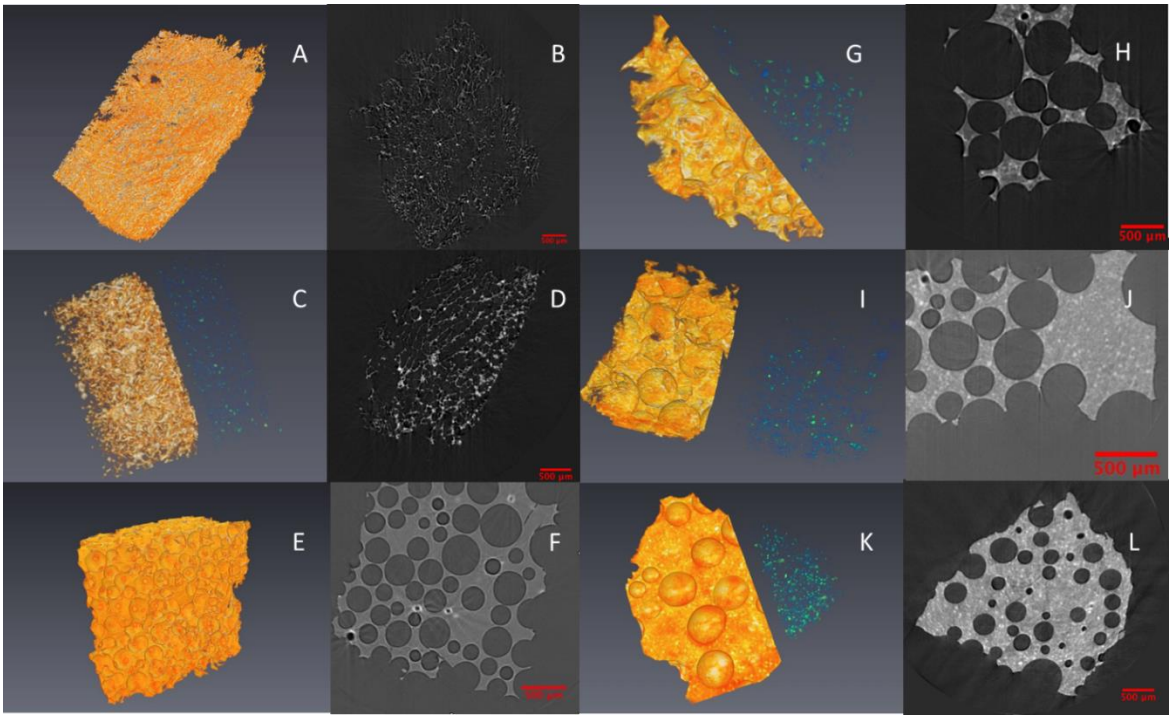

Figure 2 Avizo rendering pictures (3D &2D) of micro-ct data of scaffolds. Figure 2A&B PCL:HA (100:0); Figure 2C&D PCL:HA (80:20) ;Figure 2E&F PETA: HA (100:0) Figure 2G&H PETA: HA (85:15) scaffolds; Figure 2I&J PETA: HA (80:20) scaffolds; Figure 2K&L PETA: HA (75:25) scaffolds. Each scale bar in the 2D pictures indicates 500µm.

This is attributed to increased polymer solution viscosity correlated with reduced N_2O expansion and mobility. In addition, the inclusion of 20% HA to PCL scaffolds increased the porosity from 78.0% (PCL:HA 100:0) to 87.6% (PCL:HA 80:20) (Figure 3.2A&C).

3.3.3. Mechanical testing

Figure 3.3B shows the compressive yield strength of the foamed and solid PCL:HA (100:0, 80:20), PETA:HA (100:0, 85:15, 80:20, 75:25) samples.

Compressive strength of solid PCL:HA (100:0, 80:20) samples are significantly higher than corresponding PETA:HA (100:0, 80:20) samples. When comparing among porous scaffolds, PETA:HA (100:0, 80:20) scaffolds are either the same as or stronger than PCL:HA (100:0, 80:20). The compressive strength of the foamed PETA:HA steadily increased with increasing HA content; however, the solid samples did not follow a similar trend. The addition of 15% HA in the foam resulted in a significant increase in compressive strength compared to the control samples and increasing the HA content beyond 15% correlated with increased compressive strength.

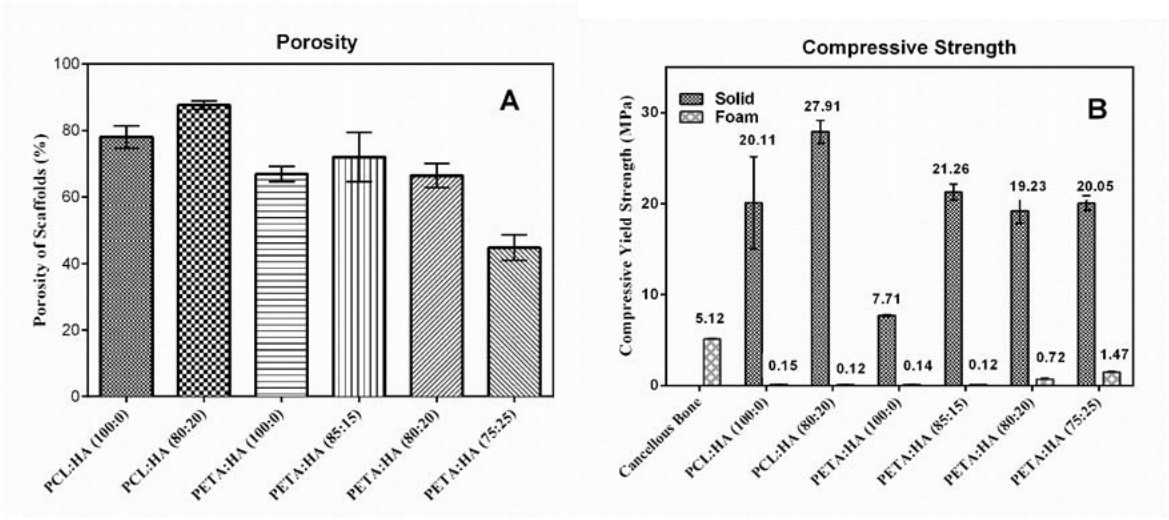

Figure 3 porosity of PETA:HA (100: 0), (85:15), (80:20), (75:25) scaffolds; B: maximum compressive strength of PETA:HA PETA:HA (100: 0), (85:15), (80:20), (75:25) composites(solid and foam)

Conversely, solid PETA:HA (85:15, 80:20, 75:25) composite scaffolds exhibited approximately the same compressive strength for all HA containing samples. It is believed that the porosity (Figure 3A) is responsible for the different trends between solid and foamed scaffolds.

3.3.4. hASC metabolic activity and proliferation on scaffolds cultured in control and osteogenic media

For cell-scaffold constructs cultured in stromal media, PETA:HA (100:0) had the highest metabolic activity after 14 days of culture. PCL:HA (100:0) had the highest levels of metabolic activity after 21 days of culture in stromal medium and no significant differences were observed from this scaffolds between any time point. In osteogenic media, PETA:HA (100:0) scaffolds again exhibited the highest metabolic activity after 7, 14 and 21 days of culture. PETA:HA (85:15 and 80:20) scaffolds had the next highest metabolic activity at all time points. PCL scaffolds showed the lowest levels of metabolic activity after 7, 14 and 21 days of culture (Figure 3.4A**)**. The addition of HA to PETA and PCL scaffolds decreased metabolic activity on constructs cultured in stromal and osteogenic media.

Significantly higher metabolic activity in was observed at all-time points for PCL:HA (100:0) and PCL:HA (80:20) scaffolds cultured in stromal media compared to osteogenic media. This data is in agreement with previous studies which indicate the metabolic activity of hASC is expected to decrease as cells commit to an osteogenic linage.(Qureshi et al., 2013; Zanetti et al., 2012b)

No differences in metabolic activity were seen in PETA:HA composite samples between stromal and osteogenic conditions. hASC cultured on HA-containing scaffolds were expected to begin differentiation into an osteogenic linage regardless of the media condition, potentially accounting for the differences in metabolic activity between HA-containing and control samples with respect to media condition. Almost no metabolic activity was measured in PETA:HA (75:25) scaffolds, likely as a result of the reduced pore size and interconnectivity.

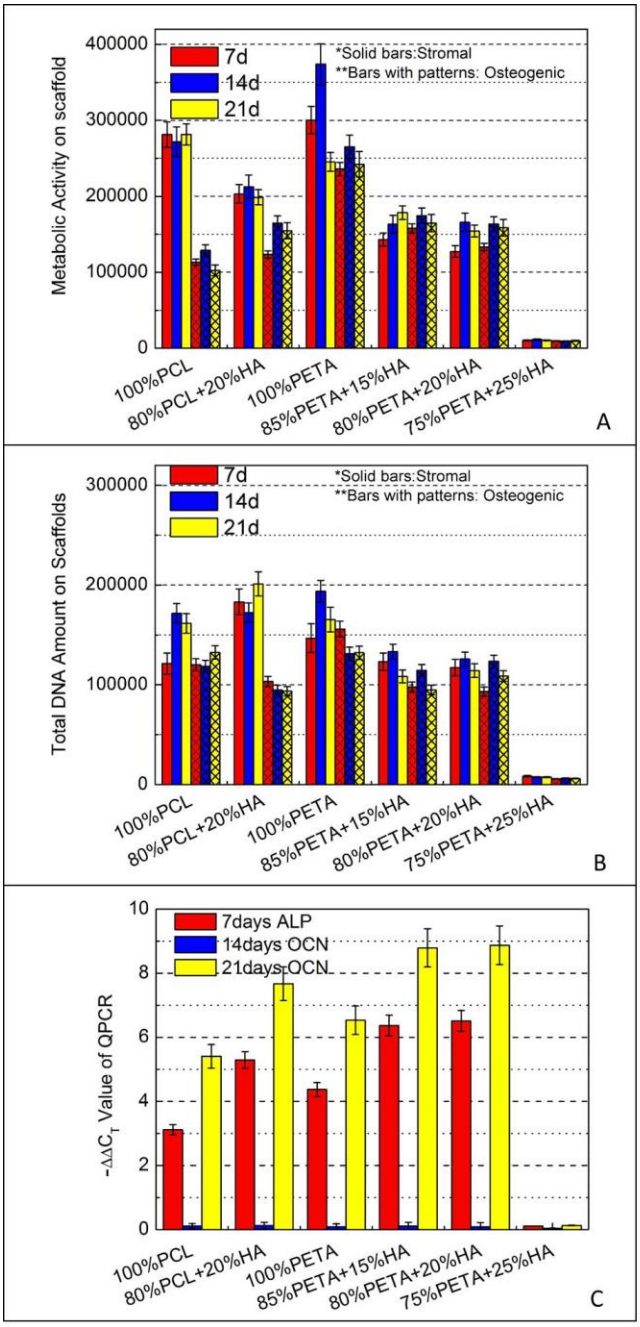

Figure 3.4 Panel A: relative metabolic activity of hASC on PETA:HA (100:0), (85:15), (80:20), (75:25) scaffolds; Panel B**:** relative DNA content of hASC on PETA:HA (100: 0), (85:15), (80:20), (75:25) scaffolds**;** Panel C: q-rtPCR analysis of ALP (7 day) and OCN (14 and 21 day) expression from hASC on PETA:HA (100:0), (85:15), (80:20), (75:25) scaffolds.

Total DNA content was quantified using Quant-iT™ PicoGreen ®, to analyze the hASC proliferation in scaffolds. Differences in DNA content, between stromal and osteogenic media conditions, were observed at the 7 day culture time point for PCL:HA (80:20), PETA:HA (85:15) and PETA:HA (80:20) composite scaffolds. When comparing samples within the stromal media treatment condition, it can be observed that the PETA:HA samples had significantly fewer cells than the PCL or PETA control. The most pronounced difference in DNA content was between PCL:HA (80:20) composites and PETA:HA scaffolds in stromal media conditions, (Figure 3.4B) where the DNA content in PCL (80:20) scaffolds was significantly higher than PETA:HA composites. At 14 and 21 days, levels of DNA content observed in both PCL scaffolds and the pure PETA scaffolds were significantly higher than the PETA:HA composites, in stromal media conditions. Within the osteogenic media treatment groups, the PETA:HA scaffolds showed slightly increased DNA content compared with the PCL:HA scaffolds, but all scaffolds contained a similar numbers of cells.

3.3.5. Quantitative real-time polymerase chain reaction (QPCR)

Bone morphogenic proteins (BMPs), known to regulate osteogenesis, act on the transcription factor core binding factor alpha1 (Cbfa1) and result in the activation of osteoblast-related genes, such as *ALP* and *OCN*. (Liu et al., 2008a; Milat & Ng, 2009) The expression of these genes are commonly used as early and middle stage markers of osteogenesis, respectively.(Burge et al., 2007) QPCR was used to assess the expression of *ALP* at the 7 day time point and *OCN* at 14 and 21 day time points (Figure 3.4C). Based on previous studies, *ALP* expression in hASC decreased dramatically after 7 days in culture and was therefore not measured at the 14 and 21 day time points in this study.(Burge et al., 2007; Zanetti et al., 2012b) The differences in the

expression of *ALP* and *OCN* in hASCs cultured on scaffolds in stromal and osteogenic media are represented in Figure 3.4C. The cells on PETA:HA (85:15) and PETA:HA(80:20) scaffolds showed similar expression of *ALP* at 7days and were significantly higher than all other PETA and PCL scaffolds. Additionally, hASC on pure PETA scaffolds had higher *ALP* expression than pure PCL control scaffolds. While hASC cultured on PCL:HA(80:20) scaffolds had higher *ALP* expression than pure PETA or PCL, the expression was still lower than PETA:HA (85:15) and PETA:HA(80:20) scaffolds. Moreover, the expression of the *OCN* marker could only be observed at 21 days of culture, with little expression at 14 days regardless of treatment. The *OCN* expression level demonstrated in hASC as a function of scaffold type was the similar to that of *ALP* expression with maximal *OCN* expression observed in PETA:HA (85:15) and PETA:HA(80:20) followed closely by *OCN* levels in PCL:HA composites. Consistent with the previously described results, cells cultured on the PETA:HA (75:25) sample did not demonstrate substantial expression of either marker, likely the result of poor cell proliferation/survival associated with the lack of a porous and interconnected structure.

3.3.6 Calcium deposition in hASC cultured in control and osteogenic media

The mineralization of different scaffold types was assessed using alizarin red staining, which stains calcium-rich deposits. hASC cultured on the PETA composites in stromal and osteogenic media were tested against PCL and PCL:HA scaffolds. (Figure 3.5A)

As expected, alizarin red staining was significantly higher in hASC cultured in osteogenic media compared to samples cultured in stromal media. (Zanetti et al., 2012b) Also, hASC cultured in osteogenic media showed a significant increase in staining with respect to increased

time in culture. Except for PETA:HA (75:25), all scaffolds showed significant differences in the calcium deposition at 14 days between stromal and osteogenic media.

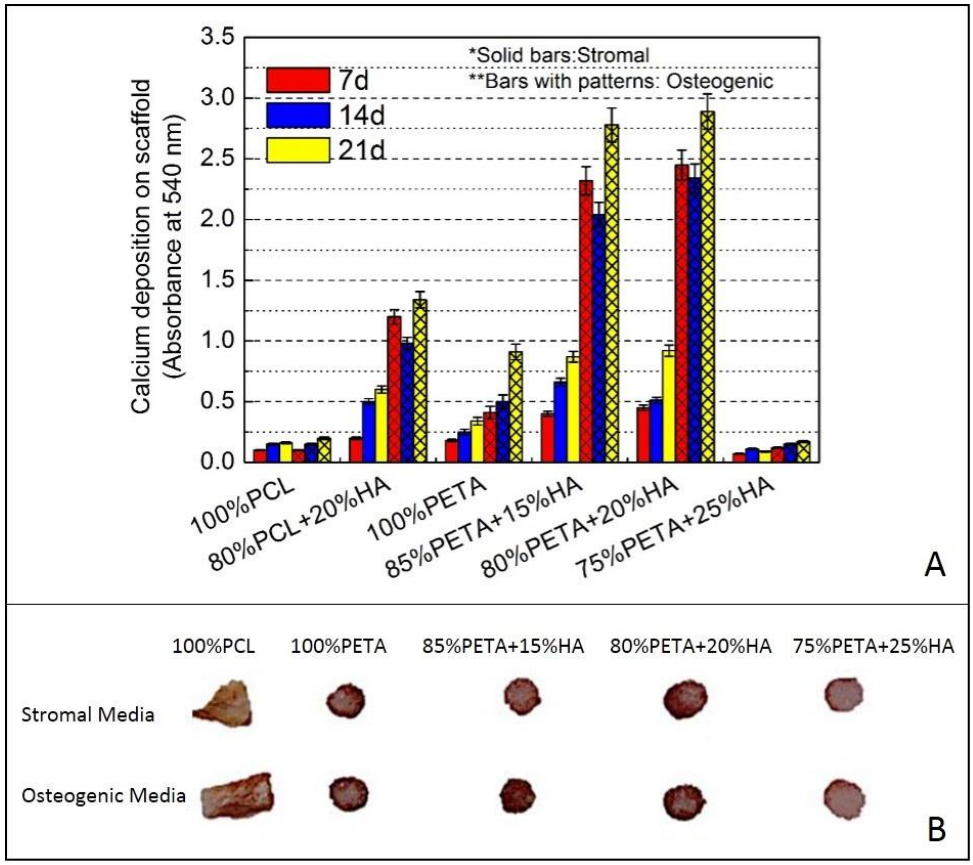

Figure 3.5 Alizarin red stain of PETA:HA as a function of scaffold composition, media treatment and time. Panel A, quantitative analysis of staining on scaffolds loaded with hASC and cultured in stromal and osteogenic media for 7, 14 and 21 days. Panel B**,** cross section of each type of scaffold stained with alizarin red on 21 days.

Both PETA: HA (80:20) and PETA:HA (85:15) cultured in osteogenic media demonstrated significantly increased staining compared to all other experimental samples and controls. Almost no calcium deposition, however, was observed at 14 and 21 day culture time points in PETA:HA (75:25).

3.3.7 *In vivo* study

Radiography

Observed behavior and weight gain were normal (90.7 ± 5.9 g) for all rats after surgery. Foamed thiol-acrylate nanocomposite implants showed some increase in radiographically detectable opacity 3 weeks after implantation compared to immediately after surgery, and the opacity increased further by 6 weeks after implantation. The increasing intensity of bone scaffolds is consistent with scaffold calcification (Figure 3.6). Rats implanted with pre-molded samples, had a lower increase in radioopacity by 6 weeks after implantation compared to rats implanted with PETA+HA foamed *in situ*.

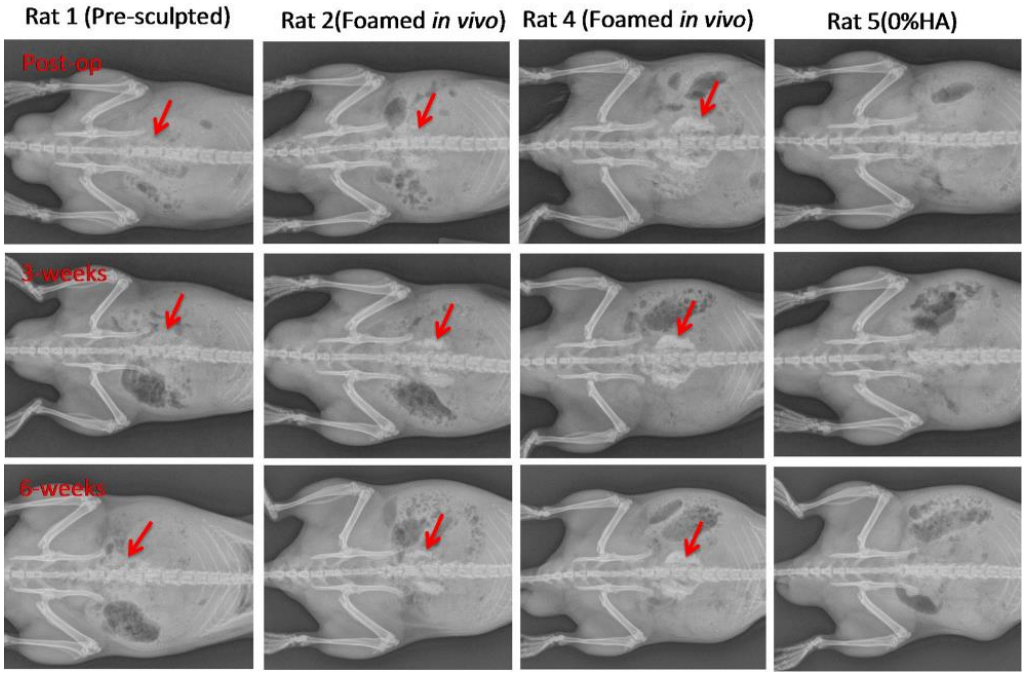

Figure 3.6 Radiographs of *in vivo* study

No evidence of calcification was observed in implants of 0% HA pre-sculpted PETA. This is consistent with the *in vitro* osteogenesis target gene expression results.

Microcomputed Tomography

The micro-CT results support the radiographic findings. The light colored regions indicate densification in the scaffolds in Figure 3.7. *In vivo*, *in situ* polymerized scaffolds had the greatest amount of densification six weeks after surgery.

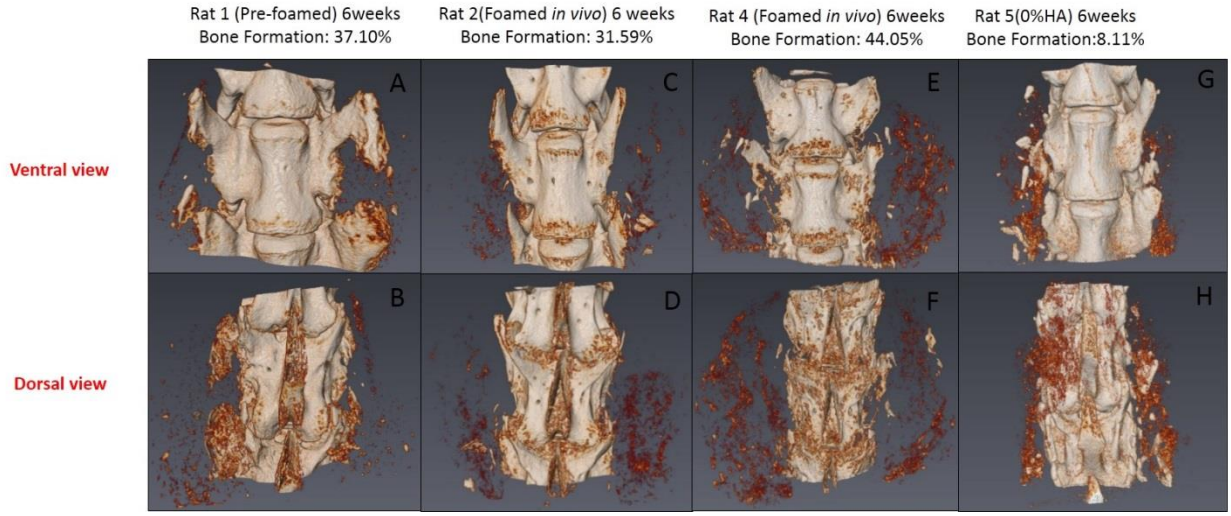

Figure 3.7 Micro-CT data of the L4 (top) and L5 (bottom) vertebral bodies from the *in vivo* study. The light colored regions indicate densification in scaffolds.

Analysis of Bone Formation using histology

Histological examination was performed on pre-sculpted PETA:HA (80:20), PETA:HA (80:20) foamed *in situ*, and PETA:HA (100:0) foamed *in situ*. The essential step of decalcifying and staining the spinal column poses a problem in analyzing tissues for bone formation evaluating the calcified areas. For this reason, tissue morphology is considered a reliable parameter to measure bone formation(Schulte et al., 2013). Each cohort was examined six weeks post-op.

Treatment cohort 1 (pre-sculpted PETA:HA (80:20)proved to be biocompatible, support cell growth, and induce osteogenesis in tissue growing into the foam structure. Figure 3.8A shows that the PETA:HA (80:20) implant is partially demarcated by fibrosis and multifocal fibrocartilage formation, which incorporates multifocal, small areas of endochondral ossification.

Figure 3.8D contains the implant surrounded by fibrous tissue, fibrocartilage, and peripheral endochondral ossification. The appearance of cells chondrocytic in appearance, a tide mark, and an ossified site present around the implant site indicate that the PETA:HA (80:20) scaffold have the potential to induce endochondral ossification.

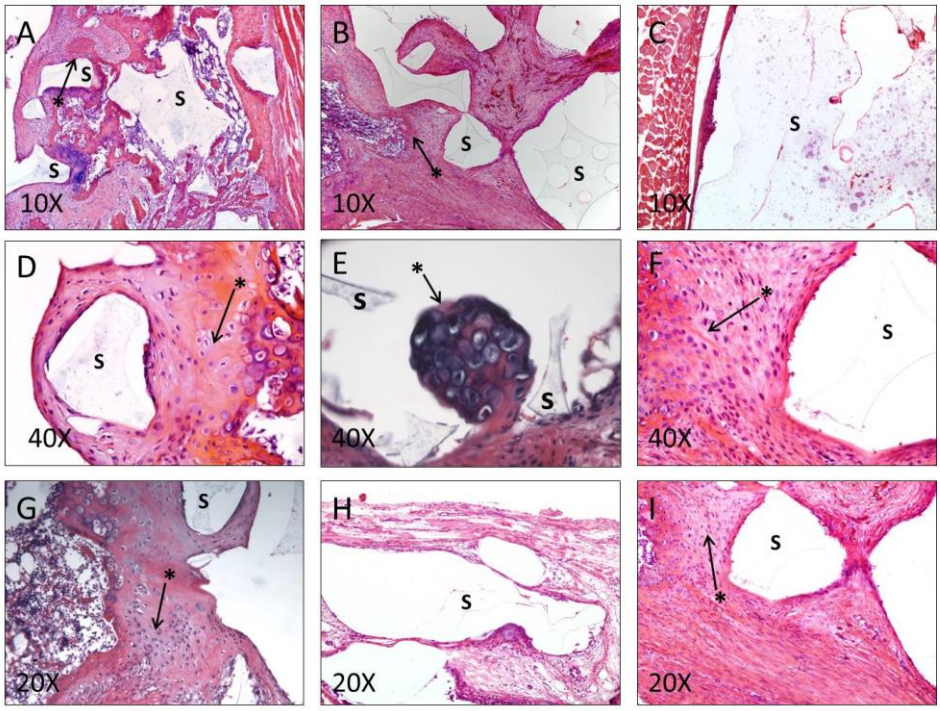

Figure 8 Histology analysis using Hematoxylin and eosin staining. A medial cut was made on the spinal column of each rat. The progress of this specimen guides the analysis of the other specimens. Figures 8A, 8B, 8D, 8F, and 8I: Rat was treated with the pre-sculpted PETA:HA (80:20) scaffold. Figure 8C, 8E, and 8G: Rats were treated with PETA:HA (80:20) scaffold foamed *in situ*. Figure 8H: Rat was treated with PETA:HA (100:0) foamed in situ. **S**: scaffold implants; *****: site endochondral ossification

Figure 3.8B shows that the polymer implant is segmentally demarcated by fibrous and fibrocartilagenous tissues with an ossified rim blending into pre-existing trabecular bone. The findings in Figure 3.8B are further supported by Figure 3.8I and Figure 3.8F.

Treatment 2 (PETA:HA 80:20 *in situ*) was also shown to be biocompatible, support bone growth, and induce osteogenic differentiation. In cohort 2, histological changes are characterized by ostegenic activity around the implant site. Figure 3.8C shows a large accumulation of polymer implant near the skeletal muscle of the rat, surrounded by a thin layer of fibrous tissue with a focal area also containing macrophages. Figure 3.8E shows the presence of a cavitation lined by 1-3 layers of spindled cells (fibroblasts) containing the scaffold and a sprouting nidus of endochondral ossification. Figure 3.8G shows that in the area adjacent to the polymer-occupied cavitation, there are fibrous tissues and a region of endochondral ossification.

Histological analysis of cohort 3 PETA:HA (100:0) indicates that the lack of nanoscale HA reduces the osteogenic properties of the scaffolds. In Figure 3.8H, the scaffold is surrounded by a very thin layer of fibrous tissue, indicating a reduction in the formation of organized tissue in the implant region.

3.4. Discussion

Bone tissue engineering involving polymer/ceramic composites presents an attractive alternative approach to the repair and regeneration of damaged or traumatized bone tissue. (Gaalen et al., 2008; Pallua & Suscheck, 2010b). Several studies have previously explored the potential use of thiol-acrylate chemistry for biomedical devices, but radical based photoinitiators are usually used to drive the polymerization process.(Rydholm et al., 2008; Rydholm et al., 2006;

Zanetti et al., 2012b) A non-radical based polymerization method is potentially less cytotoxic and therefore more amenable to *in situ* polymerization. The amine catalyzed Michael addition for thiol-acrylate polymerization described in this study has potential advantages compared to photoinitiated reactions because the chain propagation does not require a free radical initiator during the polymerization reaction. The mechanism of this amine-catalyzed reaction has been previously investigated.(Bounds et al., 2013; Garber et al., 2013a) The general reaction occurs via the formation of a catalyst/comonomer molecule by the Michael addition of a secondary amine across the alkene end group found in acrylate monomers. The *in situ* catalyst produced reacts with a trifunctional thiol and trifunctional acrylates forming a high-density cross-linked copolymer. The step growth nature and the incorporation of the tertiary amine catalyst reduce concerns about potential leaching of free radical initiators and unreacted monomer. This reaction, therefore, is potentially more attractive for *in situ* polymerization for bone formation than comparative free radical-based methods.

The PCL-based scaffold was synthesized via a thermal precipitation method resulting in pore size, volume, and interconnectivity that are largely independent of solution viscosity.(Qureshi et al., 2012) Results showed that such characteristics were directly influenced by the viscosity of the stock solution in the polymerization of PETA composites. (Barby & Haq, 1985). It is well documented that an interconnected pore structure can help support cell migration, cell differentiation, nutrient transport (Di Maggio et al., 2011; Lawrence & Madihally, 2008) and, in some cases, formation of blood vessels. (Mehrkens et al., 2009; Papadimitropoulos et al., 2011; Scherberich et al., 2007) Because HA was found to decrease interconnectivity, it was expected that the highest HA concentration sample, PETA:HA (75:25), would not provide a

suitable environment for cell in-growth and nutrient/waste transport. Electron microscopy images and micro-CT analysis indicate PETA:HA (75:25) scaffolds lack interconnectivity of the void volume providing for cell penetration and nutrient/waste transport required for cell growth and differentiation. The analysis of cell viability and expression of osteogenic markers further supported this hypothesis.

The decreased metabolic activity of PETA:HA composites compared to the PETA control is likely related to differences in cell function, not cell number, attributed to osteogenic differentiation of hASC. The decreased cell proliferation and metabolic activity also had an inverse relationship with the increased calcium deposition and expression of osteogenic markers. This data further supports the hypothesis that hydroxyapatite induces osteogenesis, resulting in decreased metabolic activity and proliferation. (Bernhardt et al., 2009; He et al., 2010)

Calcium deposition correlated with the expression of *ALP* and *OCN* in hASC cultured on PETA:HA (85:15) and PETA:HA (80:20) scaffolds, which were significantly greater than PCL:HA (80:20), pure PCL, and PETA control scaffolds in both media conditions, providing a further indication that scaffolds composed of PETA may be an appropriate material for the repair of bone defects. Increased alizarin stain uptake in PETA: HA (80:20) and PETA:HA (85:15), compared to PCL:HA (80:20), does not correlate with increased cell density or metabolic activity but does correlates with increased *ALP* and *OCN* expressionPETA is better able to induce the expression of osteogenic markers than PCL, but further comparisons at differing concentrations and with other degradable resins are required to test this hypothesis. . Cross sectional images of PETA:HA (75:25) scaffolds demonstrate poor alizarin red penetration providing further support that the void volume in not substantially interconnected.

Although increasing HA content resulted in reduced pore size and interconnectivity, it provided a more solid and stronger structure for the scaffold. Other studies have shown a similar trend of decreasing porosity with increasing HA content.(Zhang & Ma, 1999) The increase in compressive strength seen in solid samples is predictable and similar to that seen with other nanoscale polymer fillers.(Ahn et al., 2004; Reynaud et al., 2001) As porosity played no role in the solid samples, the increase in viscosity with increasing HA content beyond 15% did not significantly affect the mechanical strength. Histological results demonstrated that both the pre-sculpted and foamed *in situ* PETA:HA (80:20) scaffolds induced endochondral ossification. Radiography results indicating increased densification further supported these findings. During the *in vivo* study, the structure of the *in situ* polymerized foam sample may have been disrupted when the surgical site was closed during the surgery. Poor porosity and interconnectivity could be the reason why the densified regions of the radiographs were non-continuous. Overall results suggest that PETA:HA scaffolds could be a suitable substrate for bone regeneration.

3.5. Conclusion

By gas foaming thiol-acrylate based copolymers synthesized via Michael addition with an *in situ* amine-catalyst, a porous polymeric scaffold with bone-like morphology was developed as a potential graft or augment in critical-sized bone defect repair. Not only does PETA:HA composite have substantial porosity and interconnectivity, it also demonstrates adequate mechanical strength as compared to cortical bone. Compared to PCL:HA composites, both PETA:HA (85:15) and PETA:HA (80:20) scaffolds showed higher mineral deposition and *ALP* and *OCN* expression level. Overall, the PETA:HA had higher compressive strength and improved cytocompatibility compared to PCL controls. Mesenchymal cells cultured on PETA

based scaffolds had a greater expression of osteogenic markers and the scaffolds exhibited significantly greater mineralization than hASC cultured on PCL controls. The *in vivo* study demonstrated that animals injected with PETA:HA composites showed no signs of surgical site or systemic toxicity and that PETA:HA composites induced osteogenesis *in vivo*. Additionally, the study serves as a proof-of-concept that gas foaming of thiol-acrylate polymers *in vivo* may be used to conformally fill irregular sized defects.

3.6. References

Ahlmann, E., Patzakis, M., Roidis, N., Shepherd, L., Holtom, P. 2002. Comparison of anterior and posterior iliac crest bone grafts in terms of harvest-site morbidity and functional outcomes. *J Bone Joint Surg Am*, **84-A**(5), 716-20.

Ahn, S.H., Kim, S.H., Lee, S.G. 2004. Surface‐modified silica nanoparticle‐reinforced poly (ethylene 2, 6‐naphthalate). *Journal of Applied Polymer Science*, **94**(2), 812-818.

Aust, L., Devlin, B., Foster, S., Halvorsen, Y., Hicok, K., Du Laney, T., Sen, A., Willingmyre, G., Gimble, J. 2004. Yield of human adipose-derived adult stem cells from liposuction aspirates. *Cytotherapy*, **6**(1), 7-14.

Barby, D., Haq, Z. 1985. Low density porous cross-linked polymeric materials and their preparation and use as carriers for included liquids, Google Patents.

Bernhardt, A., Despang, F., Lode, A., Demmler, A., Hanke, T., Gelinsky, M. 2009. Proliferation and osteogenic differentiation of human bone marrow stromal cells on alginate-gelatine-hydroxyapatite scaffolds with anisotropic pore structure. *J Tissue Eng Regen Med*, **3**(1), 54-62.

Bohner, M. 2010. Resorbable biomaterials as bone graft substitutes. *Materials Today*, **13**(1-2), 24-30.

Bounds, C.O., Upadhyay, J., Totaro, N., Thakuri, S., Garber, L., Vincent, M., Huang, Z., Hupert, M., Pojman, J.A. 2013. Fabrication and Characterization of Stable Hydrophilic

Microfluidic Devices Prepared via the in Situ Tertiary-Amine Catalyzed Michael Addition of Multifunctional Thiols to Multifunctional Acrylates. *ACS applied materials & interfaces*, **5**(5), 1643-1655.

Burge, R., Dawson-Hughes, B., Solomon, D.H., Wong, J.B., King, A., Tosteson, A. 2007. Incidence and Economic Burden of Osteoporosis-Related Fractures in the United States, 2005–2025. *Journal of Bone and Mineral Research*, **22**(3), 465-475.

Degasne, I., Basle, M.F., Demais, V., Hure, G., Lesourd, M., Grolleau, B., Mercier, L., Chappard, D. 1999. Effects of roughness, fibronectin and vitronectin on attachment, spreading, and proliferation of human osteoblast-like cells (Saos-2) on titanium surfaces. *Calcif Tissue Int*, **64**(6), 499-507.

Di Maggio, N., Piccinini, E., Jaworski, M., Trumpp, A., Wendt, D.J., Martin, I. 2011. Toward modeling the bone marrow niche using scaffold-based 3D culture systems. *Biomaterials*, **32**(2), 321-9.

Gaalen, S.v., Kruyt, M., Meijer, G., Mistry, A., Mikos, A., Beucken, J.v.d., Jansen, J., Groot, K.d., Cancedda, R., Olivo, C., Yaszemski, M., Dhert, W. 2008. Chapter 19 - Tissue engineering of bone. in: *Tissue Engineering*, (Eds.) B. Clemens van, T. Peter, L. Anders, H. Jeffrey, F.W. David, C. Ranieri, D.d.B. Joost, P.T.A.L.J.H.D.F.W.R.C.J.D.d.B. Jérôme SohierA2 - Clemens van Blitterswijk, S. Jérôme, Academic Press. Burlington, pp. 559-610.

Garber, L., Chen, C., Kilchrist, K.V., Bounds, C., Pojman, J.A., Hayes, D. 2013. Thiol-acrylate nanocomposite foams for critical size bone defect repair: A novel biomaterial. *Journal of Biomedical Materials Research Part A*, **10**(12), 3531-3541.

Gertzman, A.A., Sunwoo, M.H. 2000. Malleable paste for filling bone defects, Google Patents.

He, J., Genetos, D.C., Leach, J.K. 2010. Osteogenesis and trophic factor secretion are influenced by the composition of hydroxyapatite/poly(lactide-co-glycolide) composite scaffolds. *Tissue Eng Part A*, **16**(1), 127-37.

Ho, S.T., Hutmacher, D.W. 2006. A comparison of micro CT with other techniques used in the characterization of scaffolds. *Biomaterials*, **27**(8), 1362-1376.

Hutmacher, D.W. 2000. Scaffolds in tissue engineering bone and cartilage. *Biomaterials*, **21**(24), 2529-2543.

Karageorgiou, V., Kaplan, D. 2005. Porosity of 3D biomaterial scaffolds and osteogenesis. *Biomaterials*, **26**(27), 5474-91.

Lawrence, B.J., Madihally, S.V. 2008. Cell colonization in degradable 3D porous matrices. *Cell Adhesion & Migration*, **2**(1), 9-16.

Levine, B. 2008. A New Era in Porous Metals: Applications in Orthopaedics. *Advanced Engineering Materials*, **10**(9), 788-792.

Liu, Q., Cen, L., Yin, S., Chen, L., Liu, G., Chang, J., Cui, L. 2008a. A comparative study of proliferation and osteogenic differentiation of adipose-derived stem cells on akermanite and β-TCP ceramics. *Biomaterials,* **29**(36), 4792-4799.

Liu, Q., Cen, L., Yin, S., Chen, L., Liu, G., Chang, J., Cui, L. 2008b. A comparative study of proliferation and osteogenic differentiation of adipose-derived stem cells on akermanite and β-TCP ceramics. *Biomaterials*, **29**(36), 4792-4799.

Livak, K.J., Schmittgen, T.D. 2001. Analysis of relative gene expression data using real-time quantitative PCR and the 2(-Delta Delta C(T)) Method. *Methods*, **25**(4), 402-8.

Lopez, M.J., McIntosh, K.R., Spencer, N.D., Borneman, J.N., Horswell, R., Anderson, P., Yu, G., Gaschen, L., Gimble, J.M. 2009. Acceleration of spinal fusion using syngeneic and allogeneic adult adipose derived stem cells in a rat model. *Journal of Orthopaedic Research*, **27**(3), 366-373.

Mehrkens, A., Muller, A.M., Schafer, D., Jakob, M., Martin, I., Scherberich, A. 2009. Towards an intraoperative engineering of osteogenic grafts from the stromal vascular fraction of human adipose tissue. *Swiss Medical Weekly*, **139**(23-24), 23S-23S.

Milat, F., Ng, K.W. 2009. Is Wnt signalling the final common pathway leading to bone formation? *Molecular and cellular endocrinology*, **310**(1-2), 52-62.

Otsu, N. 1975. A threshold selection method from gray-level histograms. *Automatica*, **11**(285-296), 23-27.

Pallua, N., Suscheck, C.V. 2010a. *Tissue engineering: from lab to clinic*. Springer Verlag.

Pallua, N., Suscheck, C.V. 2010b. *Tissue Enginnering: from lab to clinic*. Springer Verlag.

Papadimitropoulos, A., Scherberich, A., Guven, S., Theilgaard, N., Crooijmans, H.J., Santini, F., Scheffler, K., Zallone, A., Martin, I. 2011. A 3D in vitro bone organ model using human progenitor cells. *Eur Cell Mater*, **21**, 445-58.

Qureshi, A.T., Monroe, W.T., Dasa, V., Gimble, J.M., Hayes, D.J. 2013. miR-148b–Nanoparticle conjugates for light mediated osteogenesis of human adipose stromal/stem cells. *Biomaterials*, **34**(31), 7799-7810.

Qureshi, A.T., Terrell, L., Monroe, W.T., Dasa, V., Janes, M.E., Gimble, J.M., Hayes, D.J. 2012. Antimicrobial biocompatible bioscaffolds for orthopaedic implants. *Journal of Tissue Engineering and Regenerative Medicine*, n/a-n/a.

Reynaud, E., Jouen, T., Gauthier, C., Vigier, G., Varlet, J. 2001. Nanofillers in polymeric matrix: a study on silica reinforced PA6. *Polymer*, **42**(21), 8759-8768.

Rydholm, A.E., Held, N.L., Benoit, D.S.W., Bowman, C.N., Anseth, K.S. 2008. Modifying network chemistry in thiol-acrylate photopolymers through postpolymerization functionalization to control cell-material interactions. *Journal of Biomedical Materials Research Part A*, **86A**(1), 23-30.

Rydholm, A.E., Reddy, S.K., Anseth, K.S., Bowman, C.N. 2006. Controlling network structure in degradable thiol-acrylate biomaterials to tune mass loss behavior. *Biomacromolecules*, **7**(10), 2827-2836.

Scherberich, A., Galli, R., Jaquiery, C., Farhadi, J., Martin, I. 2007. Three-dimensional perfusion culture of human adipose tissue-derived endothelial and osteoblastic progenitors generates osteogenic constructs with intrinsic vascularization capacity. *Stem cells*, **25**(7), 1823-9.

Schulte, F.A., Ruffoni, D., Lambers, F.M., Christen, D., Webster, D.J., Kuhn, G., Müller, R. 2013. Local Mechanical Stimuli Regulate Bone Formation and Resorption in Mice at the Tissue Level. *PloS one*, **8**(4), e62172.

Singh, R., Lee, P.D., Lindley, T.C., Dashwood, R.J., Ferrie, E., Imwinkelried, T. 2009. Characterization of the structure and permeability of titanium foams for spinal fusion devices. *Acta Biomater*, **5**(1), 477-87.

Sundelacruz, S., Kaplan, D.L. 2009. Stem cell-and scaffold-based tissue engineering approaches to osteochondral regenerative medicine. *Seminars in cell & developmental biology*. Elsevier. pp. 646-655.

Topart, P., Vandenbroucke, F., Lozac'h, P. 2005. Tisseel versus tack staples as mesh fixation in totally extraperitoneal laparoscopic repair of groin hernias. *Surgical Endoscopy And Other Interventional Techniques*, **19**(5), 724-727.

Yeh, J.C., Tucker, N. 2005. The Use of Tisseel in Oculoplastics. *Invest. Ophthalmol. Vis. Sci.*, **46**(5), 4252.

Zanetti, A.S., McCandless, G.T., Chan, J.Y., Gimble, J.M., Hayes, D.J. 2012. Characterization of novel akermanite:poly-ε-caprolactone scaffolds for human adipose-derived stem cells bone tissue engineering. *Journal of Tissue Engineering and Regenerative Medicine*, n/a-n/a.

Zanetti, A.S., Sabliov, C., Gimble, J.M., Hayes, D.J. 2013. Human adipose‐derived stem cells and three‐dimensional scaffold constructs: A review of the biomaterials and models currently used for bone regeneration. *Journal of Biomedical Materials Research Part B: Applied Biomaterials*, **101**(1), 187-199.

Zhang, R., Ma, P.X. 1999. Poly(alpha-hydroxyl acids)/hydroxyapatite porous composites for bone-tissue engineering. I. Preparation and morphology. *J Biomed Mater Res*, **44**(4), 446-55.

CHAPTER 4 TARGETING CALCIUM MAGNESIUM SLICATES FOR POLYCAPROLACTONE/CERAMIC COMPOSITE SCAFFOLDS[3]

4.1 Introduction

In order to properly facilitate bone regrowth, synthetic composite scaffolds, grafts and augments must be biocompatible, biodegradable, and provide adequate structural support for cell migration, as well as waste and nutrient transport. These characteristics may be achieved by manipulating tunable physical properties, such as porosity, modulus, degradation rate, absorption rate, and swelling by modifications with the inclusion of copolymers and ceramic phases as synthetic composite scaffolds.(Larrañaga et al., 2014; Wang et al., 2014) Synthetic bioceramics, in particular calcium phosphates, have demonstrated high biocompatibility, osteoconductivity, and osteoinductivity. These ceramics seek to mimic the natural hydroxyapatite (HA) crystal formation found in bone.(Hench & Paschall, 1973; Hench et al., 1971; Pallua & Suschek, 2010) Recently, silicon-based glass-ceramics, have been explored as an alternative to calcium phosphates. Some members of this group have demonstrated desirable mechanical strength, high bioactivity, and have been shown to enhance cell adhesion, proliferation, and mineralization of extracellular matrix.(Gu et al., 2011; Kotobuki et al., 2005; Liu et al., 2008a)

Akermanite ($Ca_2MgSi_2O_7$), a calcium, magnesium silicate, has been demonstrated to have improved osteogenic properties compared to calcium phosphates ($Ca_3(PO_4)_2$).(Haimi et al., 2008; Sun et al., 2006) These properties may be attributed to the presence of Ca^{2+}, Mg^{2+}, and Si^{4+} ions, which increases recruitment and osteogenic commitment of hASCs.(Gu et al., 2011; Liu et al., 2008a) In addition to superior osteogenic properties, akermanite ($Ca_2MgSi_2O_7$) exhibits a stable degradation rate, an important scaffold design consideration for bone regrowth.(Sun et al.,

[3] Reprinted with the permission of ACS Biomaterials Science &Engineering (Appendix C)

2006; Wu & Chang, 2007b) Structurally similar to akermanite ($Ca_2MgSi_2O_7$), diopside ($CaMgSi_2O_6$) also supports osteoblast culture (Sun et al., 2006) and precipitation of surface apatite.(Iwata et al., 2004a) The inclusion of diopside in Al_2O_3/diopside ceramic composites has been shown to increase calcium deposition in simulated body fluid (SBF).(Zhang et al., 2010b) This may be due to the structural similarities between akermanite and diopside. The structural similarities of each ceramic presented herein can be seen in the crystal structures in order of most three-dimensional to least three-dimensional in Figure 4.1. Although its potential as a biomaterial has only recently been explored, merwinite has also been shown to induce apatite formation(Hafezi-Ardakani et al., 2011) and osteoblast proliferation. (Ou et al., 2008) Monticellite has been shown to possess similar properties, increasing apatite formation in simulated body fluid (SBF) and stimulating osteoblast growth and adhesion *in vitro*. (Chen et al., 2008)

While possessing favorable characteristics for osteoinduction, the clinical translation of such bioactive glass-ceramics is severely limited by their brittle nature in pure form. However, these mechanical limitations may be overcome by the fabrication of ceramic-polymer composites. The inclusion of a polymer phase lends mechanical strength and tunable rheological properties.(Zanetti et al., 2012a) Combined with the osteoconductive and osteoinductive properties of bioactive ceramics, a more clinically relevant scaffold, graft or augment can be fabricated.(Zanetti et al., 2013a) Natural compounds, including collagen and chitosan have been employed in such composites.(Peter et al., 2010; Rodrigues et al., 2003) However, the ability to control the chemical composition, as well as mechanical and biological properties make biocompatible synthetic polymers a potentially more desirable alternative. Polycaprolactone

(PCL), an FDA-approved material, displays high biocompatibility and a low degradation rate, making it an ideal polymer phase for the slow growth process of bone regeneration.(Zanetti et al., 2012a; Zanetti et al., 2013a)

Over 200,000 liposuction procedures are performed in the United States annually, and from the resulting lipoaspirate, a great deal of hASCs can be derived. Multipotent hASCs have been demonstrated to have similar morphology and differentiation capacity to those mesenchymal stem cells isolated from bone marrow.(Levi & Longaker, 2011a) The hASCs are capable of differentiating along the adipocyte, chondrocyte, neuronal, osteoblast, and skeletal myocyte pathways. Abundant bone tissue engineering studies, as well as clinical trials, have been conducted and shown impressive results by using hASCs.(Aksu et al., 2008; Cui et al., 2007; Gabbay et al., 2006; Gimble et al., 2007; Yoon et al., 2007)

Herein, we present the preparation and comparison of composite polymer-ceramic biodegradable materials composed of diopside ($CaMgSi_2O_6$), akermanite ($Ca_2MgSi_2O_7$), monticellite ($CaMgSiO_4$), and merwinite ($Ca_3MgSi_2O_8$). Each ceramic was synthesized, characterized via X-ray diffraction, and incorporated into composite PCL:ceramic scaffolds. Mechanical testing was used to determine compressive yield strength and Young's modulus for each scaffold. Human adipose-derived stem cells (hASCs) viability and *in vitro* osteogenesis were evaluated for each composite scaffold through extractive studies. To confirm osteogenic properties, metabolic activity, calcium deposition, DNA content, and osteogenic markers alkaline phosphatase (*ALP*) and osteocalcin (*OCN*), were quantified.

4.2. Materials and Methods

4.2.1. Synthesis of diopside ($CaMgSi_2O_6$), akermanite ($Ca_2MgSi_2O_7$), monticellite ($CaMgSiO_4$), and merwinite ($Ca_3MgSi_2O_8$)

Diopside ($CaMgSi_2O_6$), akermanite ($Ca_2MgSi_2O_7$), monticellite ($CaMgSiO_4$), and merwinite ($Ca_3MgSi_2O_8$) were synthesized by conventional ceramic methods with $CaCO_3$ (99.95%), $MgCO_3$ (98.95%), and SiO_2 (99.999%). All reagents were stoichiometrically weighed, mixed, and grounded in an agate mortar and pestle (~ 20 min.), and powders were pressed into ~1 cm pellets and annealed in alumina boats. After an initial calcination at 950 °C at a rate of 100 °C/h for 48 h, multiple heat treatments were carried out up to 1300 °C at a rate of 100 °C with intermediate grinding and re-pelletizing until reaching phase equilibrium. Monticellite ($CaMgSiO_4$) was obtained with heat treatments up to 1100 °C. Figure 4.1 shows the crystal structures of the four ceramic materials considered in this work.

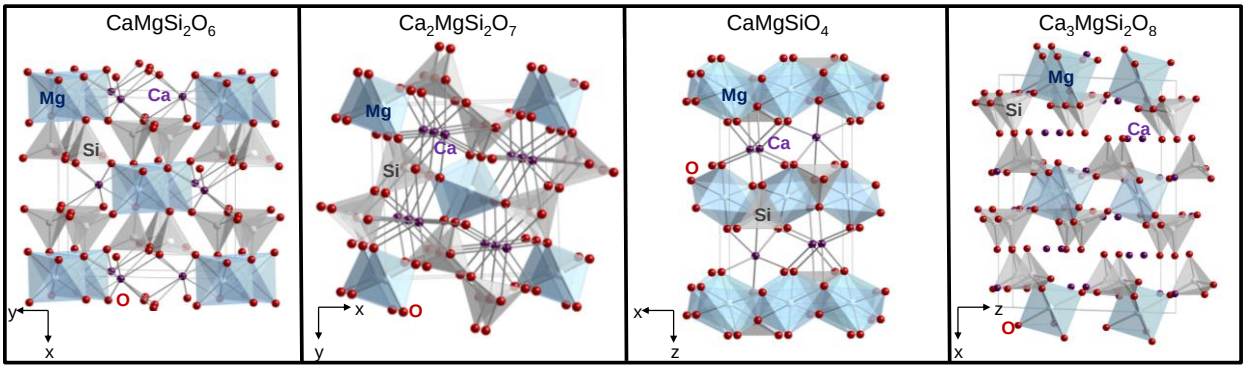

Figure 4.1 Crystal structures of $CaMgSi_2O_6$, $Ca_2MgSi_2O_7$, $CaMgSi_2O_4$, and $Ca_3MgSi_2O_8$. Purple spheres are Ca, red spheres are O, grey and blue polyhedra are Si and Mg, respectively.

4.2.2 Characterization of ceramics by powder X-ray diffraction

Diopside ($CaMgSi_2O_6$), akermanite ($Ca_2MgSi_2O_7$), monticellite ($CaMgSiO_4$), and merwinite ($Ca_3MgSi_2O_8$) were characterized by powder X-ray diffraction using a Bruker D8

Advance X-ray diffractometer operating at 40 kV and 30 mA with a Cu Kα radiation source with a LYNXEYE XE detector. X-ray diffraction data were collected using Bragg Brentano geometry from 2θ of 10° to 80° using a step size of 0.02 at a rate of 1s per step. Phase purity was determined from calculated powder diffraction patterns.(Clark et al., 1969; Kuz'micheva et al., 1995; Moore & Araki, 1972; Subbotin et al., 2008) The model of X-ray data (Table 4.1) of diopside ($CaMgSi_2O_6$), akermanite ($Ca_2MgSi_2O_7$), monticellite ($CaMgSiO_4$), and merwinite ($Ca_3MgSi_2O_8$) were refined using TOPAS 4.2.[8]

Table 4.1 Unit cell parameters of akermanite ($CaMgSi_2O_6$), diopside ($Ca_2MgSi_2O_7$), monticellite ($CaMgSiO_4$), and merwinite ($Ca_3MgSi_2O_8$)

Unit Cell Parameters				
Compound	$CaMgSi_2O_6$	$Ca_2MgSi_2O_7$	$CaMgSiO_4$	$Ca_3MgSi_2O_8$
System	monoclinic	tetragonal	orthorhombic	monoclinic
Space Group	$C2/c$	$P\bar{4}2_1m$	$Pbnm$	$P2_1/c$
a (Å)	9.74825(48)	7.9087(42)	4.7977(17)	13.1745(66)
b (Å)	8.92577(43)	-	11.0409(43)	5.2694(20)
c (Å)	5.25162(24)	5.0458(27)	6.3556(22)	9.3006(41)
β (°)	105.8862(30)	-	-	92.004(40)
V (Å^3)	439.495(37)	316.17(38)	336.66(21)	645.26(49)

4.2.3 Fabrication of ceramic scaffolds

Diopside ($CaMgSi_2O_6$), akermanite ($Ca_2MgSi_2O_7$), monticellite ($CaMgSiO_4$), and merwinite ($Ca_3MgSi_2O_8$) powders (~1 g) were used to prepare the pure ceramic scaffolds as previously described. The polyurethane foam templates 5 mm (height) x 10 mm (diameter) filled

with diopside, akermanite, monticellite and merwinite slurry mixtures were incubated overnight at 60 °C.

This was followed by annealing at 500 °C for 5 hours (after ramping up at a rate of 50 °C/h from room temperature.) in a box furnace, yielding porous diopside, akermanite, monticellite and merwinite scaffolds.

4.2.4 Fabrication and characterization of PCL and PCL:ceramic scaffolds

Fabrication of PCL and PCL:ceramic scaffolds

A 10% (wt/vol) PCL solution in 10 mL of 1,4- dioxane was prepared. Akermanite, merwinite, monticelite, and diopside were added to PCL individually at different weight ratios in a PDMS mold with 10 mm x 5 mm wells, frozen overnight at -80 ^{o}C and lyophilized in a freeze-drier for 24 hours before use.

Micro-CT analysis and pore size determination

Two-dimensional (2-D) microcomputed tomography (μ-CT) imaging on pure akermanite, monticellite, and diopside scaffolds was performed (40 kV and 540 ms) to obtain 0.04 mm slices every 0.9° throughout a 360° rotation (SkyScan 1074, Skyscan n.v., Belgium). Three-dimensional (3-D) files were reconstructed from 2-D images. Volume renderings were generated through AVIZO 7.0.1 (Visualization Services Group)(Chen et al., 2014). Pore size was measured through AVIZO 7.0.1 as well. Merwinite scaffolds were too fragile to image.

4.2.5 Porosity calculation based on micro-ct

To analyze the three-dimensional data, two dimensional slices were read into a custom MATLAB code. For each slice the grayscale image was thresholded using Otsu's method (Otsu,

1975) and then converted into a binary image. Morphological operations were performed to remove small imaging artifacts, and isolate interior and exterior pores(Chen et al., 2014). After quantifying solid and void pixels, porosity was calculated as follows: $\emptyset = \frac{V_{pores}}{V_{pores}+V_{solid}} \times 100\%$

4.2.6 Compression test

Composite and PCL composite scaffolds, molded into a 5 mm (height)×10 mm (diameter) cylinder shape, were subjected to compression strain and the ultimate compressive strain tests. Results were reported at 80 percent elongation at a compression rate of 1mm/min. Five samples were tested for each group. The compressive strain of pure ceramic scaffolds was reported when the samples reached the failure point using an Instron Mechanical Test System 5696, at an extension rate of 0.5 mm/min.(Garber et al., 2013b)

4.2.7 Inductively coupled plasma atomic emission spectroscopy (ICP-OES)

0.1 gram of each ceramic were gas sterilized and then extracted in 5 mL of stromal media for 7 days (n=3) at 37 ^{o}C. The supernatants were then collected and filtered through 0.22 μm sterile filters after centrifugation of media from undissolved ceramic. Prior to elemental analysis (ICP-OES), solutions were acidified with 1 mL of nitric acid, transferred to weighed ICP-OES tubes, agitated for 2.5 h and diluted to a final volume of 10 mL with DI water. The final vials were massed and run on a Varian Vista MPX.(Smoak et al., 2014)

4.2.8 hASCs isolation and culture

Liposuction aspirates from subcutaneous adipose tissue were obtained from at least three donors. All tissues were obtained with informed consent under a clinical protocol reviewed and approved by the Institutional Review Board at the Pennington Biomedical Research Center.

Isolation of hASCs was performed according to previous work.(Gimble et al., 2010) The initial passage of the primary cell culture was referred to as "Passage 0" (p0). The cells were passaged after trypsinization and plated at a density of 5,000 cells/cm^2 (''Passage 1'') for expansion on T125 flasks in order to attain 80% confluency.(Garber et al., 2013b)

4.2.9 Extract cytotoxicity

Ceramic extractives from the degradation test were filtered (0.22 μm pore size) and pipetted (100 μL/well) into a 96-well plate previously sub-cultured with hASCs (2,500 cells/well) and incubated in a CO_2 incubator at 37 °C containing 5% CO_2 for 24 hours. The cellular viability on scaffold cultures was determined using the alamarBlue® assay. 10 μL alamarBlue® reagent was added to each well which were then re-incubated at 37 °C in 5% CO_2 for 2 hours. The fluorescence was measured using a fluorescence plate reader at an excitation wavelength of 530 nm and an emission wavelength of 595 nm. The tissue culture treated plastic 96-well plate served as a control substrate.(Garber et al., 2013b)

4.2.10 hASCs loading on scaffolds and culture

5 μL (1.0 × 104 cells/μL) of Passage 2 from each donor (n = 3) were pooled and directly loaded on the top of each sample. After 30 min of incubation at 37 °C and 5% CO_2, the opposite side of each sample was loaded with the same number of cells by the same approach. Experimental groups included: Ceramics (akermanite, merwinite, monticellite, or diopside):PCL, 75:25; 50:50; 25:75; and pure PCL, 0:100. Scaffolds loaded with hASCs were immediately transferred to new 48-well plates and cultured in stromal media (DMEM, 10% FBS, and 1% triple antibiotic solution) for 3 days followed by sample collection to assess cell viability with alamarBlue® stain.

4.2.11 In vitro hASCs viability on scaffolds with alamarBlue® stain

The viability of cells within the scaffolds in stromal media was determined after 3 days using an alamarBlue® metabolic activity assay. The scaffolds were removed from culture, washed three times in PBS, and incubated with 10% alamarBlue® in Hank's balanced salt solution (HBSS) without phenol red (pH 7) for 90 min. Aliquots (100 μL) of alamarBlue®/HBSS were placed in a 96-well plate in triplicate, and the fluorescence was measured at an excitation wavelength of 530 nm and an emission wavelength of 595 nm using a fluorescence plate reader.(Zanetti et al., 2012a)

4.2.12. Osteogenic extract study

Each of the ceramics were suspended in DMEM F12 (0.5 g in 50 Ml) and placed on a shaker at medium speed for 7 days at 37 ^{o}C. After this time period, each solution containing ionic products from the ceramics dissolution was filtered with sterile 0.22 μm filters and normalized to a 7.0 Ph. The media were then supplemented with 10% FBS and 1% triple antibiotics. HASCs were cultured in stromal medium, osteogenic medium, and the adjusted ceramic extractives for 21 days. The alamarBlue® conversion was measured at 7, 14, and 21 days. Culture medium was removed from each scaffold, which was then washed three times in phosphate buffered saline (PBS) and incubated with 10% alamarBlue® in Hank's balanced salt solution (HBSS) without phenol red (Ph 7) for 120 minutes. The fluorescence of three aliquots (100 μL) from each scaffold was measured at an excitation wavelength of 530 nm and an emission wavelength of 595 nm using a fluorescence plate reader (Wallac 1420 multilabel hts counter). HASCs calcium deposition (cells cultured with stromal, osteogenic medium and ceramic extractives) was assessed after 7, 14, and 21 days of culture by alizarin red staining.

Wells of sterile tissue culture plates containing the cultured hASCs were washed with 0.9% NaCl and fixed with 10% formaldehyde for 10 minutes at RT. Wells were then stained with 2% alizarin red for 10 minutes and washed with DI water three times to remove excess stain, avoiding damage to the cells. Wells were then destained with 10% cetylpyridinium chloride monohydrate for 4 hours at room temperature with constant agitation. Total DNA content was used to determine the cell count on each scaffold as previously described.(Liu et al., 2008a) 0.5 Ml proteinase K (Sigma-Aldrich) at a concentration of 0.5 mg/Ml were added to each well, and plates were kept at 56 ºC overnight to lyse the hASCs and release DNA. Aliquots (50 µL) were mixed with equal volumes of 0.1 g/Ml Picogreen dye solution in 96-well plates. Samples were then excited at 480 nm with a plate reader. Samples prepared without cells were used as blank controls. Total RNA was extracted from cell-scaffold constructs as previously described.(Zanetti et al., 2012a) Total RNA to Cdna EcoDry Premix (ClonTech) was used for Cdna synthesis. Qrt-PCR was performed using 2× iTaq™ SYBR® green supermix with ROX (Biorad) and primers for alkaline phosphatase (*ALP*) and osteoscalcin (*OCN*)(Zanetti et al., 2012a) to quantify osteogenic target gene expression of hASCs loaded onto the scaffolds and cultured in either stromal or osteogenic media for 7, 14, and 21 days. Reactions were performed with a MJ Mini™ Thermal Cycler (BioRad). The sequences of PCR primers (forward and backward, 50-30) were as follows: ALP, 5'-AATATGCCCTGGAGCTTCAGAA-3' and 5'-CCATCCCATCTCCCAGGAA-3';OCN, 5'-GCCCAGCGGTGCAGAGT-3' and 5'-TAGCGCCTGGGTCTCTTCAC-3'.Samples were normalized (ΔCt) against the house keeping gene 18S Rrna and the – ΔΔCt value of *ALP* and *OCN* in scaffolds cultured in osteogenic and control media was calculated using the ΔΔCt method.(Livak & Schmittgen, 2001a)

4.2.13. Statistical analysis

All results were expressed as mean ± SEM. Data was analyzed with one-way analysis of variance (ANOVA), followed by Tukey's minimum significant difference (MSD) post hoc test for pairwise comparisons of main effects. For all comparisons, a P-value < 0.05 was considered significant. All significant differences among groups have been mentioned in the results and discussion section.

4.3. Results and Discussion

4.3.1 Powder X-ray diffraction

A minor impurity is observed and the results indicate the phase targeted. The diffraction results of the targeted $CaMgSiO_4$ resulted in a two phase refinement of monticellite (95.9%) and merwinite (4.10%). Multiple subsequent heat treatments up to 1100 °C led to the increasing stability of merwinite. Figure 4.2 shows the X-ray powder diffraction patterns of diopside ($CaMgSi_2O_6$), akermanite ($Ca_2MgSi_2O_7$), monticellite ($CaMgSiO_4$), and merwinite ($Ca_3MgSi_2O_8$).

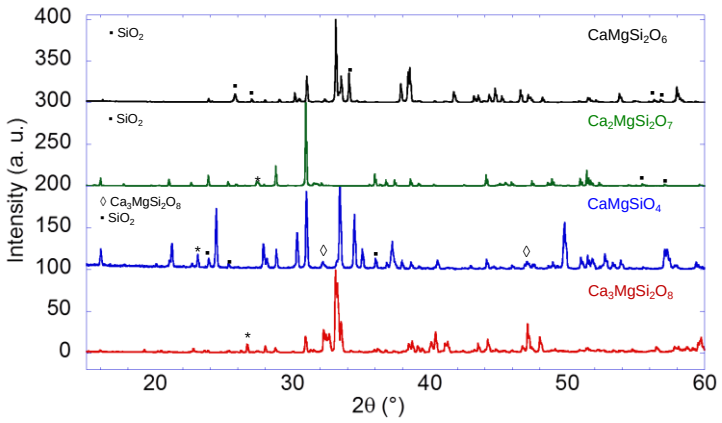

Figure 4.2 Powder X-ray diffraction patterns of $CaMgSi_2O_6$ (black), $Ca_2MgSi_2O_7$ (green), $CaMgSi_2O_4$ (blue), and $Ca_3MgSi_2O_8$ (red). * represents unidentified reflections

4.3.2 Micro-Ct and porosity analysis of 100% ceramic scaffolds (Figure 4.3)

Micro-CT images and porosity analysis revealed that monticellite was the most porous ceramic scaffold (34.17±13.07), followed by diopside (33.99±11.89), and akermanite (32.41±11.32). There does not appear to be any significant difference in the porosity of these scaffolds. The average pore size of diopside, akermanite and monticellite scaffolds is 0.844±0.157 mm, 0.838±0.172 mm, and 0.844±0.178 mm respectively. These results suggest that the differences in mechanical strength between the ceramic scaffolds are due to differences in three-dimensionality and crystal structure, not to the porosity of the material.

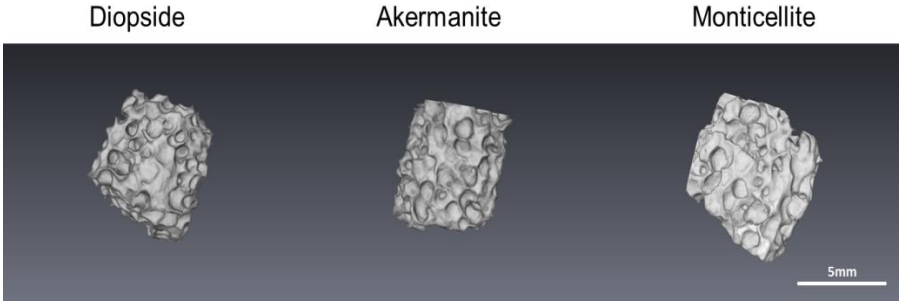

Figure 4.3 Micro-CT analysis of 100% ceramic scaffolds made diopside, akermanite and monticellite

4.3.3 Compression analysis of 100% ceramic scaffolds

The 100 % ceramic scaffolds showed significant differences in compressive strength from one another, as shown in Figure 4.4. Among the pure ceramic scaffolds, diopside ($CaMgSi_2O_6$) scaffolds had the greatest compression strength (0.27 MPa), twice as strong as to akermanite ($Ca_2MgSi_2O_7$) with 0.12 MPa and six times stronger than monticellite ($CaMgSi_2O_4$)(0.04 MPa) scaffolds.

The compressive strength was significantly different between all groups. Merwinite ($Ca_3MgSi_2O_8$), in sharp contrast to diopside, was powdery after the annealing of poly-urethane and poly vinyl alcohol, yielding 0 MPa compression strength.

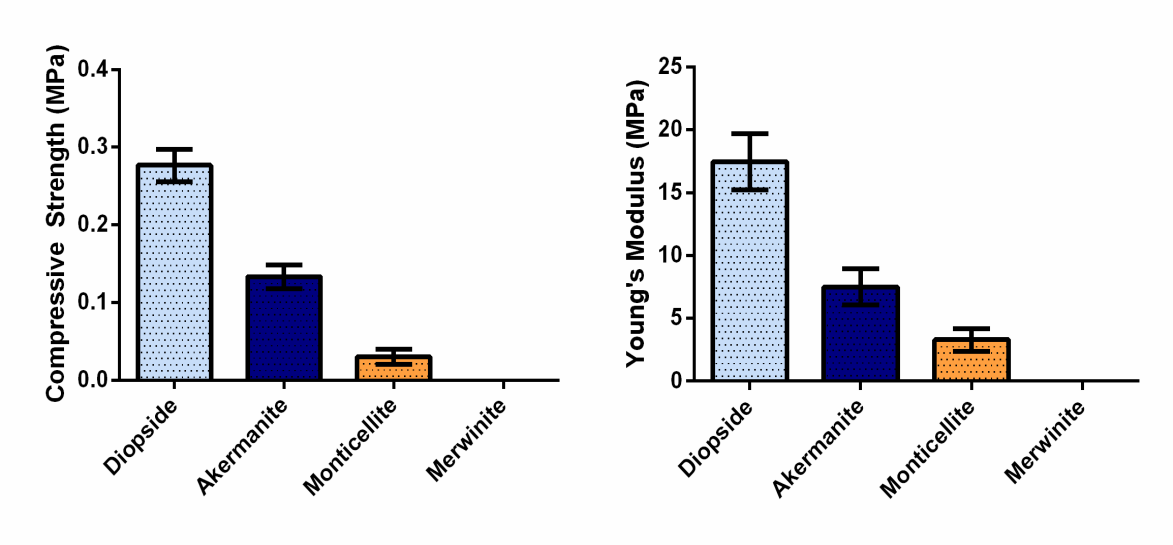

Figure 4.4 Compressive strength and Young's modulus of 100% ceramic scaffolds made with diopside, akermanite, monticellite and merwinite respectively.

Diopside is monoclinic, akermanite is tetragonal, and monticellite and merwinite are octahedral and monoclinic, respectively(Wu & Chang, 2007b) These differences in structural dimensionality of the four silicates most likely contribute to differences in degradation and mechanical strength. Merwinite's insubstantial three-dimensional structure may explain its low mechanical strength, ruling it out as a viable candidate for bone scaffold composites.

4.3.4. ICP-OES (Figure 4.5)

The Ca, Mg and Si concentrations in $CaMgSi_2O_6$, $Ca_2MgSi_2O_7$, and $CaMgSiO_4$ extractives were significantly higher in the ceramic experimental groups than in the stromal medium control.

Crystal structure may affect the degradation rates of the ceramics, leading to differences in their subsequent release profiles.(Ducheyne et al., 1993; Radin & Ducheyne, 1994) Additionally, diopside, akermanite, and monticellite absorb over 50% of phosphorus from stromal medium. Merwinite precipitates almost all of the phosphorus as well as the magnesium from stromal medium.

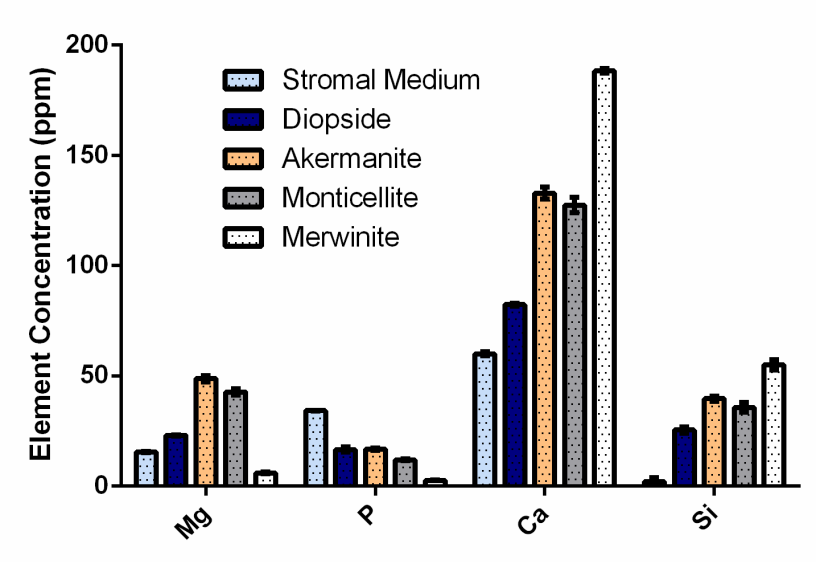

Figure 4.5 ICP-OES analysis of ceramic extractives from diopside, akermanite, monticellite and merwinite.

4.3.5 Compression test of ceramic/PCL scaffolds

Compressive strength of all types of ceramic/PCL scaffolds are reported in Figure 4.6. In general, PCL/ceramic composite scaffolds reach highest compressive strength at a 75:25 ratio of PCL to ceramics. Further increasing the amount of ceramics to 50% in the PCL/ceramic composite scaffolds causes the compressive strength to decrease. When the ceramic ratio reaches 75% in the composite scaffolds, the compressive strength of scaffolds drops below 0.02MPa regardless of the ceramic type.

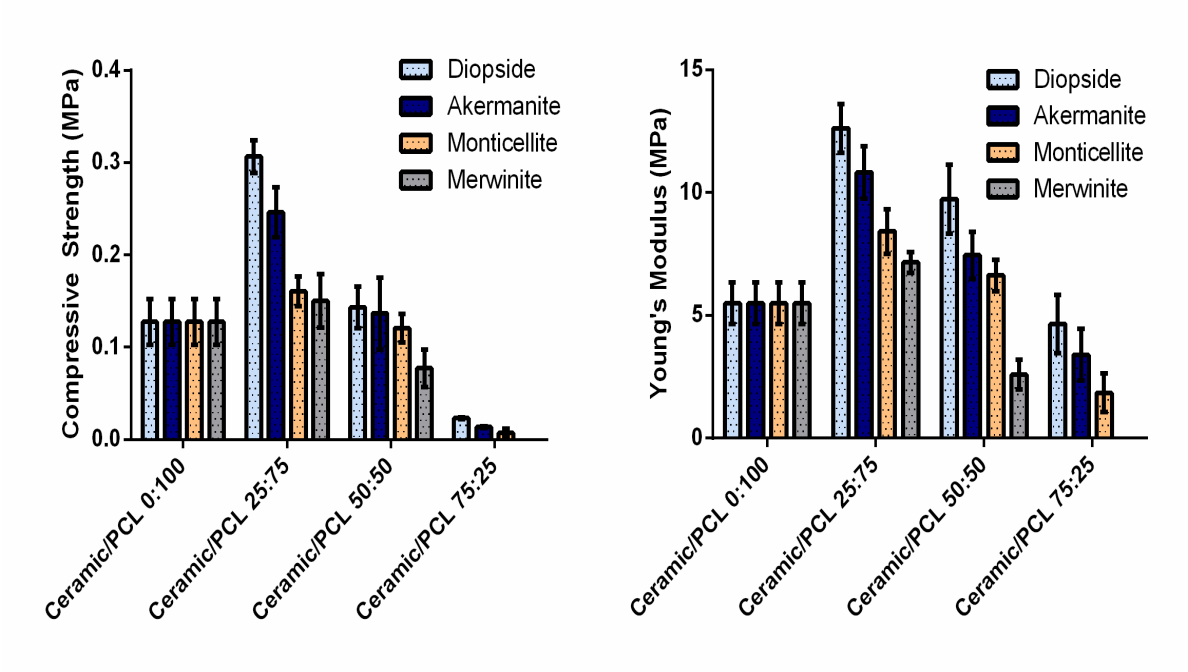

Figure 4.6 Compressive strength and Young's modulus of PCL: ceramic composite scaffolds

It should be noted that merwinite/PCL, 75:25 scaffolds maintain little integrity during normal handling and were consequently difficult to measure under compression test conditions due to its low mechanical strength. Because all of the composite scaffolds were made via a thermal-precipitation method, the ceramic phases tended to precipitate to the lower part of the PCL/ceramic mixture in 1,4-dioxane. Phase separation may explain why the mechanical strength of PCL/ceramic scaffolds decrease dramatically when ceramics comprise over 25% of the composite.

When compared, the compressive strength of PCL/ceramic (75:25) composite scaffolds followed a trend similar to that of the pure ceramic scaffolds. PCL/diopside (75:25) composite scaffolds exhibit the greatest mechanical strength, followed by PCL/akermanite (75:25), PCL/monticellite (75:25), and PCL/merwinite (75:25) composite scaffolds. PCL/ceramic (50:50)

scaffolds all exhibited similar mechanical properties, indicating that varying concentrations of PCL affects the performance of ceramics in the scaffolds.

4.3.6 Viability of hASCs after acute exposure (24 hours) to the seven-day media extractives of different ceramic powders

alamarBlue® assay was used to determine the effect of ceramic component ions on hASCs metabolic activity when cultured in the ceramic extracts (Figure 4.7). Cells exposed to diopside extract and akermanite extract showed 80 % metabolic activity compared to the control, which was cultured in stromal medium containing no ceramic extracts. There were no statistical differences shown between the metabolic activity of hASCs cultured in diopside extracts, akermanite extracts and monticellite extracts. However, hASCs cultured in merwinite extracts were shown to exhibit significantly lower metabolic activity than those cultured in diopside extracts, akermanite extracts, and the control. Even so, the cells cultured in merwinite extracts showed above 70% relative metabolic activity.

4.3.7. Viability of hASCs on scaffolds for 3 days in stromal media

After characterization of the effects of ceramic extracts on hASCs cultured on sterile tissue culture plates, the viability of cells cultured on PCL scaffolds containing varying concentrations of ceramic additives was measured (Figure 8). Results from the alamarBlue®metabolic assay showed that the diopside and akermanite composites showed no significant difference from the control containing no ceramic additives. Composite scaffolds containing diopside and akermanite were shown to support the highest levels of relative hASCs metabolic activity.

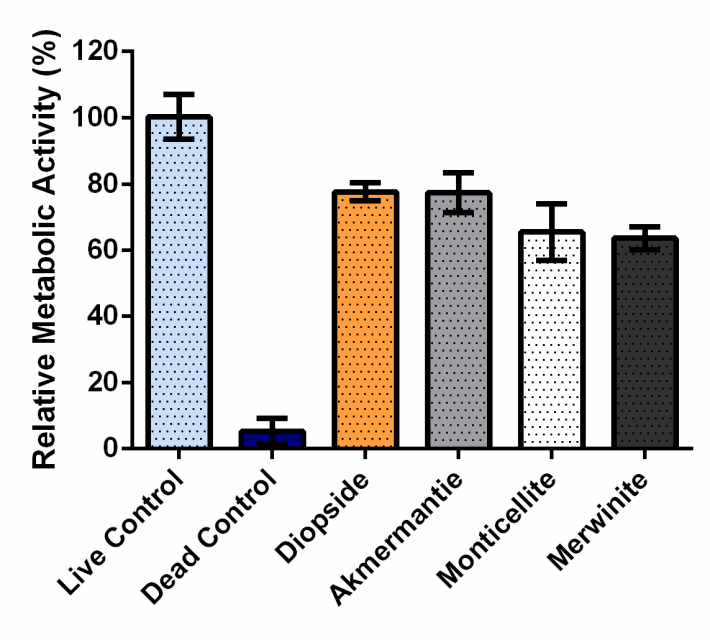

Figure 4.7 Viability of hASCs after acute exposure (24 hours) to the 7 days media extractives of different ceramic powder. *, significantly different, P<0.05

The merwinite additives at 25% and 50% as well as the monticellite additives at 25% and 75% displayed no statistical differences in metabolic activity from the scaffold control containing no ceramics. The merwinite additives at 75% formed a scaffold with very poor mechanical strength and unstable structure. It failed to support hASCs growth, likely due to its rapid degradation in stromal medium.

4.3.8. Osteogenesis study of hASCs cultured with ceramic extractives

Alizarin red staining was performed to evaluate the mineral deposition of hASCs cultured with ceramic extractives (Figure-4.9A). All groups showed peak mineralization at 21 days of culture.

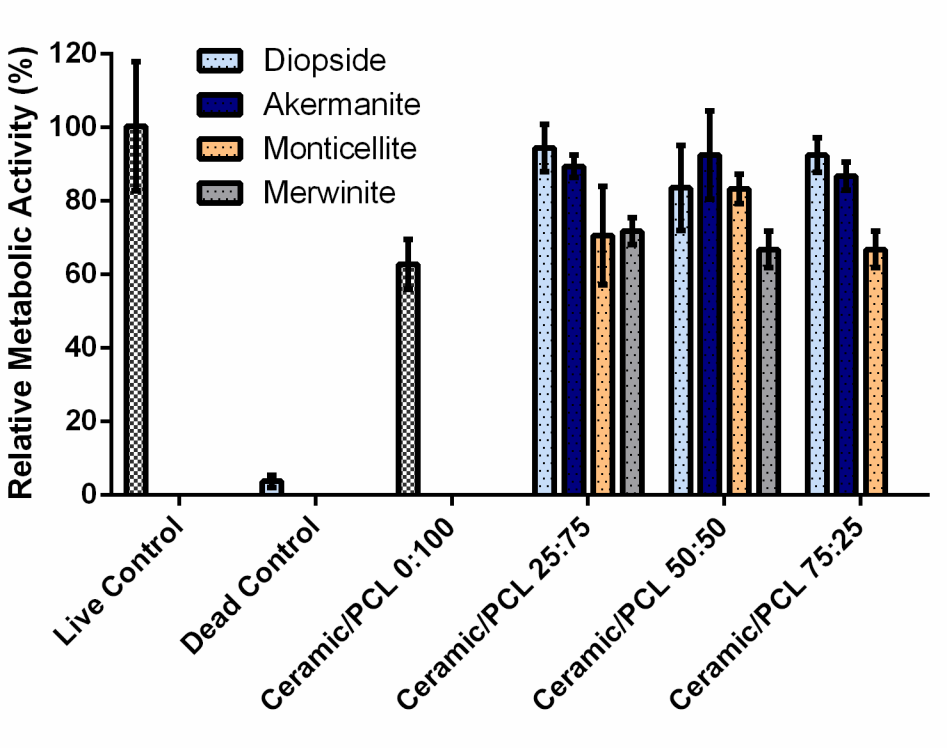

Figure 4.8 Viability of hASCs on Scaffolds for 3 days in Stromal Media

Among the ceramic groups, hASCs cultured with akermanite extractives showed the highest level of calcium deposition, followed by monticellite and diopside. Merwinite exhibited the lowest level of calcium deposition, lower than stromal medium negative control. Each of the ceramic extractives displayed significantly lower osteogenic induction based on calcium deposition in comparison to the positive control, osteogenic medium. qRT-PCR was performed to assess the expression of commonly used osteogenic stage markers and total DNA content was quantified using Quant-iT™ PicoGreen®, to analyze the hASCs proliferation in each group.(Burge et al., 2007) The activation of genes such as *ALP* and *OCN*, indicative of osteoblast activity, is the result of the osteogenic regulation and action on the transcription factor core binding factor alpha1 (Cbfa1) by bone morphogenic proteins (BMPs).(Liu et al., 2008a; Milat & Ng, 2009) *ALP* expression was measured 7 days after culture and *OCN* expression was measured

after 14 and 21 days (Figure 4.8B). Both *ALP* and *OCN* up-regulation was observed in cultures containing diopside, akermanite and monticellite extractives. Conversely, hASCs culture containing merwinite extractives exhibited down regulation of *ALP* and *OCN* in comparison to the stromal medium group. Among the ceramic groups, akermanite demonstrated the highest *ALP* and *OCN* expression levels, followed by monticellite and diopside. This trend was in accordance with calcium deposition levels. The metabolic activity (Figure 4.9C) and proliferation (Figure 4.9D) of hASCs cultured in stromal medium, osteogenic medium, and ceramic extractives was also studied. Osteogenic medium displayed the lowest metabolic activity at both 7 and 14 day time points. Calcium deposition and qRT-PCR data suggests that the hASCs were committed to an osteogenic lineage at these time points, which has been demonstrated to decrease metabolic activity.(Qureshi et al., 2013; Zanetti et al., 2012a) For the same reason, akermanite and monticellite groups also exhibited decreased metabolic activity compared to diopside and merwinte groups. Merwinite still shows a significant decrease in metabolic activity 21 days after culture and a decrease in total cell number, as indicated by total DNA analysis (Figure 4.9D). Merwinite appeared to have a significantly decreased total cell number at 21 days due to cell death. Merwinite still shows a significant decrease in metabolic activity 21 days after culture and a decrease in total cell number, as indicated by total DNA analysis (Figure 4.9D). Merwinite appeared to have a significantly decreased total cell number at 21 days due to cell death. The most distinct difference in DNA content was seen between stromal medium and osteogenic medium.

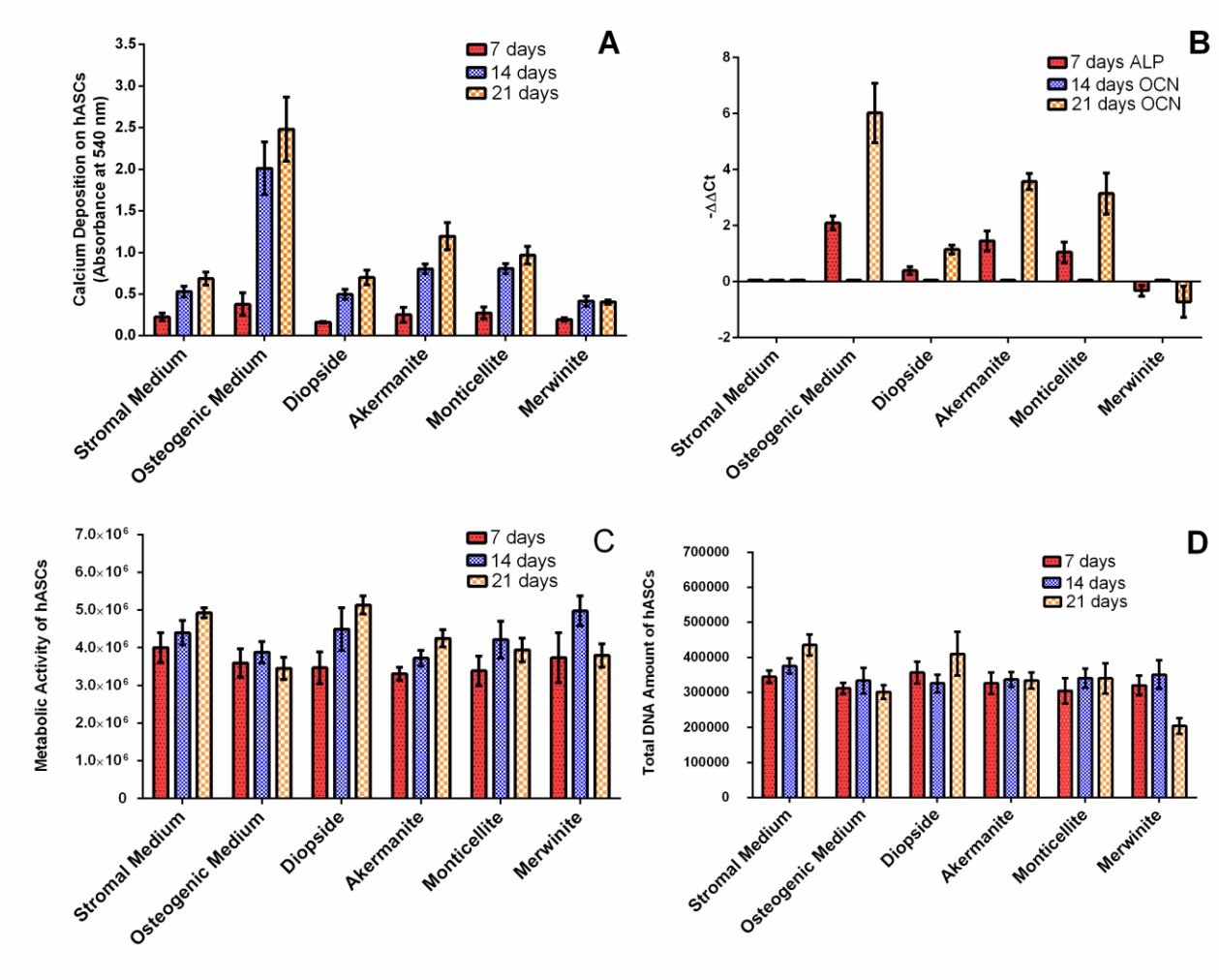

Figure 4.9 Osteogensis study. A: calcium depostion of hASC cultured with diopside, akermanite, monticellite and merwinite extractives repectively; B: q-rtPCR analysis of ALP (7 day) and OCN (14 and 21 day) expression from hASC cultured with diopside, akermanite, monticellite and merwinite extractives repectively; C: metabolic activity hASC cultured with diopside, akermanite, monticellite and merwinite extractives repectively; D:total DNA amount of hASC cultured with diopside, akermanite, monticellite and merwinite extractives repectively.

When correlated with calcium deposition, gene expression, and metabolic activity, the steady number of cells between 7 and 21 indicates that hASCs have a lower proliferation rate when committed to an osteogenic lineage. Akermanite and monticellite showed similar to trends to osteogenic medium, further indicating similar osteogenic pathways are activated by the media and ceramic induction.

The hASC cultured in ceramic extractives has lower levels of osteogenic marker expression compared to the positive control group, osteogenic medium. One hypothesis is that this phenomena is related to the amounts of phosphorus absorption in the ceramics. Phosphorus is important for cellular structure and function.(DiBartola & Willard, 2006) Phosphorous influx into osteoblasts by means of a sodium-dependent phosphate co-transporter mechanism has recently shown to trigger osteopontin mRNA and protein synthesis and to subsequently regulate mineralization.(Beck et al., 2000) In addition, different ceramics release varying amounts of calcium, magnesium and silicon, which are the crucial elements that stimulate gene transcription during osteogenesis.(Gu et al., 2011) It is well known that calcium plays a crucial role in the process of bone mineralization. However, the ability for extracellular calcium to regulate cell-specific responses has not been proven until recently.(Yamaguchi et al., 1998) Increased extracellular calcium binding to G-protein-coupled extracellular calcium-sensing receptors has been previously shown to induce osteoblast proliferation and chemotaxis. (Xynos et al., 2001) Silicon plays a role in cross-linking glycosaminoglycan molecules with collagen and the mineralization of human primary osteoblasts.(Seaborn & Nielsen, 2002) Likewise, Mg has a close relationship with the bone tissue mineralization,(Di Mario et al., 2004; Kim et al., 2003b; LeGeros, 1990) and Mg-substituted tricalcium phosphate, has been demonstrated to stimulate adhesion and proliferation of human osteoblast cells compared to calcium phosphate controls.(Sader et al., 2009) While merwinite was shown to release the greatest amount of calcium, it also absorbed a high level of phosphorus from stromal medium, which led to cell death and impeded the osteogenic differentiation. It is likely that as a result of severe hypophosphatemia in merwinite extractives, exposed hASCs have osteogenic failure and cell

death in 21 days. Furthermore, the increased level of silicon released by merwinite may be responsible for the inhibition of cell proliferation observed.(Wu & Chang, 2007b) High silicone concentration could induce cellular vacuole formation,(Valerio et al., 2004) which is often associated with apoptosis or cell degeneration.(Serre et al., 1998) Diopside, on the other hand, released only 44.8% of the magnesium and 61.3% of the calcium when normalized to release from akermanite. Lower levels of these crucial ions may have led to the decreased osteogenic properties observed.

4.4. Conclusion

The dimensionality of the crystal structure of ceramics plays an important role in the fabrication of ceramic/polymer composite scaffolds. Increased three-dimensionality allows for better stability and higher mechanical strength of the ceramic scaffolds, as well as limiting scaffold phosphorous absorption from the environment. Furthermore,composite scaffolds provide greater stability to support hASCs attachment and growth than pure ceramics. The composites containing ceramics were also shown to degrade more slowly and maintain a relatively intact structure after prolonged exposure to cell medium compared to polymer scaffolds without ceramic additives as well as pure ceramic scaffolds. Overall, akermanite and monticellite-containing composites exhibit better osteogenic properties than those containing diopside and merwinite, suggesting that they might be the better ceramics for fabricating tissue engineered bone scaffolds.

4.5 References

Aksu, A.E., Rubin, J.P., Dudas, J.R., Marra, K.G. 2008. Role of gender and anatomical region on induction of osteogenic differentiation of human adipose-derived stem cells. *Annals of plastic surgery*, **60**(3), 306-322.

Beck, G.R., Zerler, B., Moran, E. 2000. Phosphate is a specific signal for induction of osteopontin gene expression. *Proceedings of the National Academy of Sciences*, **97**(15), 8352-8357.

Burge, R., Dawson-Hughes, B., Solomon, D.H., Wong, J.B., King, A., Tosteson, A. 2007. Incidence and Economic Burden of Osteoporosis-Related Fractures in the United States, 2005–2025. *Journal of Bone and Mineral Research*, **22**(3), 465-475.

Chen, C., Garber, L., Smoak, M., Fargason, C., Scherr, T., Blackburn, C., Bacchus, S., Lopez, M.J., Pojman, J.A., Del Piero, F. 2014. In vitro and in vivo characterization of Pentaerythritol Triacrylate-co-Trimethylolpropane Nanocomposite scaffolds as Potential Bone Augments and Grafts. *Tissue Eng Part A*.

Chen, X., Ou, J., Kang, Y., Huang, Z., Zhu, H., Yin, G., Wen, H. 2008. Synthesis and characteristics of monticellite bioactive ceramic. *J. Mater. Sci. Mater. Med.*, **19**(3), 1257-1263.

Clark, J.R., Appleman, D.E., Papike, J. 1969. Crystal-chemical characterization of clinopyroxenes based on eight new structure refinements. *Mineral. Soc. Am., Spec. Pap.*, **2**, 31-50.

Cui, L., Liu, B., Liu, G., Zhang, W., Cen, L., Sun, J., Yin, S., Liu, W., Cao, Y. 2007. Repair of cranial bone defects with adipose derived stem cells and coral scaffold in a canine model. *Biomaterials*, **28**(36), 5477-5486.

Di Mario, C., Griffiths, H., Goktekin, O., Peeters, N., Verbist, J., Bosiers, M., Deloose, K., Heublein, B., Rohde, R., Kasese, V. 2004. Drug‐eluting bioabsorbable magnesium stent. *Journal of interventional cardiology*, **17**(6), 391-395.

DiBartola, S., Willard, M. 2006. Disorders of phosphorus: hypophosphatemia and hyperphosphatemia. *Fluid, Electrolyte, and Acid-Base Disorders in Small Animal Practice. 3rd edn. Ed S. P. DiBartola. Elsevier Science, St Louis, MO, USA*, 195-209.

Ducheyne, P., Radin, S., King, L. 1993. The effect of calcium phosphate ceramic composition and structure on in vitro behavior. I. Dissolution. *Journal of Biomedical Materials Research*, **27**(1), 25-34.

Gabbay, J.S., Heller, J.B., Mitchell, S.A., Zuk, P.A., Spoon, D.B., Wasson, K.L., Jarrahy, R., Benhaim, P., Bradley, J.P. 2006. Osteogenic Potentiation of Human Adipose–Derived Stem Cells in a 3-Dimensional Matrix. *Annals of plastic surgery*, **57**(1), 89-93.

Garber, L., Chen, C., Kilchrist, K.V., Bounds, C., Pojman, J.A., Hayes, D. 2013. Thiol-acrylate nanocomposite foams for critical size bone defect repair: A novel biomaterial. *J. Biomed. Mater. Res., Part A*, **101**(12), 3531-3541.

Gimble, J.M., Guilak, F., Bunnell, B.A. 2010. Clinical and preclinical translation of cell-based therapies using adipose tissue-derived cells. *Stem Cell Research & Therapy*, **1**.

Gimble, J.M., Katz, A.J., Bunnell, B.A. 2007. Adipose-derived stem cells for regenerative medicine. *Circulation research*, **100**(9), 1249-1260.

Gu, H., Guo, F., Zhou, X., Gong, L., Zhang, Y., Zhai, W., Chen, L., Cen, L., Yin, S., Chang, J., Cui, L. 2011. The stimulation of osteogenic differentiation of human adipose-derived stem cells by ionic products from akermanite dissolution via activation of the ERK pathway. *Biomaterials*, **32**(29), 7023-7033.

Hafezi-Ardakani, M., Moztarzadeh, F., Rabiee, M., Talebi, A.R. 2011. Synthesis and characterization of nanocrystalline merwinite ($Ca_3Mg(SiO_4)_2$) via sol–gel method. *Ceram. Int.*, **37**(1), 175-180.

Haimi, S., Suuriniemi, N., Haaparanta, A.-M., Ellä, V., Lindroos, B., Huhtala, H., Räty, S., Kuokkanen, H., Sándor, G.K., Kellomäki, M. 2008. Growth and osteogenic differentiation of adipose stem cells on PLA/bioactive glass and PLA/β-TCP scaffolds. *Tissue Eng., Part A*, **15**(7), 1473-1480.

Hench, L.L., Paschall, H.A. 1973. Direct chemical bond of bioactive glass-ceramic materials to bone and muscle. *Journal of Biomedical Materials Research*, **7**(3), 25-42.

Hench, L.L., Splinter, R.J., Allen, W.C., Greenlee, T.K. 1971. Bonding mechanisms at the interface of ceramic prosthetic materials. *Journal of Biomedical Materials Research*, **5**(6), 117-141.

Iwata, N.Y., Lee, G.-H., Tokuoka, Y., Kawashima, N. 2004. Sintering behavior and apatite formation of diopside prepared by coprecipitation process. *Colloids Surf., B*, **34**(4), 239-245.

Kim, S., Lee, J., Kim, Y., Riu, D.-H., Jung, S., Lee, Y., Chung, S., Kim, Y. 2003. Synthesis of Si, Mg substituted hydroxyapatites and their sintering behaviors. *Biomaterials*, **24**(8), 1389-1398.

Kotobuki, N., Ioku, K., Kawagoe, D., Fujimori, H., Goto, S., Ohgushi, H. 2005. Observation of osteogenic differentiation cascade of living mesenchymal stem cells on transparent hydroxyapatite ceramics. *Biomaterials*, **26**(7), 779-785.

Kuz'micheva, G., Zharikov, E., Denisov, A. 1995. X-ray structural study of synthetic gehlenites $Ca_2Al(AlSi)O_7$ and akermanites $Ca_2MgSi_2O_7$ doped with chromium ions. *Russ. J. Inorg. Chem.*, **40**(9), 1368-1374.

Larrañaga, A., Diamanti, E., Rubio, E., Palomares, T., Alonso-Varona, A., Aldazabal, P., Martin, F.J., Sarasua, J.R. 2014. A study of the mechanical properties and cytocompatibility of lactide and caprolactone based scaffolds filled with inorganic bioactive particles. *Mater. Sci. Eng., C*, **42**(0), 451-460.

LeGeros, R.Z. 1990. Calcium phosphates in oral biology and medicine. *Monographs in oral science*, **15**, 1-201.

Levi, B., Longaker, M.T. 2011. Concise Review: Adipose-Derived Stromal Cells for Skeletal Regenerative Medicine. *Stem Cells*, **29**(4), 576-582.

Liu, Q., Cen, L., Yin, S., Chen, L., Liu, G., Chang, J., Cui, L. 2008. A comparative study of proliferation and osteogenic differentiation of adipose-derived stem cells on akermanite and β-TCP ceramics. *Biomaterials*, **29**(36), 4792-4799.

Livak, K.J., Schmittgen, T.D. 2001. Analysis of relative gene expression data using real-time quantitative PCR and the $2^{-\Delta\Delta CT}$ Method. *Methods*, **25**(4), 402-8.

Milat, F., Ng, K.W. 2009. Is Wnt signalling the final common pathway leading to bone formation? *Molecular and cellular endocrinology*, **310**(1-2), 52-62.

Moore, P., Araki, T. 1972. Atomic arrangement of merwinite, $Ca_3 Mg (SiO_4)_2$, an unusual dense-packed structure of geophysical interest. *American Mineralogist*, **57**, 1355-1374.

Otsu, N. 1975. A threshold selection method from gray-level histograms. *Automatica*, **11**(285-296), 23-27.

Ou, J., Kang, Y., Huang, Z., Chen, X., Wu, J., Xiao, R., Yin, G. 2008. Preparation and in vitro bioactivity of novel merwinite ceramic. *Biomed. Mater.*, **3**(1), 015015.

Pallua, N., Suschek, C.V. 2010. *Tissue engineering: from Lab to Clinic*. Springer.

Peter, M., Binulal, N.S., Nair, S.V., Selvamurugan, N., Tamura, H., Jayakumar, R. 2010. Novel biodegradable chitosan–gelatin/nano-bioactive glass ceramic composite scaffolds for alveolar bone tissue engineering. *Chemical Engineering Journal*, **158**(2), 353-361.

Qureshi, A.T., Monroe, W.T., Dasa, V., Gimble, J.M., Hayes, D.J. 2013. miR-148b–Nanoparticle conjugates for light mediated osteogenesis of human adipose stromal/stem cells. *Biomaterials*, **34**(31), 7799-7810.

Radin, S., Ducheyne, P. 1994. Effect of bioactive ceramic composition and structure on in vitro behavior. III. Porous versus dense ceramics. *Journal of biomedical materials research*, **28**(11), 1303-1309.

Rodrigues, C.V.M., Serricella, P., Linhares, A.B.R., Guerdes, R.M., Borojevic, R., Rossi, M.A., Duarte, M.E.L., Farina, M. 2003. Characterization of a bovine collagen–hydroxyapatite composite scaffold for bone tissue engineering. *Biomaterials*, **24**(27), 4987-4997.

Sader, M.S., LeGeros, R.Z., Soares, G.A. 2009. Human osteoblasts adhesion and proliferation on magnesium-substituted tricalcium phosphate dense tablets. *Journal of Materials Science: Materials in Medicine*, **20**(2), 521-527.

Seaborn, C., Nielsen, F. 2002. Dietary silicon and arginine affect mineral element composition of rat femur and vertebra. *Biological trace element research*, **89**(3), 239-250.

Serre, C., Papillard, M., Chavassieux, P., Voegel, J., Boivin, G. 1998. Influence of magnesium substitution on a collagen–apatite biomaterial on the production of a calcifying matrix by human osteoblasts. *Journal of biomedical materials research*, **42**(4), 626-633.

Smoak, M., Chen, C., Qureshi, A., Garber, L., Pojman, J.A., Janes, M.E., Hayes, D.J. 2014. Antimicrobial cytocompatible pentaerythritol triacrylate-co-trimethylolpropane composite scaffolds for orthopaedic implants. *J. Appl. Polym. Sci.*, **131**(22), 1-7.

Subbotin, K., Iskhakova, L., Zharikov, E., Lavrishchev, S. 2008. Investigation of the crystallization features, atomic structure, and microstructure of chromium-doped monticellite. *Crystallogr. Rep.*, **53**(7), 1107-1111.

Sun, H., Wu, C., Dai, K., Chang, J., Tang, T. 2006. Proliferation and osteoblastic differentiation of human bone marrow-derived stromal cells on akermanite-bioactive ceramics. *Biomaterials*, **27**(33), 5651-5657.

Valerio, P., Pereira, M.M., Goes, A.M., Leite, M.F. 2004. The effect of ionic products from bioactive glass dissolution on osteoblast proliferation and collagen production. *Biomaterials*, **25**(15), 2941-2948.

Wang, J., Guo, J., Liu, J., Wei, L., Wu, G. 2014. BMP-Functionalised Coatings to Promote Osteogenesis for Orthopaedic Implants. *Int. J. Mol. Sci.*, **15**(6), 10150-10168.

Wu, C., Chang, J. 2007. Degradation, bioactivity, and cytocompatibility of diopside, akermanite, and bredigite ceramics. *J. Biomed. Mater. Res., Part B*, **83**(1), 153-160.

Xynos, I.D., Edgar, A.J., Buttery, L.D.K., Hench, L.L., Polak, J.M. 2001. Gene-expression profiling of human osteoblasts following treatment with the ionic products of Bioglass® 45S5 dissolution. *Journal of Biomedical Materials Research*, **55**(2), 151-157.

Yamaguchi, T., Chattopadhyay, N., Kifor, O., Butters, R.R., Sugimoto, T., Brown, E.M. 1998. Mouse osteoblastic cell line (MC3T3-E1) expresses extracellular calcium (Ca2+o)-sensing receptor and its agonists stimulate chemotaxis and proliferation of MC3T3-E1 cells. *Journal of Bone and Mineral Research*, **13**(10), 1530-1538.

Yoon, E., Dhar, S., Chun, D.E., Gharibjanian, N.A., Evans, G.R. 2007. In vivo osteogenic potential of human adipose-derived stem cells/poly lactide-co-glycolic acid constructs for bone regeneration in a rat critical-sized calvarial defect model. *Tissue Engineering*, **13**(3), 619-627.

Zanetti, A.S., McCandless, G.T., Chan, J.Y., Gimble, J.M., Hayes, D.J. 2012. Characterization of novel akermanite:poly-ε-caprolactone scaffolds for human adipose-derived stem cells bone tissue engineering. *Journal of Tissue Engineering and Regenerative Medicine*.

Zanetti, A.S., McCandless, G.T., Chan, J.Y., Gimble, J.M., Hayes, D.J. 2013. In vitro human adipose-derived stromal/stem cells osteogenesis in akermanite: poly-ε-caprolactone scaffolds. *Journal of biomaterials applications*, **28**(7), 998-1007.

Zhang, M., Liu, C., Zhang, X., Pan, S., Xu, Y. 2010. Hydroxyapatite/diopside ceramic composites and their behaviour in simulated body fluid. *Ceramics International*, **36**(8), 2505-2509.

CHAPTER 5. SUMMARY AND FUTURE WORK

The step growth nature of the amine catalyzed Michael addition reaction alleviated the concern of unreacted monomer or radicals leaching into the body as would typically occur using a chain-growth mechanism involving a free-radical process. *In situ* polymerization opens the opportunity for the development of absorbable foams for the conformal repair of critical sized tissue defects, which can be easily delivered in the clinical surgical setting. This represents a substantial improvement over PCL, which are foamed externally prior to surgical insertion, and methylmethacrylate bone cements, which are largely inert, non-porous, and permanent. The SEM analysis, mechanical testing, and micro CT data prove that there is no distinct difference between the PETA-co-TMPTMP foam made *in situ* and *in vitro*. While this material has many advantages, future work includes the development of a homogenous HA containing polymer network, osteogenic studies and improved mechanical strength of the foamed PETA-co-TMPTMP with varying HA amounts. It is clear that scaffold technology plays a critical role in the success of the current stem cell based bone tissue engineering paradigms. While a variety of different materials, both ceramics and polymers have been tested in combination with hASC, Lendeckel et al. and others note that composite scaffolds may offer a better clinical outcome as a result of improved mechanical and biological properties.(Lendeckel et al., 2004) Calcium phosphate nanoscale ceramic particles of HA and β-TCP will be used as the inorganic osteogenic phase and thixotropic agent in future studies.

By gas foaming thiol-acrylate based copolymers synthesized via Michael addition with an *in situ* amine-catalyst, a porous polymeric scaffold with bone-like morphology was developed as a potential graft or augment in critical-sized bone defect repair. Not only does PETA:HA

composite have substantial porosity and interconnectivity, it also demonstrates adequate mechanical strength as compared to cortical bone. Compared to PCL:HA composites, both PETA:HA (85:15) and PETA:HA (80:20) scaffolds showed higher mineral deposition and *ALP* and *OCN* expression level. Overall, the PETA:HA had higher compressive strength and improved cytocompatibility compared to PCL controls. Mesenchymal cells cultured on PETA based scaffolds had a greater expression of osteogenic markers and the scaffolds exhibited significantly greater mineralization than hASC cultured on PCL controls. The *in vivo* study demonstrated that animals injected with PETA:HA composites showed no signs of surgical site or systemic toxicity and that PETA:HA composites induced osteogenesis *in vivo*. Additionally, the study serves as a proof-of-concept that gas foaming of thiol-acrylate polymers *in vivo* may be used to conformally fill irregular sized defects.

The dimensionality of the crystal structure of ceramics plays an important role in the fabrication of ceramic/polymer composite scaffolds. Increased three-dimensionality allows for better stability and higher mechanical strength of the ceramic scaffolds, as well as limiting scaffold phosphorous absorption from the environment. Furthermore, composite scaffolds provide greater stability to support hASCs attachment and growth than pure ceramics. The composites containing ceramics were also shown to degrade more slowly and maintain a relatively intact structure after prolonged exposure to cell medium compared to polymer scaffolds without ceramic additives as well as pure ceramic scaffolds. Overall, akermanite and monticellite-containing composites exhibit better osteogenic properties than those containing diopside and merwinite, suggesting that they might be the better ceramics for fabricating tissue engineered bone scaffolds.

APPENDIX A: APPROVAL FROM JOURNAL OF BIOMEDICAL MATERIALS RESEARCH: PART A

Copyright Clearance Center

Confirmation Number: 11302681
Order Date: 02/24/2015

Customer Information

Customer: Cong Chen
Account Number: 3000892434
Organization: Cong Chen
Email: cchen19@tigers.lsu.edu
Phone: +1 (225)6630689
Payment Method: Invoice

This is not an invoice

Order Details

Journal of biomedical materials research. Part A

Billing Status: N/A

Order detail ID:	66211054
ISSN:	1552-4965
Publication Type:	e-Journal
Volume:	
Issue:	
Start page:	
Publisher:	JOHN WILEY & SONS, INC.
Author/Editor:	Society for Biomaterials ; et al

Permission Status: Granted
Permission type: Republish or display content
Type of use: Republish in a thesis/dissertation
Order License Id: 3575570398820

Requestor type	Author of requested content
Format	Electronic
Portion	chapter/article
Number of pages in chapter/article	11
Title or numeric reference of the portion(s)	Thiolâacrylate nanocomposite foams for critical size bone defect repair: A novel biomaterial
Title of the article or chapter the portion is from	Journal of Biomedical Materials Research Part A
Editor of portion(s)	James M. Anderson
Author of portion(s)	Cong Chen
Volume of serial or monograph	101
Issue, if republishing an article from a serial	12
Page range of portion	3531-3541
Publication date of portion	April 29, 2013
Rights for	Main product
Duration of use	Life of current edition
Creation of copies for the disabled	yes
With minor editing privileges	yes
For distribution to	United States
In the following language(s)	Original language of publication

With incidental promotional use	no
Lifetime unit quantity of new product	Up to 499
Made available in the following markets	education
The requesting person/organization	Louisiana State University
Order reference number	
Author/Editor	Cong Chen
The standard identifier	Chapter2
The proposed price	non profit
Title	Cong Chen's dissertation
Publisher	LSU
Expected publication date	Aug 2015
Estimated size (pages)	200

Note: This item was invoiced separately through our **RightsLink service.** More info **$ 0.00**

Total order items: 1 **Order Total: $0.00**

APPENDIX B: APPROVAL FROM TISSUE ENGINEERING PART:A

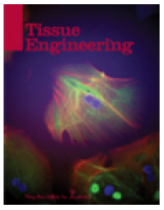

Title: In Vitro and In Vivo Characterization of Pentaerythritol Triacrylate-co-Trimethylolpropane Nanocomposite Scaffolds as Potential Bone Augments and Grafts

Author: Cong Chen, Leah Garber, Mollie Smoak, et al

Publication: Tissue Engineering Part A

Publisher: Mary Ann Liebert, Inc.

Date: Jan 1, 2015

Permissions Request

Mary Ann Liebert, Inc. publishers does not require authors of the content being used to obtain a license for their personal reuse of full article, charts/graphs/tables or text excerpt.

BACK CLOSE WINDOW

APPENDIX C: APPROVAL FROM ACS BIOMATERIALS SCIENCE &ENGINEERING

RightsLink®

Home | Create Account | Help | Live Chat

Title:	Targeting Calcium Magnesium Silicates for Polycaprolactone/Ceramic Composite Scaffolds
Author:	Cong Chen, Pilanda Watkins-Curry, Mollie Smoak, et al
Publication:	ACS Biomaterials Science & Engineering
Publisher:	American Chemical Society
Date:	Feb 1, 2015

LOGIN

If you're a copyright.com user, you can login to RightsLink using your copyright.com credentials. Already a **RightsLink user** or want to learn more?

PERMISSION/LICENSE IS GRANTED FOR YOUR ORDER AT NO CHARGE

This type of permission/license, instead of the standard Terms & Conditions, is sent to you because no fee is being charged for your order. Please note the following:

- Permission is granted for your request in both print and electronic formats, and translations.
- If figures and/or tables were requested, they may be adapted or used in part.
- Please print this page for your records and send a copy of it to your publisher/graduate school.
- Appropriate credit for the requested material should be given as follows: "Reprinted (adapted) with permission from (COMPLETE REFERENCE CITATION). Copyright (YEAR) American Chemical Society." Insert appropriate information in place of the capitalized words.
- One-time permission is granted only for the use specified in your request. No additional uses are granted (such as derivative works or other editions). For any other uses, please submit a new request.

BACK | CLOSE WINDOW

VITA

Mr. Cong Chen was born in China in 1986. He received his M. Sc. degree in biological and agricultural engineering in August, 2011 from Louisiana State University. Mr. Chen started his Ph.D. program in the college of Engineering at Louisiana State University in the fall of 2011 with a concentration in biomedical engineering. He plans to work as a post-doctorate after he graduates.